Characterization of the early stages in biofilm development

By

S. MARAIS

Thesis presented in partial fulfillment of the requirements for the degree of Master of Science at the University of Stellenbosch

Supervisor: Prof. G.M. Wolfaardt

Co-supervisor: Dr. D.G. Bessarabov

March 2004

DECLARATION

I, the undersigned hereby declare that the work contained in this thesis is my own original work and has not previously in its entity or in part been submitted at any university for a degree.

SIGNATURE:

DATE:

ABSTRACT

Complex biofilm communities have extensively been studied in the past. Less work has been done on the early stages of biofilm formation. This study aimed to assess initial colonization patterns of biofilms on different surfaces and under different environmental conditions with application of novel methods describing biofilm surface profiles. Biofilms were cultivated on glass, polyvinylchloride (PVC) and polished stainless steel. Results from microscopy, followed by mathematical analysis and contact angle measurements proved that glass was the most appropriate substrate for this study. More extensive extracellular polymeric substances (EPS) production and apparently less cell attachment were observed on PVC and polished stainless steel surfaces. Two different series of experiments were conducted where biofilms were cultivated on the glass. Biofilm morphology was analysed under various conditions of temperature and nutrient concentration. Different temperature conditions were 8°C, 22°C and 37°C and different nutrient concentrations were 0.1%, 1% and 10% Tryptic Soy Broth (TSB). After obtaining samples after 1, 2, 3 and 4 days respectively, the biofilm surfaces were visualised using atomic force microscopy (AFM) and epifluorescence microscopy. Less cell attachment was displayed at lower temperatures and nutrient limitations. The roughness profile of the early stages of biofilm development was explored by the novel application of various existing statistical methods. Benoit software was applied for the statistical analysis of various data sets obtained from AFM imaging, using power spectrum, variogram and wavelet methods to determine the Hurst exponent. The variogram method proved to be the most suitable to describe biofilm surface profiles with consistent values of ± 0.9, indicating that biofilm growth behaviour will continue in a similar pattern. Fractal dimension values of images obtained from epifluorescence microscopy was determined by the box dimension method. The values described the self-affine patterns displayed by biofilms. Using the results of these investigations, a series of models concerning the initial stages of biofilm formation was compared to describe the development of colony patterns. This study showed that the AFM and epifluorescence microscopy can be used as analytical tools for raw data assembly. It also demonstrated a novel application of existing statistical methods in order to describe the early stages of biofilm formation. Using this approach it was shown that the early stages of biofilm formation display certain colony patterns that can be

described and predicted. Such information may be used in efforts to control biofilm formation.

OPSOMMING

Komplekse biofilmgemeenskappe is reeds breedvoerig in die verlede bestudeer. Minder werk is op vroeë stadiums van biofilmvorming gedoen. Hierdie studie het gepoog om die aanvanklike koloniseringspatrone van biofilmvorming op verskillende substrate en onder verskillende omgewingstoestande kwantitatief te bepaal met nuwe metodes om die oppervlakprofiele van biofilms te beskryf. Biofilms is gekweek op glas, polivinielchloried (PVC) en gepoleerde vlekvrye staal. Resultate van mikroskopie, gevolg deur wiskundige analise en kontakhoek-metings het getoon dat glas die mees geskikte substraat vir hierdie studie is. Die produksie van meer ekstrasellulêre polimeriese substanse (EPS) en oënskynlik minder selaanhegting is waargeneem op PVC en gepoleerde vlekvrye staal oppervlaktes. Twee verskillende reekse eksperimente is uitgevoer waar biofilms op glas gekweek is. Biofilm-morfologie is geanaliseer onder verskillende toestande van temperatuur en nutriënt-konsentrasie. Verskillende temperatuur-toestande was 8°C, 22°C en 37°C en verskillende nutriënt-konsentrasies was 0.1%, 1% en 10% *Tryptic Soy Broth* (TSB). Nadat monsters onderskeidelik na 1, 2, 3 en 4 dae verkry is, is die biofilm oppervlaktes gevisualiseer deur atoomkrag mikroskopie (AFM) en epi-fluoressensie mikroskopie. Minder selaanhegting is waargeneem by laer temperature en nutriënt-beperkinge. Die grofheidsprofiele van die vroeë stadium van biofilm-ontwikkeling is ondersoek deur die nuwe toepassing van verskeie bestaande statistiese metodes. Benoit-sagteware is gebruik om die statistiese analise van verskeie data-stelle van AFM beelde te ondersoek deur *power spectrum*, *variogram* en *wavelet* -metodes te gebruik om die Hurst-eksponent te bepaal. Die *variogram* metode het voorgekom as die mees geskikte om biofilm oppervlakprofiele te beskryf met konstante waardes van ± 0.9, wat aandui dat biofilm groei sal aanhou in 'n soortgelyke patroon. Fraktale dimensie-waardes van beelde wat met epi-fluoressensie mikroskopie verkry is bepaal deur toepassing van Benoit-sagteware se *box dimension* metode. Die waardes beskryf die selfherhalende patrone wat deur biofilms gedemonstreer word. Deur die resultate van hierdie ondersoeke te gebruik, is 'n reeks modelle aangaande die aanvanklike stadiums van biofilmvorming vergelyk om die ontwikkeling van koloniepatrone te beskryf. Hierdie studie het getoon dat die AFM en epi-fluoressensie mikroskopie gebruik kan word as analitiese gereedskap vir rou data-versameling. 'n Nuwe toepassing van bestaande statistiese metodes om die vroeë

stadiums van biofilmvorming te beskryf, is ook gedemonstreer. Deur hierdie benadering te gebruik, is getoon dat die vroeë stadiums van biofilmvorming sekere koloniepatrone aandui wat beskryf en voorspel kan word. Sulke inligting kan gebruik word in pogings om biofilmvorming te beheer.

ACKNOWLEDGEMENTS

I would like to express my gratitude towards:

Prof. G.M. Wolfaardt (supervisor) and Dr. D.G. Bessarabov (co-supervisor) for their advice and support, and for giving me the opportunity to undertake this study.

Friends and family for their loyalty, friendship and support.

LIST OF TABLES

LIST OF FIGURES

CHAPTER 1: GENERAL INTRODUCTION AND OBJECTIVES

1.1 Introduction

Biofilms are populations or communities of microorganisms adhering to surfaces. These microorganisms are usually encased in a matrix of extracellular polymeric substances (EPS) that they synthesize. Most of the EPS of biofilms are polymers containing sugars such as glucose, galactose, mannose, fructose, rhamnose, N-acetylglucosamine and others (Nguyen and Schiller, 1989). Biofilms may form on solid substrates in contact with moisture, on soft tissue surfaces in living organisms or at liquid-air interfaces. They are consequently found in many environmental, industrial and medical systems. The adherent bacteria produce microcolonies, leading to the development of biofilms, which initially may be composed of only one type of bacteria, but frequently develop to contain several bacteria living in a complex community (Costerton, *et al.*, 1995).

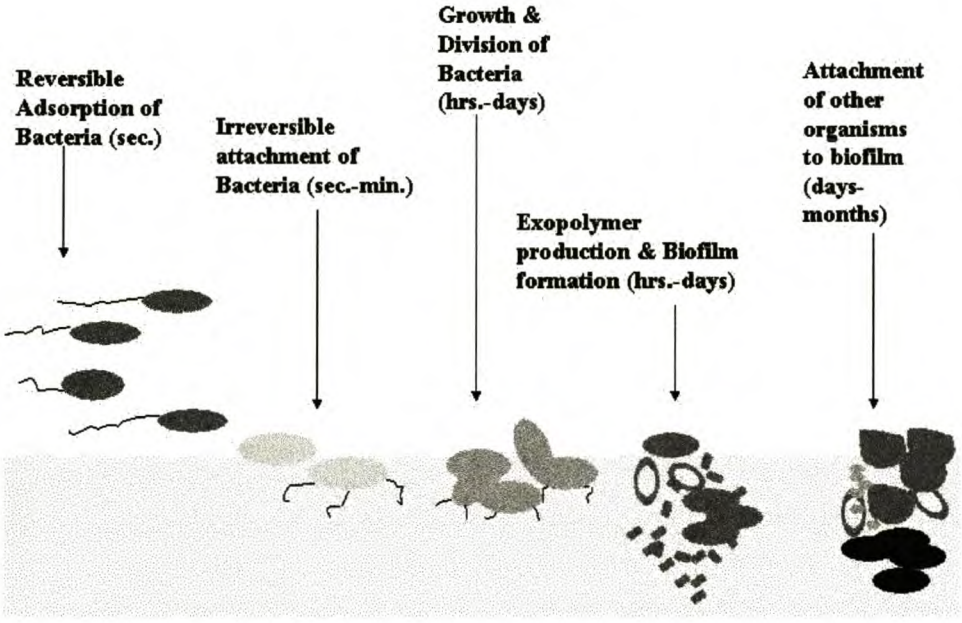

Figure 1.1 The different stages during the biofilm formation process, including the time scale of these events (Adapted from Allison and Hughes, 1992).

The formation of biofilms follows a course of which the nature can be predicted and recorded (Fig. 1.1). The process is believed to begin when bacteria sense certain environmental parameters that trigger the transition from planktonic (free-swimming) growth to life on a surface (Fletcher *et al.*, 1986; Nyvad and Kilian, 1990; Poulsen *et al.*, 1993; Wang *et al.*, 1996; Williams and Fletcher, 1996; O'Toole and Kolter, 1998;

O'Toole *et al.*, 2000). When organic matter is present, a conditioning film of adsorbed components is formed on the surface prior to the arrival of the first organisms. The adsorbed materials condition the surface of the substrate and appear to increase the probability of the attachment of planktonic bacteria. This changes the chemical and physical properties of the substrate. Microorganisms are transported to the surface through diffusion, convection, sedimentation or active movement. These free floating or planktonic bacteria encounter the conditioned surface and form a reversible, sometimes transient attachment, often within minutes. After initial attachment, they often rearrange themselves in microcolonies. This attachment, called adsorption, is influenced by electrical charges on the bacteria, by Van der Waals forces, and by electrostatic attraction (Razatos *et al.*, 1998).

The final stage in the irreversible adhesion of a cell to an environmental surface is associated with the production of EPS. Attachment of adhering microorganisms is strengthened through EPS production and unfolding of cell surface structures termed holdfasts. The surface growth of attached microorganisms continues together with continued secretion of EPS. This layer of EPS and bacteria subsequently now entrap materials such as clay, organic materials, dead cells and precipitated minerals adding to the bulk and diversity of the biofilm habitat. The EPS matrix also has the potential to physically prevent access of certain antimicrobial agents into the biofilm by acting as an ion exchanger, thereby restricting diffusion of compounds from the surrounding milieu into the biofilm (Gilbert and Foley, 1997).

Biofilms have beneficial and detrimental attributes, depending on where they are found, and the composition of species (Bryers and Characklis, 1982; Costerton *et al.*, 1995; Stoodley *et al.*, 1999). Often, biofilms are unwanted, and related to diverse problems such as microbially induced corrosion of oilrigs and pipelines, food and drinking water contamination, dental caries and periodontal diseases, as well as a variety of biomaterial-related infections in humans. Not all biofilms are unwanted, however, and in sewage treatment, biofilms are needed for efficient degradation of xenobiotics, while *Lactobacillus* biofilms form part of the normal indigenous bacterial population in humans and their maintenance is essential in the prevention of disease.

Prevention of biofilm formation is often difficult because of the numerous attachment and adhesion mechanisms shown by bacteria, and therefore removal strategies are

often necessary. Pasmore *et al.* (2002) found that cells were most readily removed from the smoothest, most hydrophilic, neutral surfaces, with removal becoming more difficult after longer attachment times. This finding correlates with the observation that surfaces with these characteristics are most resistant to biofilm initiation. Therefore, it is possible to produce a surface from which bacteria can be more readily removed. Total removal of biofilms is only possible when biofilms are directly accessible, as e.g. on exterior parts of the human body. Dental biofilms can be removed by mechanical cleansing, in combination with the use of surface-active substances, like in dentifrices and mouth washes. Bacteria adhering to contact lenses can be removed by rubbing the lenses between the fingers in combination with cleansing solutions. The strength of biofilm adhesion to a substratum surface, i.e. the ease with which it can be removed, is greatly dependent on the strength with which the initially adhering organisms bind to the substratum surface and cohesiveness of the conditioning film (Busscher *et al.*, 1995), which makes initial microbial adhesion and surface growth an important issue of research.

1.2 Recent studies on the characterization of biofilms

Various techniques have been used to study biofilms. A major problem is the inability to study them as they develop in natural settings. Morphological observation of microbial population has been done by optical microscopy, scanning electron microscopy (SEM) (Shapiro, 1987; Tommaso *et al.*, 2002) and magnetic resonance force microscopy (MRFM) (Noble, 1995). SEM techniques have been used in the past to image biological samples (Shapiro, 1987; Tessele *et al.* 2002), but these have severe limitations as SEM requires a conductive layer and examination under vacuum, which may damage the surfaces of samples. This method is not suitable for the hydrated nature of biological samples like biofilms, because the three-dimensional structure of, e.g. the EPS is lost. On the other hand, confocal scanning laser microscopy (CSLM) has the ability to produce images of fully hydrated material at various depths, and the development of procedures to study biofilms with this instrument has given new information on the structure of microbial biofilms (Zottola, 1997). These studies showed that bacterial cells are located in discrete microcolonies embedded in a matrix permeated by well-defined channels. Binnig and Rohrer (1984) invented the Scanning Tunnelling Microscope (STM) which makes use of a tungsten wire from which a stream of electrons "tunnels" across to the sample. It has been found that the STM

technique has a major drawback when used for biological applications, because the tip may puncture and penetrate the cell, and as a result, the inside of the cell is imaged (Ruppersberg *et al.*, 1989). Furthermore, the sample surface needs to be conducting and this usually requires coating which might damage biological samples.

Binnig and colleagues also developed the Atomic Force Microscope (AFM), which uses a sharp tip placed at the end of a flexible cantilever to scan across the surface of a sample, sensing the topography of a sample (Binnig *et al.*, 1986). The major advantages of AFM are the ability to cover the magnification range of both optical and electron microscopy, but under natural conditions with minimal sample preparation, and the production of three-dimensional images of the surfaces. Biofilms are relatively soft; therefore minimization of force interactions between the AFM tip and the sample surface is required for non-destructive imaging of most samples. Initially, AFM studies were aimed at visualization of biofilm morphology, roughness, nanostructure and structural order, and these investigations have been performed on a large number of biofilm samples (Jasche *et al.*, 1994; Gunning *et al.*, 1996; Xu *et al.*, 1996). More recently, the spectrum of AFM applications to biofilms has broadened substantially. In addition to high-resolution profiling of surface morphology and nanostructure, AFM allows determination of surface roughness values and fractal analysis. In spite of the many advantages that AFM offers in surface roughness analysis, there are disadvantages associated with using AFM, such as inaccurate roughness analyses due to the imaging of artifacts (Kiely and Bonnell, 1997). Therefore, alternative methods have also been investigated, such as statistical methods for the characterisation of surface roughness.

1.3 Fractal analysis and mathematical characterization

Fractal geometry has been used by geologists, economists and recently by microbiologists for quantifying the roughness of an object (Kaandorp, 1994; Russ, 1994). The surface enlargement coefficient of roughness, fractal dimension of surface, biofilm compactness, and solids hold-up were found to be good measures of biofilm structure complexity (Picioreanu *et al.*, 1998). Fractal dimension measurements are becoming increasingly useful for surface characterization as it becomes apparent that standard engineering roughness calculations do not completely represent the properties of the surface being studied. Shortcomings of conventional techniques such as R_a

(average roughness) and R_t (maximum feature height) are apparent when the differences in measured roughness between two surfaces are small, but the differences in other characteristics are apparently large (Chesters *et al.*, 1989). Fractal analysis can be used to distinguish between surfaces with the same average roughness (R_a) values as an alternative to characterize surface texture.

Hermanowicz *et al.* (1995) used fractal dimension to describe biofilm morphology. Images of biofilm sections were obtained with CSLM, and fractal dimensions were estimated from the slopes of cross-correlation functions. During investigations of the fractal structure of *Escherichia coli* and *Bacillus subtilis* colonies growing on agar plates, it was demonstrated that in limited nutrients, the colonies developed a self-similar shape (is exactly or approximately similar to a part of itself) corresponding to the geometry of diffusion-limited aggregates (Vicsek *et al.*, 1990).

Matsuura and Miyazima (1992) grew *Aspergillus oryzae* in various environmental conditions and analyzed the self-affinity. The occurrence of self-affine fractal scaling means that a small part of the surface of the biological system looked the same as the whole structure after this small part was expanded in an anistrophic way. The Eden model (Eden, 1961) was used to describe growth behavior under favorable conditions and diffusion limited aggregation (DLA) to describe growth behavior under unfavorable conditions. In the Eden model a cluster made of identical units or "particles" (corresponding to the bacteria) is generated on lattice by adding new particles to the growing cluster at sites randomly chosen from the set of sites adjacent to the cluster. In the DLA model typical examples of fractal growth in nature (smoke, dust and haze) was simulated by Witten *et al.* (1981) and called DLA. In the glucose-rich condition, the *Aspergillus oryzae* colonies showed a homogeneous and smooth growth front (Eden-like) on the solid agar and a ramified front on the semi-liquid agar. In the glucose poor-condition, the colony surfaces become rough even on the solid agar, and the colonies showed a ramified pattern on the semi-liquid agar (DLA-like). It was further concluded that the growth behavior was fast effuse at the higher temperature and became dense at lower temperature.

Although biofilm structure has been studied extensively, the attempts to quantify the structure are much fewer and limited to calculating fractal dimension. This study focuses on the analysis of images of biofilms obtained with AFM. Various analyses

have been developed to utilize the numerical data of surface height provided by AFM, including the root-mean square of height, fractal analysis and Power Spectrum Density (PSD) analysis (Gouyet, 1996). These analyses aimed at finding appropriate morphological parameters to interpret physical properties of the film or studying the growth mechanism of film. Michaels (2002) successfully used various statistical methods to explore the roughness profiles of a platinum catalyst embedded in a membrane. The statistical analysis of various data sets for a surface of a platinum-containing membrane was investigated using Hurst exponent. This theory will be applied in this study to compare the feasibility of the different equations for calculating fractal values to mathematically and statistically describe biofilm development under different conditions.

1.4 Advantages of early stage studies

The early stages of biofilm development on solid substrata begin with formation of a molecular film on which microbes settle and replicate, forming a confluent but heterogeneous matrix of which the negative effects are an ongoing area of concern. Control of oral plaque build up is a fundamental problem in dental hygiene (Marsh, 1999). In order to control the buildup of plaque, chemicals can be used to detach bacteria from the tooth surface or kill the bacteria within plaque. An alternative is to stop the bacteria from attaching to the surface by using chemicals called anti-adhesins. This leads to the interest to examine the initial events of plaque formation by studying attachment of primary colonizers. Preventing the initial attachment stage would help addressing the problem of biofilm formation. In such a case, it will be a benefit to better understand the process of initial attachment. This could include defining patterns of biofilm development during the initial stages.

The initial development stages also play a large role during biofilm protection against disinfectants (Davies, 1994) as shown by experiments indicating that biofilm bacteria may be 150-3000 times more resistant to free chlorine than free-floating bacteria. In order to destroy the cells responsible for forming the biofilm, the disinfectant must probably first react with the surrounding polysaccharide network. Biofilm bacteria often produce more exopolymers after biocide treatment to further protect themselves (Costerton, and Stewart, 2001). Despite the great interest in biofilms, little is known about the molecular basis of biofilm development and biofilm-specific antibiotic

resistance. This theory applies to other problem areas. Initial attachment of bacteria and subsequent biofilm formation on equipment surfaces subjected to food contact and handling in food processing environments, is a significant potential source of contamination that upon deattachment, may result in food spoilage or possible transmission of diseases. Equipment surfaces used in food processing environments are indeed major sources of microbial contamination; joints, pits and cracks on areas of equipment that are more prone to collection of soil and bacteria, thus facilitating microbial attachment (Notermans, 1991). The contamination of food processing environments by biofilms emphasizes the importance of studying bacterial attachment and inactivation and thereby motivates the importance to produce environments and surfaces that do not encourage the development of biofilms. Most studies focus on mature, established biofilms, because they are easier to study, and to detect their implications.

1.5 Objectives of this research

The working hypothesis of this study was that the initial stages of biofilm formation occur in an orderly fashion, which, if well defined, can be used to predict the behavior of microbes when they first colonize surfaces. This implies that if this is true, primary colonization is not a random event. However, it was further hypothesized that various environmental factors could influence the patterns of primary colonization. To test this hypothesis, the overall goal of this study was therefore to follow an experimental approach to visualize the initial stages of biofilm formation, and to use a mathematical equation to quantify initial biofilm formation and the resulting patterns. The specific objectives were to:

1) Select a model system that would allow primary colonization of test surfaces
2) Use AFM to observe initial stages of biofilm formation on the test surfaces
3) Measure primary colonization under different environmental conditions, including type of attachment surface, nutrient conditions, and temperature
4) To use fractal analysis to quantitatively describe primarily colonization on the different test surfaces under different environmental conditions.

CHAPTER 2: LITERATURE REVIEW

2.1 Implications of the biofilm mode of growth

2.1.1 Medicine

Biofilms can be a serious threat to health for patients in whom artificial substrates have been introduced. Patients with indwelling catheters for urine excretion or continuous ambulatory peritoneal dialysis (CAPD) are subject to frequent and persistent bouts of infection. These recurrent infections are due to the accumulation of mixed biofilms on the artificial surfaces provided by the catheter (Velraeds, *et al.*, 1997) or other body implants (Van der Mei, *et al.*, 1997). Fragments of biofilm that slough off at intervals can spread the infection to distant locations within the body. Consequently, infection of a biomaterial implant can result in re-operation, osteomyelitis, or amputation (Gristina, 1987). Biofilm formation can also occur on contact lenses, and these biofilms are thought to contribute to keratitis (Elder *et al.*, 1995; Gorlin *et al.*, 1996; McLaughlin-Borlace *et al.*, 1998). Infections in humans are especially troublesome, since biofilm organisms are protected against the host immune system and cannot be easily eradicated with antibiotics. The EPS in which the bacteria live protects them from the effects of antibiotics and accounts for the persistence of the infection even during vigorous chemotherapy (Jarlier and Nikaido, 1994).

Tissue surfaces such as teeth and intestinal mucosa, which are constantly bathed in a rich aqueous medium, rapidly develop a complex aggregation of microorganisms. A classic example is the biofilm on our teeth, leading to the development of cavities when bacteria such as *Streptococcus mutans* degrade sugars to organic acids (Landa *et al.*, 1996). The ability of oral bacteria to store iodophilic polysaccharides or glycogen-like molecules inside their cells is associated with dental caries since these storage compounds may extend the time during which lactic acid formation may occur. This prolonged exposure to lactic acid results in decalcification of tooth enamel. Dental plaque is one of the most-studied biofilm communities and a number of recent reviews have covered the structure and composition of oral communities (Kolenbrander and London, 1993; Whittaker *et al.*, 1996; Singleton *et al.*, 1997; Burne *et al.*, 1999; Dibdin and Wimpenny, 1999; Kolenbrander *et al.*, 1999; Marsh, 1999).

2.1.2 Industry

Biofilms have useful applications in industry, because of the production of EPS. This biopolymer is used as a thickening agent in a variety of food and consumer products (Notermans, *et al.*, 1991; Flint, *et al.*, 1997). Gellation of some biopolymers can occur upon addition of divalent cations, such as calcium and magnesium. The electrostatic interaction between carboxylate functional groups on the polysaccharide and the divalent cations results in a bridging effect between polymer chains. Bridging and cross-linking of the polymers help to stabilize the biofilm, making it more resistant to shear.

Industrial biofilm contamination and fouling occurs in nearly every industrial water-based process, including water treatment and distribution, pulp & paper manufacturing, and the operation of cooling towers (Flemming and Geesey, 1991). For example, biofilms are notorious for causing pipe plugging, corrosion, water contamination and the accelerated corrosion of machine surfaces (Flemming, 1996) causing billions of dollars to be lost in industrial productivity and both product and capital equipment damage each year.

Even in the papermaking process, several problems are caused by biofouling of surfaces in the wet end of paper machines (Blanco *et al.,* 1996). Biofilms detaching from machine surfaces can break the paper web, causing downtime that can cost up to $30,000 per hour in modern machines. Furthermore, coloured EPS can spoil paper products, beacause coloured deposits are visible in white products. The content of live microbes in the paper product may increase to numbers intolerable in food-quality packaging paper and paperboard.

2.1.3 Environment

The complex ecological systems of biofilms can have a significant impact on the surrounding environment. Humans have made considerable use of microbial biofilms, primarily in the area of habitat remediation. Bacteria within biofilms can break down contaminants in soil and water and are often used for remediation purposes. Water treatment plants, waste water treatment plants, as well as septic systems associated with private homes remove pathogens and reduce the amount of organic matter in the water or waste water through interaction with biofilms (Massol-Deya, *et al.*, 1995).

Biofilms found on the solid supports in sewage-treatment plants, play an essential role in processing of sewage water before it is discharged into rivers.

Eutrophication is another environmental problem. The discharge of phosphate to water streams, coming from agricultural, industrial or domestic activities is the main reason responsible for this problem. In solving this problem, biological phosphorous removal is gaining advantage over chemical precipitation as there is a reduction in the emission of solids, while less operational costs are involved (Toerien *et al.*, 1990).

Plants also commonly have microbial populations associated with their external tissues. Such plant microbe association typically occurs in the rhizosphere and implies a relationship between the plant roots and root hairs and a complex microbial community (Campbell and Greaves, 1990). The rhizosphere association is mutualistic. Plant roots secrete significant amounts of sugars, amino acids, vitamins and plant hormones, which stimulate microbial growth in the immediate vicinity of the root. This relationship may also be important to the plant in that the microbial population may facilitate the absorption of nutrients by the plant from the soil.

2.1.4 Cell survival and metabolic ability

Biofilm-grown bacteria are notorious for their resistance to a range of antimicrobial agents including clinically relevant antibiotics. Despite the focus of modern microbiology research on pure culture, planktonic bacteria, it is now widely recognized that most bacteria found in natural, clinical, and industrial settings persist in association with surfaces. These microbial communities are often composed of multiple species that interact with each other and their environment. Microbes are efficient to proliferate under conditions of low nutrient concentrations for instance portable water, especially high-purity water systems, are nutrient-limited environments, but even nutrient concentrations too low to measure are sufficient for microbial growth and reproduction (Chang *et al.*, 1991)

Studies revealed that increasing nutrient concentration increases the biofilm thickness and detachment rate (Chang *et al.*, 1991), while increasing turbulence can produce denser and thinner biofilms (Chang *et al.*, 1991). It was also found that denser and thinner biofilms are less sensitive to both shear and abrasion biofilm losses (Nicolella, *et al.*, 1997). Attachment characteristics change depending on the species or the

physiological condition of the microorganism (Characklis, 1973) and species distribution varies with turbulence (Characklis, 1971).

2.2 Studies of biofilms

2.2.1 Types of models

Early models of biofilms depicted them as a homogeneous and contiguous layer containing uniformly distributed bacterial cells. The first models in the 1970s, described biofilms as uniform steady-state films of a single species with one-dimensional mass transport and biochemical reactions. In the 1980s, stratified dynamic models of multisubstrate and multispecies biofilms were developed. The characteristic biofilm morphology could not be generated, but a given biofilm structure was used as input into the model (Kreft *et al.*, 2001). In the 1990s two-dimensional (2D) and three-dimensional (3D) models were developed, facilitated by the advances in both computational power and numerical methods. These models incorporated the whole range of transport processes as well as biofilm growth and detachment (Wimpenny and Colasanti, 1997; Noguera *et al.*, 199b; Eberl *et al.*, 2001). According to these biomass-based models (BbMs), also classified as spatially structured models, biofilm structure is an emergent property because it follows a bottom-up approach where complex communities emerge as a result of the actions and interactions of the biomass units with each other and the environment (Kreft *et al.*, 2001).

One of the keys to studying complex biological systems is to develop accurate and realistic models of natural communities in the laboratory. Progress has already been made in designing an artificial mouth (Kinniment *et al.*, 1996, Sissons, 1997) as well as a model to study catheter-induced bladder infections (Stickler *et al.*, 1993). Another bottom-up approach is the individual-based model (IbM). It attempts to represent a population or community by describing the actions and properties of the individuals comprising the population or community (Huston *et al.*, 1988; De Angelis and Gross, 1992; Grimm, 1999). In contrast to the BbM, the IbM allows individual variability and treats organisms as fundamental entities. When one of these entities changes position, its biomass, fixed and variable properties and its cell number are displaced together. Barton *et al.* (1996) summarize the use of a parallel plate flow chamber model to study initial microbial adhesion to surfaces and extends the use of flow chamber devices and data analysis to include surface growth of the initially adhering organisms. With this

system different processes in bacterial biofilm formation, i.e. conditioning film formation, initial bacterial adhesion, bacterial surface growth and bacterial detachment can be modeled and monitored *in situ*. As thickness extends to above one layer, the events are not clearly visible anymore and consequently only initial biofilm formation can be studied.

2.2.2 Microscopy

There are ranges of microscopic methods that can be applied to study biofilms (Beech *et al.*, 1996; Surman *et al.*, 1996). It was initially thought that biofilms consisted of bacteria randomly distributed within a uniform slimy matrix. However, CSLM studies have revealed the elaborate three-dimensional structure of biofilms (Costerton *et al.*, 1995; de Beer and Stoodley, 1995; de Beer *et al.*, 1994). It was found that biofilm structures take a wide variety of forms depending on their age and growing conditions. Through the examination of the internal structure of biofilms with CLSM (Lawrence *et al,* 1991), it became apparent that biofilms are often not uniform and homogeneous but full of holes and channels connected to bulk of liquid. SEM has also proven to be a method of choice to examine microbial biofilms under high resolution (Coutinho *et al.*, 1993). SEM investigations showed that even in the simplest systems of pure culture biofilms patterns of attachment are displayed as well as the subsequent growth into elaborate structures, which optimize the flow of nutrients and enhance the survival of the microorganisms on the surface. Fluorescence illumination and observation is the most rapidly expanding microscopy technique employed today, both in the medical and biological sciences. Fluorescence microscopy can also be used to detect structures, molecules or proteins within the cell (Goulian and Simon, 2000). The epifluorescence images can provide valuable information on the morphology of the biofilms forming on different substrates, and the distribution of the biofilm cells within the bulk of the biofilm layers (Donlan, 2002). Unfixed, hydrated biological samples can be investigated by this technique.

AFM has been used extensively to study microbial cells. Biologists have used AFM in combination with light microscopy (transmitted bright field, epiflourescence and surface interface) to gain both topographical and visual information from the sample (Vesenka *et al.*, 1995; Nagao and Dvorak, 1998). A number of bacterial surface layers have been studied by AFM. Examples include the real surface layer of *Deinococcus*

radiodurans (Schabert *et al.,* 1992), *Halobacterium* purple membrane (Muller *et al.,* 1995), S-layers from *Bacillus coagulans* and *Bacillus spaericus* (Ohnesorge *et al.*, 1992) and *Escherichia coli* porin surfaces (Schabert and Engel, 1994; Schabert *et al*, 1995). Other complex structures include the sheath, hoops and plugs of the surface structures of *Methanospirillium hungatei* (Southam *et al* 1993). In addition to obtaining high-resolution images of cell surface structures it is also possible to measure and model their elastic properties using the AFM. Investigations on the sheath of the methanogen *M. hungatei* illustrated this type of study (Xu *et al.*, 1996).

Bacterial cell wall structures are relatively rigid and it is possible to reveal the roughness of the surface (Gunning *et al*, 1996; Braga and Ricci, 1998). Bacterial flagella can be imaged and substructure and flagella motors have been observed (Jaschke *et al.*, 1994). AFM has been used to 'read' photoresists generated by X-ray microscopy of *E. coli.* The images revealed the outer Gram-negative envelope and internal structure attributed to chromosomal DNA (Rajyaguru *et al.*, 1997). The action of antibiotics on bacteria has been investigated by AFM. Studies include observation of the action of penicillin on *Bacillus subtilis* (Kasas *et al.*, 1994) and the use of AFM to examine changes in surface structure of *E. coli* due to exposure to the β-lactam antibiotic cefodizime (Braga and Ricci, 1998).

In addition to imaging bacteria deposited onto solid supports it is also possible to use AFM to investigate the formation and structure of biofilms formed at interfaces or on solid surfaces. AFM has been used to study biofilms formed on glass (Surman *et al.*, 1996), metal surfaces (Bremer *et al.*, 1992; Steele *et al.*, 1994; Beech, 1996; Beech *et al.*, 1996), and hydrous Fe (III)-oxides of soil (Maurice *at al.*, 1996). Studies of hydrated bacterial biofilms formed on copper surfaces have revealed that the bacteria are observed bound adjacent to pits with EPS extending into the pits (Bremer *et al.*, 1992). This is important because metal ion binding by EPS has been suggested as a basis for pit corrosion of copper surfaces (Geesey *et al.*, 1986; Jolley *et al.,* 1988). Studies of *Pseudomonas* species biofilms also illustrated the importance of EPS in film formation (Beech *et al.*, 1996). Related studies of bacterial biofilms on steel surfaces have highlighted the presence of EPS, and have been used to examine pitting of the surface caused by biofilm formation (Steele *et al.*, 1994; Beech, 1996; Beech *et al.*, 1996). AFM has also demonstrated the importance of EPS in *Pseudomonas putida*

biofilms formed at oil-water interfaces, and then imaged by light and electron microscopy (Parker *et al.*, 1995). If biofilm formation is modeled by growing such biofilms at flat oil-water interfaces, AFM images can be obtained for samples of these flat biofilms pulled from the interface onto mica substrates by Langmuir-Blodgett techniques (Gunning *et al.*, 1996). In addition to visualizing the packing of the bacteria it is also possible to identify remnants of bacterial flagella trapped within the EPS. There is, however, further scope for the use of AFM to study the early stages of biofilm formation and/or the efficiency of present, or novel cleaning methods for removing such biofilms.

2.2.3 Principles of Atomic Force Microscopy

Scanning probe microscopy began in 1982 when Gerd Binnig and Heinrich Rohrer of IBM Zurich revolutionized microscopy through the invention of the scanning tunneling microscope (STM) (Binnig and Rohrer, 1984). This microscope is capable of imaging at the Angstrom scale, allowing examination of the surface of conductors with atomic resolution. The STM triggered the development of a variety of scanning probe microscopes (SPM). Refinements and new types of SPMs have appeared and the AFM is perhaps the most versatile member of the family of these microscopes. In 1986 Binnig and colleagues announced the development of the AFM (Binnig *et al.*, 1986). Commercial AFMs began to appear in the early 1990s and have evolved through several generations.

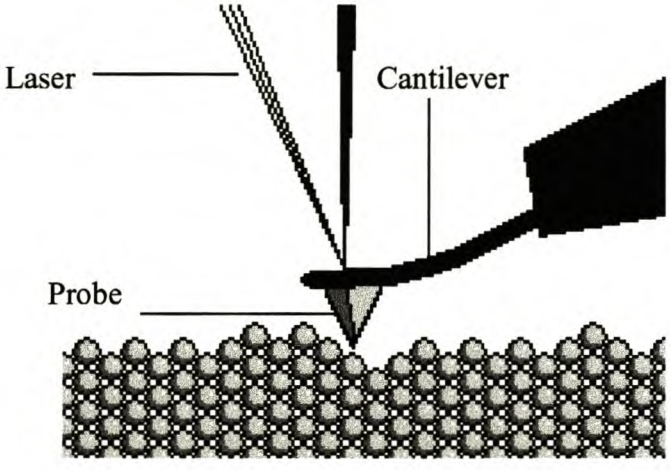

Figure 2.1 A schematic representation of AFM operation (Adapted from Morris *et al.*, 1999).

The operation of this instrument is illustrated in Figure 2.1. The goal of an AFM is to measure very small forces at very small distances in order to get images at the molecular level. The forces are typically in the nano Newton range. The probe/sample forces are measured by placing the probe on a very small spring cantilever, which deflects as features are encountered on the sample surface. The laser light is focused on the backside of the cantilever. After reflecting off the cantilever, the light is reflected by a mirror onto the surface of the multisection photodetector. The motion of the probe is therefore sensed by the displacement of the reflected beam on the multisection photodetector. The detector signal is used for feedback control to adjust the tip-sample distance during the scanning. The sensor output is compared with a set voltage, and the z feedback signal. A picture of the surface can be reconstructed and the surface topography is visualized with the use of computer graphics. Since the topographic information is stored in the computer, features relating to the surface, such as the average roughness, size of cells, distances and angles between objects, can be calculated easily.

An equivalent sample can be visualized using an AFM with minimal preparation, unlike SEM, which requires a conductive coating of metal or carbon (Au/Pd- or C-sputter coating) on most samples. This layer can cover finer features and the vacuum required by SEM can deform biological samples. AFM can scan a sample under ambient conditions, even under a layer of solution, with the only restriction that the objects of interest must be held securely on the substrate. This potential to image biological systems in real time, under natural conditions, with molecular or even submolecular resolution has clearly been of interest to biologists (Vesenka *et al*, 1995 and Nagao and Dvorak 1998).

2.2.4 Statistical methods

Benoit Mandelbrot was largely responsible for the present interest in fractal geometry. He showed how fractals could occur in many different places in both mathematics and elsewhere in nature. A popular representation of fractal geometry lies within the Mandelbrot set, named after its creator Benoit Mandelbrot who coined the name "fractal" from the Latin *fractus* or "to break". The Mandelbrot set is the collection of all points that remain bounded for every iteration of $\mathbf{z} \rightarrow \mathbf{z}^*\mathbf{z} + \mathbf{c}$ on the complex plane, where the initial value of $\mathbf{z}$ is 0 and $\mathbf{c}$ is a complex number constant. It is easy to see

the self-similarity inherent in linear fractal, but the complexity greatly increases once we move beyond linear fractals into the world of non-linear fractals such as the Mandelbrot set.

With fractal geometry much of what is witnessed in nature, can be modelled visually, the most recognized being coastlines and mountains. Fractals are used to model soil erosion and to analyse seismic patterns as well (Gardiner *et al.*, 1987). Where classical geometry deals with objects of integer dimensions, fractal geometry describes non-integer dimensions. Zero dimensional points, one dimensional lines and curves, two dimensional plane figures like squares and circles, and three dimensional solids such as cubes and spheres make up the world as previously understood. Many natural phenomena are better described with a dimension partway between two whole numbers, i.e. two integers. So while a straight line has a dimension of one, a fractal curve will have a dimension between one and two depending on how much space it takes up as it twists and curves (Feder, 1989). The more that flat fractal fills a plane, the closer it approaches two dimensions. Likewise, a "hilly fractal scene" will reach a dimension somewhere between two and three. So a fractal landscape made up of a large hill covered with tiny bumps would be close to the second dimension, while a rough surface composed of many medium-sized hills would be close to the third dimension.

The dimensions of Euclidean geometrical objects such as, dots, lines, planes or bodies are generally classified according to topological dimensions 0, 1, 2 and 3, respectively. There are however numerous natural and artificial geometrical objects for which this simple classification is inadequate. These objects need to be assigned intermediate dimensional values. Fractal geometry was therefore developed, since Euclidean geometry is unable to describe disordered surfaces. A definition of a fractal is a shape made of parts similar to the whole in some way. The fractal dimension (Fd) of a surface (Marchese-Ragona *et al.*, 1993) can be:

- characterised by only one number,
- correlated with observable phenomena such as cleanability, corrosion, adsorption, catalysis and degassing, and

- can often distinguish surfaces that other engineering parameters classify as being similar.

The minimum value of the fractal dimension for a line profile is 1.0, which describes a perfectly flat line that fills only a one-dimensional space (Fig. 2.2 A). The maximum value of the fractal dimension for a line profile is 2.0 (Fig. 2.2 B). This is for a line that is so rough that it forms a solid surface and consequently fills a two-dimensional space. In practice, the fractal dimension of a line profile is between 1.0 and 2.0 (Fig. 2.2 C). The minimum value of the fractal dimension for a surface contour is 2.0, which is a perfectly flat surface that fills only a two-dimensional space (Fig. 2.2 D). The maximum value of the fractal dimension for a surface is 3.0 (Fig. 2.2 E). This is for a case where the surface is so rough that it fills a three-dimensional space. In practice, the fractal dimension of a surface is between 2.0 and 3.0 (Fig. 2.2 F) (Marchese-Ragona *et al.*, 1993 and Feder, 1989).

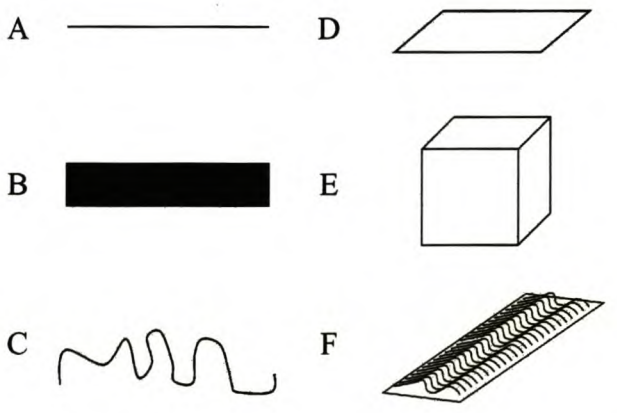

Figure 2.2 A schematic representation of surfaces with different fractal dimensions (Fd). Fd = 1.0 (A); Fd = 2.0 (B); Fd is between 1.0 and 2.0 (C); Fd = 2.0 (D); Fd = 3.0 (E); Fd is between 2.0 and 3.0 (F) (Marchese-Ragona *et al.*, 1993).

According to fractal geometry, three classes of fractals can describe strongly disordered systems, namely: surface fractal, mass fractal and pore fractal (Fig. 2.3).

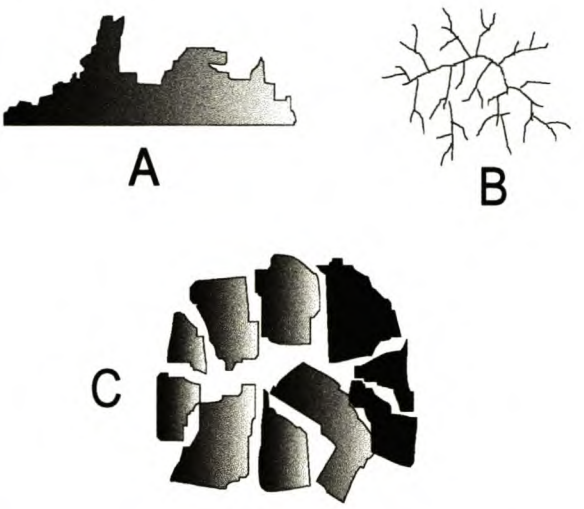

Figure 2.3 A schematic representation of different types of fractals: surface fractal (A), mass fractal (B) and pore fractal (C) (Adopted from Michaels, 2002).

The surface of an object may result in a surface fractal (Fig. 2.3 A). Otherwise, the object itself and its surface may behave as fractals, in which case the object will correspond to a mass fractal (Fig. 2.3 B). A dense object that has a distribution of holes (pores) with a fractal structure is a pore fractal (Fig. 2.3 C) (Michaels, 2002).

2.2.5 Contact angle measurements

Contact angle measurement is a simple method to determine surface tension. Surface tension reflects the change in surface free energy per unit increase in surface area (Adamson, 1990). Contact angle describes the shape of a liquid drop resting on a solid surface. Contact angles of liquids on different surfaces are used to predict wetting and adhesion properties of these solids by calculating their solid-vapour surface tension. When a drop of liquid is placed on a solid surface and the surface tension of the liquid is larger than the surface tension of the solid, it makes a definite angle of contact between the liquid and the solid phases. By drawing a tangent line from the drop shape to the touch of the solid surface, contact angle is defined as the angle between the tangent line and the solid surface (Figure 2.4).

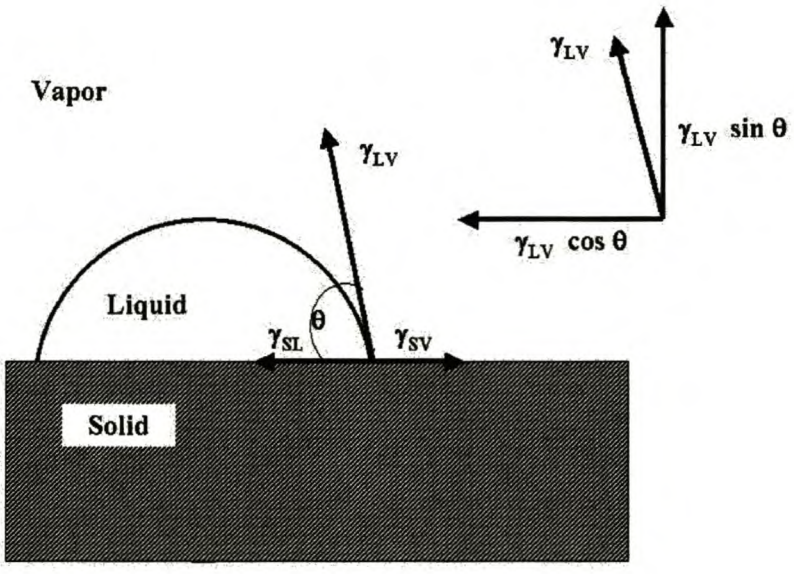

Figure 2.4 Equilibrium contact angle (Adapted from Adamson, 1990).

There is a direct relationship between the contact angle of the droplet and the interfacial tensions of the three phases that was first discovered by the British scientist Thomas Young in 1805 (Young, 1805). The contact angle is governed by the force balance at the three-phase boundary and is defined by Young's equation (Equation 2.1):

$$\gamma_{LV} \cos 0 = \gamma_{SV} - \gamma_{SL} \qquad \text{(Equation 2.1)}$$

where γ_{LV} is surface tension of the liquid in equilibrium with its saturated vapour, γ_{SV} is surface tension of the solid in equilibrium with the saturated vapour of the liquid, and γ_{SL} is the interfacial tension between the solid and the liquid. The theory is based on the equilibrium of an asymmetric sessile drop on a flat, horizontal, smooth, homogeneous, isotropic, and rigid solid surface. The measurement provides information to study the bonding energy of the solid surface and surface tension of the liquid droplet (Israelachvili, 1985). If the same liquid were used, the contact angle would decrease as surface tension of the solid increases as shown in Figure 2.5. Finally, total wetting ($0 = 0$) occurs if the surface tension of the liquid is smaller than that the surface tension of the solid.

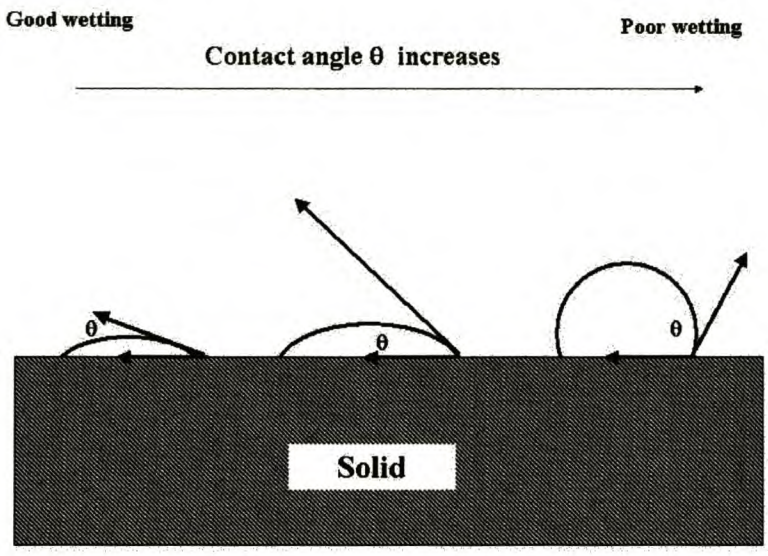

Figure 2.5 Small and large contact angles represent good and poor wetting, respectively (Adopted from Israelachvili, 1985).

The observed range is usually characterised by the measurement of the maximum (advancing angle) and the minimum (receding angle) allowed value. The measured contact angle is higher or lower than the equilibrium contact angle and is commonly called advancing and receding, according to the zone of the shown curve where the system really rests and which depends on the moving direction of the meniscus at its formation.

Applications for contact angle analysis include the analysis and evaluation of biomedical surfaces, chemical formulations, coatings, composite materials, textiles, wood, lotions, oils and soaps in cleanliness and corrosion control. Qian *et al.* (2000) conducted experiments where Barnacle larvae showed the highest settlement in glass tubes (smallest contact angle) and the lowest in Teflon tubes (largest contact angle), while *B. neritina* showed the highest larval settlement in Teflon tubes and the lowest settlement in glass tubes. Their findings concluded that biofilm formation changed the contact angles of all the tubes and the degree of change varied among the tubes. Other studies regarding hydrophobicity and surface charge measurements of several polymeric surfaces relating to specific biofilm characteristics were carried out on *Pseudomonas aeruginosa* (Pasmore *et al.*, 2002). It revealed that cells were most readily removed from the smoothest, most hydrophilic, neutral surfaces.

2.2.6 Initial attachment of microorganisms as first step in biofilm formation

Biofilms are dynamic structures and undergo a developmental process consisting of (i) initial attachment, (ii) microcolony formation, (iii) maturation and (iv) detachment. Adhesion of microorganisms to surfaces involves several steps: (i) transport to the surface, (ii) contact and initial adhesion, (iii) firmer attachment, and then (iv) growth, to form adhering microcolonies or biofilms (Sauer *et al.,* 2002). Despite the great interest in biofilms, little is known about the early stages of biofilm formation. One approach in the prevention of biofilm formation is the prevention of initial microbial adhesion. Microbial adhesion is mediated by specific interactions between cell surface structures and specific molecular groups on the substratum surface (Christensen *et al.*, 1989), or when viewed from an overall, physico-chemical view-point by non-specific interaction forces, including Lifshitz-Van der Waals forces, electrostatic forces, acid-base interactions and Brownian motion forces (Van Oss, 1994). Upon approach of a surface, organisms will be attracted or repelled by the surface, depending on the resultant of the different non-specific interaction forces. Lifshitz-Van der Waals forces and Brownian motion usually promotes adhesion, while electrostatic interactions can be either attractive or repulsive. Most organisms are negatively charged (Dankert *et al.*, 1986) and consequently a negatively charged substratum exerts a repulsive electrostatic force on the organisms. Control of the charge and hydrophobic properties of substratum surfaces is likewise a strategy to influence biofilm interaction with a substratum surface. The findings of Rupp *et al.* (2002) strengthened the hypothesis that the analysis of dynamic changes in wetting tension and wetting tension hysteresis is a sensitive analytical method for the detection of dynamic interfacial changes at biomaterial/bio system interfaces during the initial steps of biofilm.

The initial adhesion is rapid (seconds, minutes) and can be reversible or irreversible. Various groups showed that cells attach to surfaces by a portion of a cell or flagellum during the reversible attachment, after which they may either detach; or irreversibly attach (Meadows, 1971; Lawrence *et al.*, 1987; Power and Marshall, 1988). Lawrence *et al.* (1987) explained that the reason why all cells do not become irreversibly attached could be due to the fact that the cells will firstly evaluate the potential attachment sites chemically through the use of chemoreceptors. Marshall (1988) found that the presence of bound stearic acid determined whether the motile surface-associated phase of *Pseudomonas* JD8 took place. The irreversibly attached bacteria

will then grow and divide. Most data on microbial adhesion have been obtained with bacteria and have shown that adhesion depends on the surface properties of the cells and on their physiological state. The preconditioning of solid surfaces is influenced by both environmental conditions (e.g., pH, temperature) and by the surface itself (e.g., hydrophobicity, surface charge) (Gerson and Zajic, 1979).

E. coli has been found to require flagella and pili to initiate the early attachment processes (Genevaux *et al.*, 1996; Pratt and Kolter, 1998). Type I pili are absolutely essential for the initial attachment event to proceed but do not appear to play a role in moving the bacteria across the surface. The proteinaceous cell surface structures known as curli have also been implicated in early attachment events (Vidal *et al.*, 1998). Morra and Cassinelli (1996) studied the effect of the surface upon adhesion of the bacterium *Staphylococcus epidermis*, implicated in catheter-related urinary tract infections and found that electron donor-acceptor interactions play a large part in the adhesion process. Gorman *et al.* (1997) studied the same bacterium and the influence of the conditioning film upon catheter material, measuring the surface roughness using the AFM. During a scanning electron and AFM study of stainless steel, it was found that surface finishes reduce bacterial attachment and early biofilm formation. These surfaces were sandblasted, sanded and electro polished and the conclusions showed that both physical and electrochemical treatments improved resistance of stainless steel to bacterial attachment (Arnold and Bailey, 2000).

CHAPTER 3: MATERIALS AND METHODS

3.1 Experimental set-up for cultivation of biofilms

A modified Pederson device (Figure 3.1) (McCoy *et al.*, 1981; Pederson, 1982) was installed in a re-circulating loop consisting of a 20L reservoir, a centrifugal pump, and the Pederson device connected with PVC tubing. Tap water was circulated to simulate suitable conditions for biofilm development in a natural environment. The centrifugal pump was used to maintain a constant flow of tap water throughout the duration of these experiments to continuously deliver the water over the test surfaces. The modified Pederson device consisted of a coupon holder with diffusor stabilisers at both ends. In the middle were evenly distributed parallel divisions developed with enough space for 1 mm thick slides to fit into. The slides were standard size microscopic slides (76 X 26 mm).

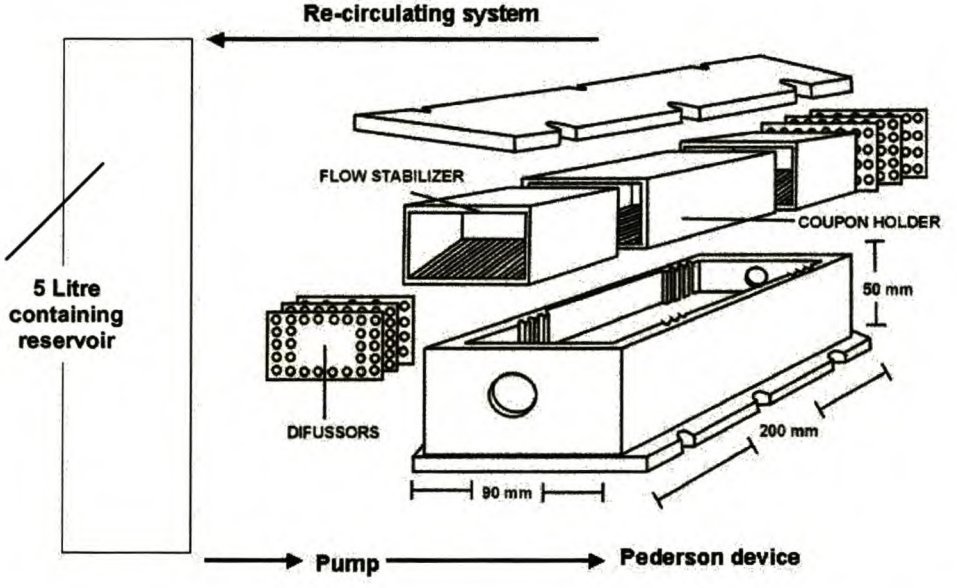

Figure 3.1 Schematic presentation of a modified device used as a system to cultivate the biofilms on slides maintaining a constant flow rate.

PVC (polyvinyl chloride), polished stainless steel (316) and glass microscope slides were used to compare biofilm development on different attachment surfaces. Based on the results from this investigation a model system was selected that would allow primary colonization of these test surfaces. The substrates were cleaned with ethanol before it was carefully placed into the evenly distributed parallel divisions. Within a few days there was evidence of biofilm development. Biofilms were cultivated for a month, and the slides were removed individually at regular intervals of 2 days, 7 days

and 10 days for polished stainless steel and PVC substrates. After 10 days the biofilm surfaces of these test surfaces became too rough for the expansion capabilities of the piezo crystals of the AFM. However, the surface of the biofilm cultivated on the glass substrate was still feasible for AFM imaging after 13 days and samples developed on the glass slides were removed at regular time intervals of 2 days, 7 days, 10 days and 13 days, respectively. Structure characterization and evaluation by means of microscopic techniques (Section 3.5 and Section 3.6) and roughness quantification with statistical methods (Section 3.7) were carried out on all the samples. The results of this preliminary experiment were used as basis for subsequent experiments to cultivate biofilms. The best results were obtained from the biofilms developed on the glass microscope slides (Chapter 4, Section 4.1.1 and 4.2.1). This was confirmed with results from contact angle measurements (Section 4.2.4).

3.2 Determination of contact angles

The experiments were performed using a Cahn microbalance DCA322 that was able to collect data at a speed of 1 Hz. The typical experimental set-up is shown in Fig.3.2. It was composed of a microbalance and a movable stage on which the liquid container is fitted. A computer controlled the stage velocity and movements and provided the software required for calculations. All DCA runs were performed at room temperature (22 ± 2 °C). Ultra pure water (18.5 MW cm produced by a Millipore Milli-Q device) was employed as the measure liquid, using only fresh liquid for each experiment. Receding angles were used for contact angle measurements. The results were described by the following equation:

$$F = F_w + F_{ic} + F_b = mg + \gamma_L p \cos\theta + (x - x_0) Adg \qquad (3.1)$$

where the three contributions to the overall force have been summarized. In equation 3.1, F_w represents the weight contribution (m is the sample mass and g is the local gravity constant), usually zeroed during the calibration routine in the experimental practice, and F_{ic} is the contribution of interfacial energetics, that is the product of the liquid surface tension (γ_l) times the sample perimeter (p) times the cosine of the product of the immersed volume (the stage displacement, x, minus the displacement at

zero depth of immerse, x_0, times the sample area) times the liquid density, d, times g.

The contact angle measurements were obtained at the following settings:

- Surface tension: 72.6 dynes/cm
- Calibration weight: 500.0 mg
- Perimeter: 12.80 mm
- Platform speed: 99.45 microns/sec
- Zero depth immersion at 0.561 mm

Contact angle measurements were determined for all three test substrates that were used for the cultivation of biofilms (PVC, polished stainless steel, and glass).

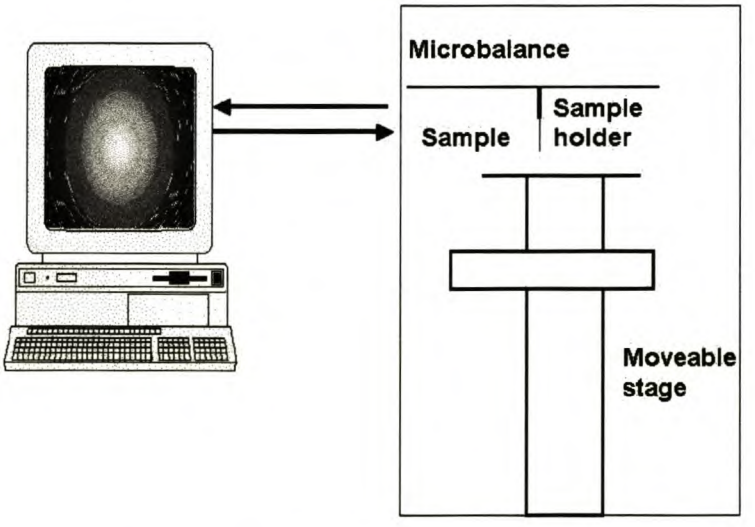

Figure 3.2 The typical experimental set-up for contact angle measurement.

3.3 Biofilm development at different nutrient concentrations

Experiments with different nutrient concentrations were set up with the glass microscope slides as substrates. The glass slides were chosen as substrates based on the preliminary experiment described in Section 3.1. The glass microscope slides used for cultivation were 76 X 26 mm and 1.0/1.2 mm thick. Heterotrophic biofilms were cultivated on the glass surfaces under aerobic conditions at room temperature. The biofilms were cultivated using a batch system. Conventional techniques were applied to prepare different concentrations of tryptic soy broth (TSB) (Difco Co.) solution for

cultivation purposes. The batch culture system was set up by preparing 0.1%, 1% and 10% TSB in a 2 L container. The growth medium was inoculated with 1 ml of tap water containing naturally-occurring microbes. The microscope slides were placed in a Perspex slide holder, which is in essence an open-ended box that allowed free flow of water over the attachment surfaces. The open-ended box was fitted with 12 corresponding grooves in the top lid and bottom portions into which the glass slides were slotted. The outside dimensions of the holder were 82 X 82 X 40 mm. An elastic band was used to keep the top cover on and the glass slides in place. The batch system was placed on a magnetic stirrer, in order to ensure that the growth medium was kept uniformly distributed through the system. The slide holder was suspended in the medium and kept at room temperature (Fig.3.3).

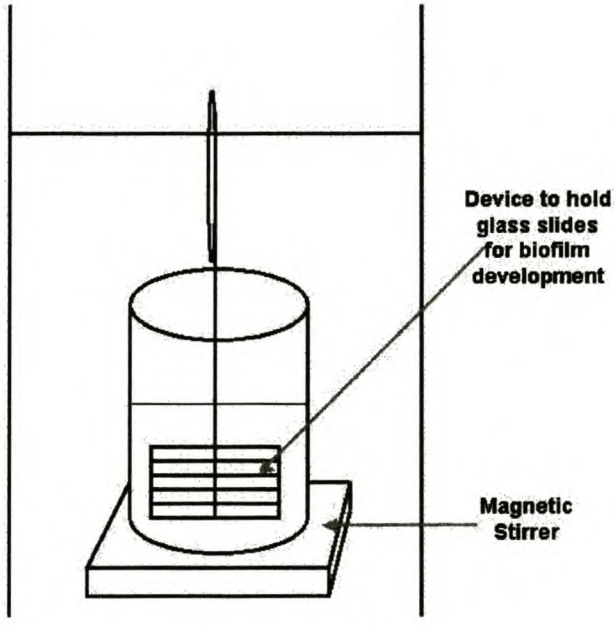

Figure 3.3 Batch culture system with biofilm growth device submerged in media.

Slides were removed daily for a period of 4 days and biofilm formation observed by means of AFM and epifluorescence microscopy.

3.4 Biofilm development at different temperatures

Experiments at different temperatures (8°C, 22°C and 37 °C, respectively) were set up with the glass microscope slides as substrates. The same batch culture setup described in Section 3.3 and Figure 3.3 was used. One percent TSB (Difco Co.) was prepared as

growth medium according to standard microbiological techniques. Inoculation, sampling frequency and microscopic analysis were similar as described in Section 3.3.

3.5 Atomic Force Microscopy

Samples were removed from the experimental set-up described in Section 3.1 at time intervals of 2, 7 and 10 days. For the investigation of biofilm development at different nutrient concentrations (Section 3.3) and different temperatures (Section 3.4), samples were removed at different time periods of 1, 2, 3 and 4 days. AFM images were acquired for biofilm surface characterization with a Topometrix Explorer TMX 2000. Scanning was carried out in non-contact mode (Russell *et al.*, 2001) using an AFM-J piezoelectric long-range dry scanner (130 µm lateral travel, 9.7 µm vertical travel) in ambient air. The scanning of the images was confined to a long-range dry scanner. I-shaped cantilevers were used for scanning. These cantilevers were single-crystal silicon with spring constants in the range of 35-65 N/m^2. The radius of the silicon tip was approximately 20 nm. In non-contact mode the operating set point was approximately 50% of the free-oscillation amplitude. The AFM images consisted of 1000 X 1000 data points. Scan areas of 20 X 20 μm^2, 50 X 50 μm^2 and 100 X 100 μm^2 were obtained for each sample. Analyses of biofilm samples were repeated at least at three different positions on each slide for each biofilm sample.

Biofilm surface characteristics were determined with line profiles (e.g., spatial series) of surface roughness, using Topometrix™ AFM software. Each spatial series of the surface roughness data consisted of 1000 equally spaced points. At least 10 profiles were recorded for each scan. The data was transferred to Excel software as an import file for further analysis. Each of the 10 line profiles was analysed with Benoit™ software (Version 1.3). The analysis with the Benoit™ software is described in Section 3.7.

3.6 Epifluorescence microscopy analysis

Sampling protocol for epifluorescence microscopy was the same as for AFM. The glass slides were cleaned on the one side to allow easier evaluation. On the other side the samples were stained with acridine orange for 10 minutes, after which the probe was gently rinsed off with sterile distilled water. Images of the biofilms were captured using a high performance CCD camera (Cohu) mounted on a Nikon Eclipse E400

epifluorescence microscope, equipped with a 60X/1.4 N.A. oil objective and appropriate filters. For each biofilm development setup, 10 images were randomly captured along the surface of the substrates. The results obtained were the averages of these experiments. The images were quantified by statistical methods as described in Section 3.8.

3.7 Statistical analysis of biofilm images obtained by AFM

The surface roughness calculations of the biofilms were determined with Benoit™ software by analysing the AFM images (Bitmap colour) as well as using Topometrix™ software to determine roughness values for the same images. Surface roughness quantification of the biofilm surface was determined by calculation of Hurst exponent, which is directly related to fractal dimension. The relationship between the fractal dimension, D, and the Hurst exponent, H, is $D = 2 - H$.

Hurst exponent was determined through the following methods performed by Benoit™ software: 1) power spectrum, 2) variogram and 3) wavelet analyses. For a self-similar profile the ratio between its vertical and horizontal ranges remain constant. Topometrix™ software (Version 3.2.02) was also used to determine fractal dimension. The following sections (3.7.1 – 3.7.3) were adapted from the Benoit™ software (Version 1.3) manual.

3.7.1 Power Spectrum

To obtain an estimate of fractal dimension, the power spectrum $P(k)$, where $k = {}^{2p}/_{l}$ is the wave number and l is the wavelength, is firstly obtained. The logarithm of $P(k)$ is then plotted versus the logarithm of k. If this trace is self-affine[1], this plot should follow a straight line with a negative slope $-b$. This exponent is related to the fractal dimension D_s as follows:

$$D_s = \frac{5-b}{2} \qquad \text{(Equation 3.2)}$$

where D_s denotes the fractal dimension estimated from the power spectrum.

[1] A series that scales time and distance by different factors.

3.7.2 Variogram

The variogram is defined as the expected value of the squared difference between two y values in a trace separated by a distance w. The sample variogram $V(w)$ of a series $y(x)$ is measured as follows:

$$V(w) = [y(x) - y(x+w)]^2 \qquad \text{(Equation 3.3)}$$

$V(w)$ is the average value of the squared difference between pairs of points at distance w. If a length span equal to w is taken, the value of the difference between $y(w)$ and $y(0)$ will be normally distributed with a variance $s(w)^2$ (where s=standard deviation) that is proportional to w^2H:

$$V(w) \approx w^{2H} \qquad \text{(Equation 3.4)}$$

To obtain the estimate of H, the average squared difference between all the pairs of points separated by a distance w is calculated as $V(w)$ in equation 3.3 for a number of window lengths, and the logarithms of $V(w)$ are plotted versus the logarithm of w. The fractal dimension of the trace can then be calculated from the relationship between the Hurst exponent H and the fractal dimension D_v:

$$D_v = 2 - H \qquad \text{(Equation 3.5)}$$

where D_v denotes the fractal dimension estimated from the variogram.

3.7.3 Wavelet

Wavelet analysis is a tool for analysis of localized variations in power b decomposing a trace into time frequency space to determine both the dominant modes of variability and how these modes vary in time. This method is appropriate where the variance does not remain constant with increasing length of the data set.

For n wavelet transforms each with a difference scaling coefficient a_i, where $S_1, S_2, ..., S_n$ are the standard deviations from zero of the respective scaling coefficients a_i, the ratio of the standard deviations $G_1, G_2, ..., G_n - 1$ are defined as:

$$G_1 = S_1/S_2, G_2 = S_2/S_3, ..., G_{n-1} = S_n - 1/S_n \qquad \text{(Equation 3.6)}$$

The average of the value of G_i is estimated as:

$$G_{avg} = \frac{\sum_{i=1}^{n-1} G_i}{n-1} \qquad \text{(Equation 3.7)}$$

The analyses (3.7.1-3.7.3) were performed on AFM images of scan areas 20μm×20μm, 50μm×50μm and 100μm×100μm, respectively. Each AFM image was analysed along ten line profiles, randomly selected. The average of these 10 line profiles for power spectrum, variogram and wavelet analysis was calculated, as well as the percentage deviation for each analysis. This methodology of using line profiles makes it possible to analyse AFM images containing artifacts, as the parts of the image containing artifacts can manually be avoided. The results obtained by these statistical methods are displayed in Tables 5.1-5.9. The results of the variables quantified by the Topometrix™ software are displayed in Tables 4.1-4.3.

3.7.4 Average roughness[2] and fractal dimension[3] determined by Topometrix™ software

The standard roughness average is the arithmetic average of the absolute values of the measured profile height deviations (Equation 3.8).

$$R_a = \frac{1}{n}\sum_{i=0}^{N}\left|Z_i - \overline{Z}\right| \qquad \text{(Equation 3.8)}$$

where n is the total number of points in the image matrix. Z_i is the height of the i-th point, which can be represented as follows:

$$\overline{Z} = \frac{1}{n}\sum_{i=0}^{N} Z_i \text{ (Average height)} \qquad \text{(Equation 3.9)}$$

The standard roughness average was used in the AFM software of Topometrix TMX 2000 AFM. This software was also used to calculate the fractal dimension as determined with the lake-filling method. In a similar way to that reported by Mandelbrot for earth coastlines, lake patterns are generated by computer simulation.

[2] Description of algorithm is according to method used by AFM software of Topometrix.
[3] Description of algorithm is according to method used by AFM software of Topometrix.

Surface topography was filled by "water" up to a given level. By using threshold detection and optimal connectivity checking algorithms, individual voids filled with "water" were isolated. The perimeter of the "lakes", defined as the number of "water" pixels on the digitized grid having non-"water" neighbours and their area, defined as the number of "water" pixels for a given void, were measured. The number of "lakes" counted at different height values is constructed into a graph from which the fractal value is derived.

3.8 Statistical analysis of biofilm images obtained by epifluorescence microscopy[4]

Benoit™ software was used for fractal dimension calculations of the biofilms. At least 10 images were analysed in each case, for: 1) box dimension, 2) perimeter-area dimension, 3) information dimension, 4) mass dimension and 5) ruler dimension analyses. Although all these self-affine methods were tested, only the box dimension method gave realistic fractal dimension values. The self-affine profile is such that the ratio between its vertical and horizontal ranges varies with scale.

The biofilm development was compared on different types of substrate, at different temperatures and in different nutrient concentrations. The average of 10 images for each condition was calculated, as well as the percentage deviation for each analysis. The results obtained by these statistical methods are displayed in Tables 5.7-5.9. The following sections (3.8.1 – 3.8.5) were adapted from the Benoit™ software (Version 1.3) manual.

3.8.1 Box Dimension

The box dimension is defined as the exponent D_b in the relationship:

$$N(d) \approx 1/d^{D_B} = d^{-D_B} \qquad \text{(Equation 3.10)}$$

where $N(d)$ is the number of boxes of linear size d necessary to cover a data set of points distributed in a two-dimensional plane. Equation 3.2 defines the dimension of objects that are Euclidean. A number of boxes proportional to $1/d$ is needed to cover a

[4] The description of the method as described by Benoit software

set of points lying on a smooth line, proportional to $1/d^2$ to cover a set of points evenly distributed on a plane. This dimension is sometimes called grid dimension, because the boxes are usually part of a grid. The boxes are placed at any position and orientation to minimize the number of boxes needed to cover the set. To measure D_b, the number of boxes of linear size d necessary to cover a set for a range of values of d, is counted. The logarithm of $N(d)$ is plotted on the vertical axis versus the logarithm of d on the horizontal axis. If the set is fractal, this plot will follow a straight line with a negative slope that equals $-D_b$. Box sizes d that follow a geometric progression e.g., d=1, 2, 4, 8 is chosen to obtain points that are evenly distributed in log-log space. For each box size the grid should be overlaid in such a way that the minimum number of boxes is occupied. The grid for each box size is rotated 90 degrees and the minimum value of $N(d)$ is plotted.

3.8.2 Perimeter Area Dimension

For this method the pattern must be a closed loop, in a two-dimensional plane, like an island. If this island is Euclidean, i.e. a circle, the area A and the perimeter P are related as follows:

$$P = 2\pi r = r\sqrt{\pi A} \approx \sqrt{A}$$

$$A = \pi r^2 = \frac{P^2}{4\pi} \approx P^2 \qquad \text{(Equation 3.11)}$$

where r is the radius of the circle. The proportionality between A and P does not depend on r. If the island had a fractal perimeter, the relationship becomes

$$P \approx \left(\sqrt{A}\right)^{D_P} = A^{D_P/2}$$

$$A \approx P^{2/D_P} \qquad \text{(Equation 3.12)}$$

where D_p is the perimeter-area dimension. If D_p=2, then the figure is space filling. If D_p is between 1 and 2, equation 3.4 shows that the perimeter of the fractal figure is longer than the perimeter of a Euclidean figure with the same area. Perimeter P and

area A with boxes of different size length d are measured to estimate D_p. The logarithm of A is plotted versus the logarithm of P on the horizontal axis. If the relationship is fractal this plot will follow a straight line with a positive slope that equals $2/D_p$.

3.8.3 Information Dimension

The information dimension effectively assigns weights to the boxes in such a way that boxes containing a greater number of points count more than boxes with less points. The information entropy $I(d)$ for a set of $N(d)$ boxes of linear size d is defined as

$$I(d) = -\sum_{i=1}^{N(d)} m_i \log(m_i) \qquad \text{(Equation 3.13)}$$

where m_i is:

$$m_i = \frac{M_i}{M} \qquad \text{(Equation 3.14)}$$

where M_i is the number of points in the i-th box and M is the total number of points in the set. For a set of points composing a smooth line, we could find

$$I(d) \approx -\log(d) \qquad \text{(Equation 3.15)}$$

Therefore, the information dimension D_i could be defined as:

$$I(d) \approx -D_i \log(d) \qquad \text{(Equation 3.16)}$$

To measure D_i the set with boxes of linear size d is covered keeping track of the mass m_i in each box and the information entropy $I(d)$ from the summation in equation 3.5 is calculated. If the set is fractal, a plot of $I(d)$ versus the logarithm of d will follow a straight line with a negative slope equal to $-D_i$.

3.8.4 Mass Dimension

For a circle of radius r drawn on a data set of points distributed in a two-dimensional plane, the number of points in the set that are inside the circle can be counted as

$M(r)$. If there are M points in the whole set, the "mass" $m(r)$ in the circle of the radius can be defined as:

$$m(r) = \frac{M(r)}{M} \qquad \text{(Equation 3.17)}$$

For a smooth line or a uniformly distributed plane, the mass within the circle of the radius r will be proportional to r and r^2 respectively. The mass dimension D_m can be defined as the exponent in the following relationship:

$$m(r) \approx r^{D_m} \qquad \text{(Equation 3.18)}$$

The mass $m(r)$ in circles of increasing radius starting from the center of the set can be measured, and the logarithm of $m(r)$ can be plotted versus the logarithm of r. If the set is fractal, the plot will follow a straight line with a positive slope equal to D_m.

3.8.5 Ruler Dimension

The ruler dimension D_r is defined as:

$$N(d) \approx d^{-D_r} \qquad \text{(Equation 3.19)}$$

where $N(d)$ is defined as the number of steps taken by walking a divider (ruler) of length d on the line. The basis of this method is that if the line is Euclidean, $D_r = 1$, then the length of the line will be a constant independent of d. To obtain D_r in practice, the number of steps $N(d)$ taken by walking a divider (ruler) of length d on the line is counted and the logarithm of $N(d)$ versus the logarithm of d. If the line is fractal, this plot will follow a straight line with a negative slope that equals $-D_r$.

CHAPTER 4: RESULTS AND DISCUSSION

4.1 Characterization of biofilm surface profiles by AFM

4.1.1 Effect of surface type

AFM images of biofilms cultivated on PVC, glass and polished stainless steel are shown in Fig. 4.1, 4.3 and 4.5, respectively. The average roughness of 10 line profiles was determined for each scan (Fig. 4.2, 4.4 and 4.6) by using Topometrix software. Visually, the number of cells on the surfaces appeared to increase over time. Consequently there was a gradual increase in the fractal dimension values for the scan ranges, and the values were higher after ten days than the values after two days (Table 4.1). In contrast, the average roughness and average height values did not show similar trends. Instead, the values showed a large degree of fluctuation. These observations suggest that fractal dimensions provide a more realistic description of the early stages of biofilm development than average height and average roughness measurements. Typical roughness profiles of biofilms can be seen in the line analysis plots (Fig. 4.2). The selected line profiles indicate the arrangement and number of cells developing over time. The profiles for the three-dimensional surface images of the surface of the biofilm cultivated on PVC suggested more EPS development than that developed on the glass substrate (Fig. 4.4). The glass substrate showed single cells on day 2 and after 13 days cells could still be distinguished. The substrate surface appeared flat with only the cells protruding (Fig. 4.3). On the contrary, the PVC substrate appeared notably different with more EPS (Fig. 4.1). There did not seem to be an increase in the number of cells over time, because the EPS layer disguised the visible cells that developed on the PVC. No cell counts have been made, and locally there must have been an increase in cell number.

The average roughness increase for the biofilms cultivated on glass was gradual, which made obtaining viable samples for AFM imaging possible even after 13 days of development. According to investigations by Pringle and Fletcher (1986), a glass substrate revealed better wetting and thus a higher hydrophobicity compared to the other substrate surfaces, which caused a reduction and delay of bacterial adherence, but over time the attachment became stronger. The development of colonies (Fig. 4.3) on the glass was slower than the development on the PVC substrate (Fig. 4.1), and this steady increase proved glass to be a better substrate for studies of initial biofilm development.

The biofilms on the polished stainless steel (Fig. 4.5) were characteristic of a very rough surface area, primarily revealing the surface features of the polished stainless steel substrate. The surface roughness profiles of the polished stainless steel substrates can be seen in the line analysis plot Fig. 4.6. These can be described as very rough with large variations in peak-valley distances. These profiles are probably not a clear indication of the development of the biofilms, because visually the images do not reveal colony development. Three-dimensional surface images did not reveal any cells except for the one or two on the 400 μm^2 and 2 500 μm^2 scan areas of day 2 (Fig. 4.5 and 4.6). Similar findings were made in previous studies. Arnold and Bailey (2000) showed that biofilm development was lower on modified stainless steel compared to unmodified surfaces. During their SEM and AFM study of stainless steel, it was found that surface finishes reduce bacterial attachment and early biofilm formation.

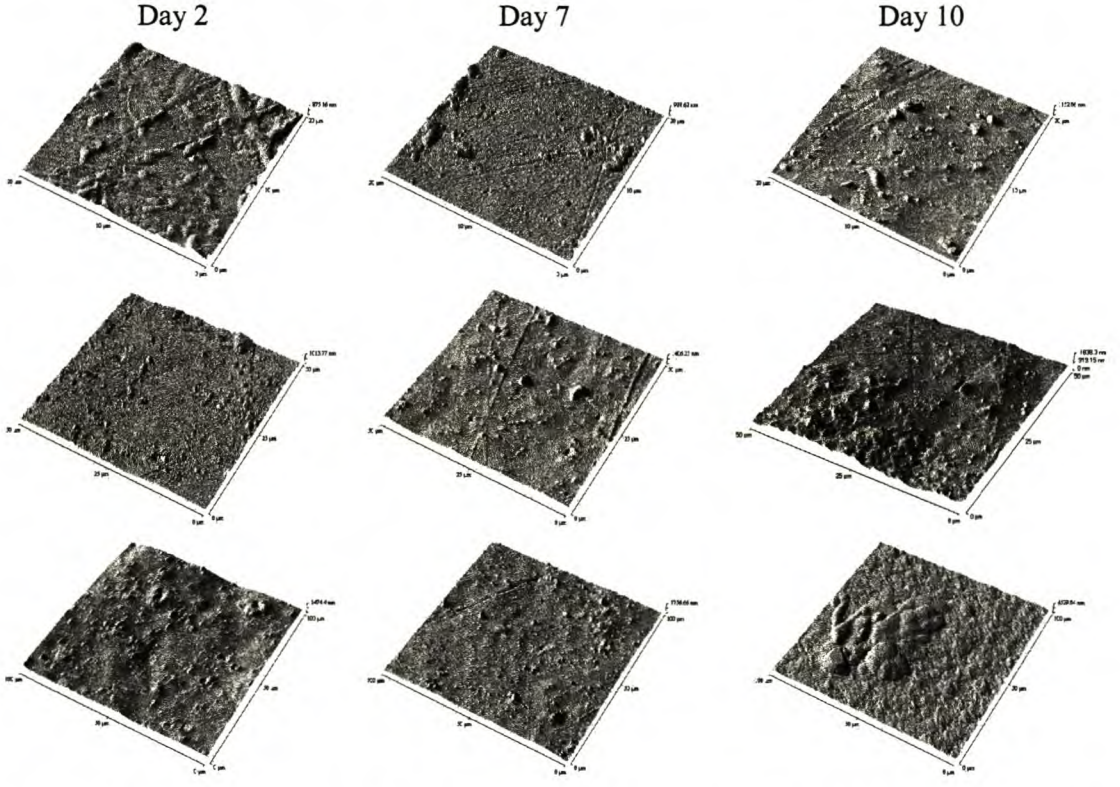

Figure 4.1 Three-dimensional AFM surface images (400 μm^2, top row; 2 500 μm^2, middle row and 10 000 μm^2, bottom row) of biofilms cultivated on a PVC substrate in a modified Pederson device after 2, 7 and 10 days, respectively.

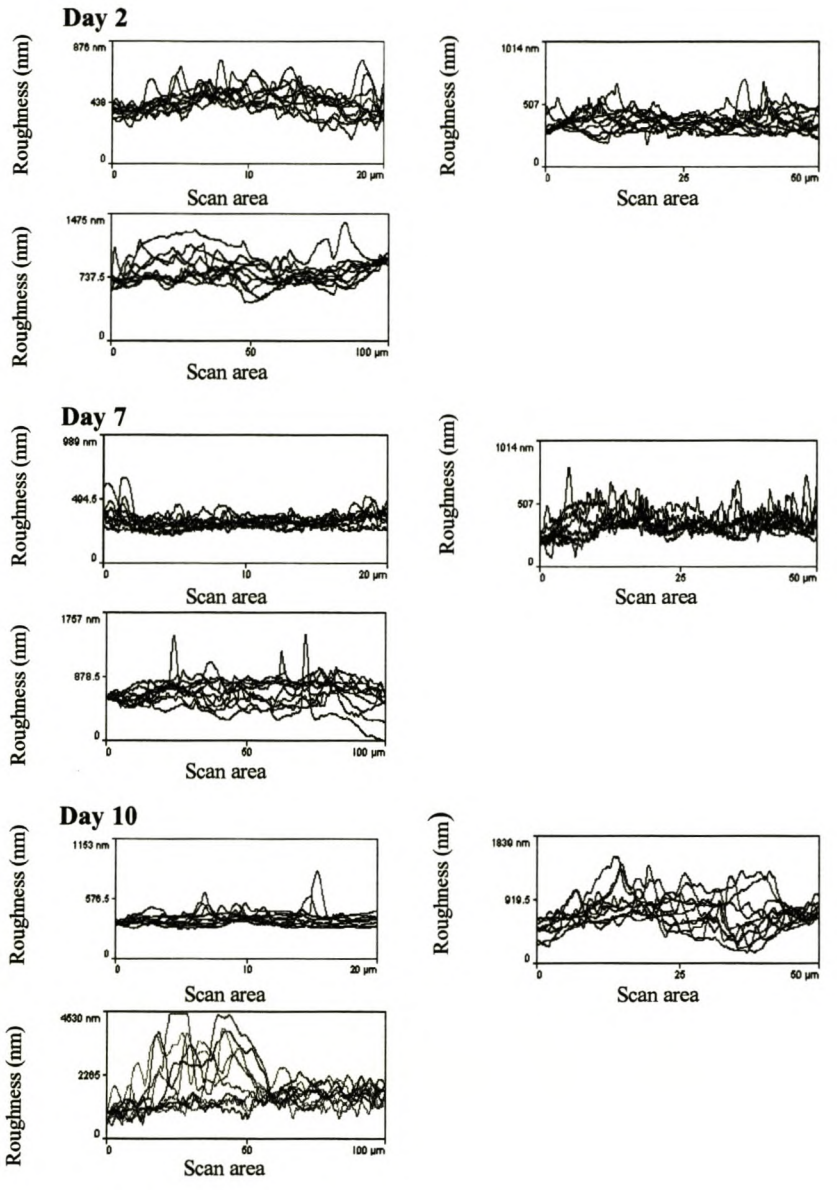

Figure 4.2 Line analysis plots (400 µm^2; 2 500 µm^2; 10 000 µm^2) of the surface roughness of biofilms cultivated on a PVC substrate in a modified Pederson device. Note the difference in scale on the vertical axis.

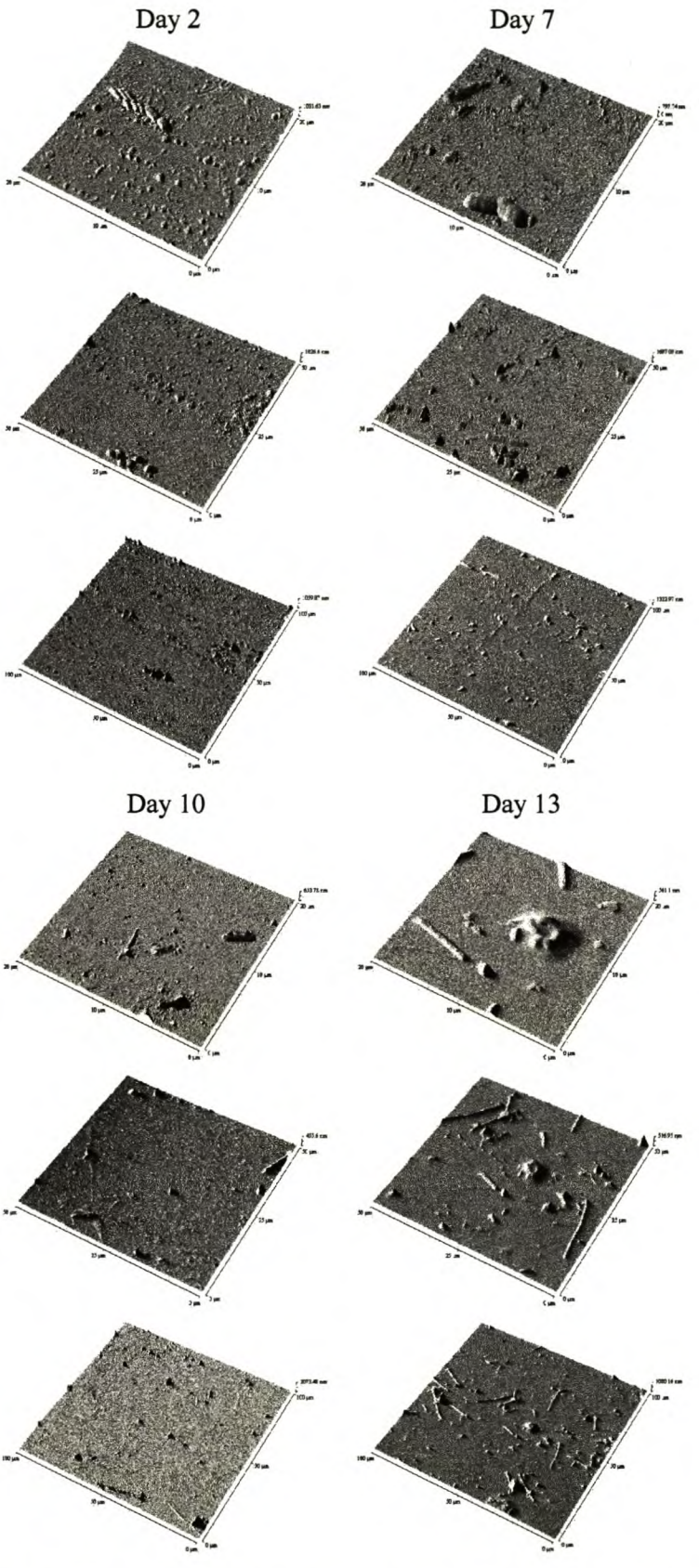

Figure 4.3 Three-dimensional AFM surface images (400 μm^2, top row; 2 500 μm^2, middle row and 10 000 μm^2, bottom row) of biofilms cultivated on a glass substrate in a modified Pederson device after 2, 7, 10 and 13 days, respectively.

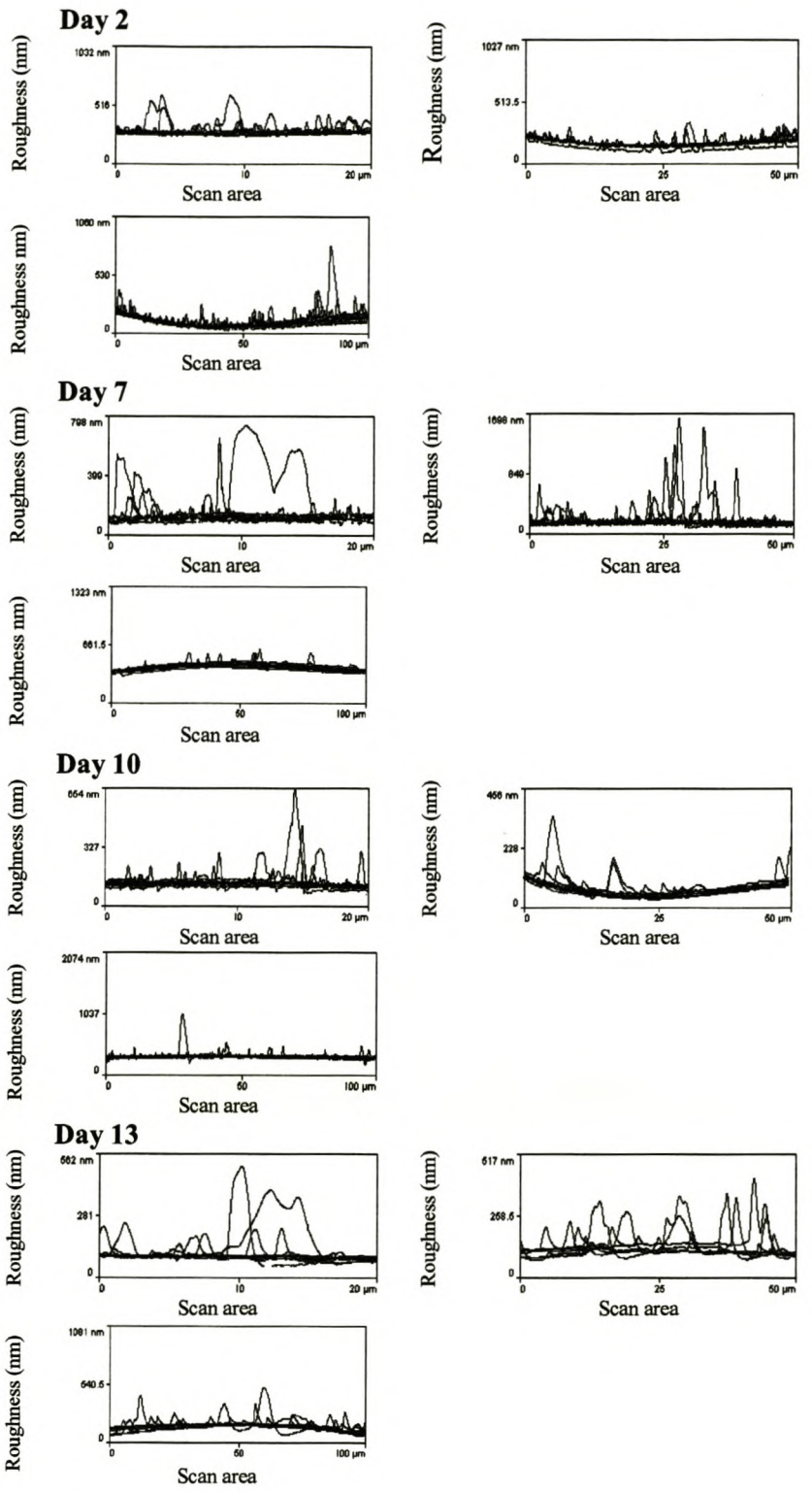

Figure 4.4 Line analysis plots (400 µm^2; 2 500 µm^2; 10 000 µm^2) of the surface roughness of biofilms cultivated on a glass substrate in a modified Pederson device.

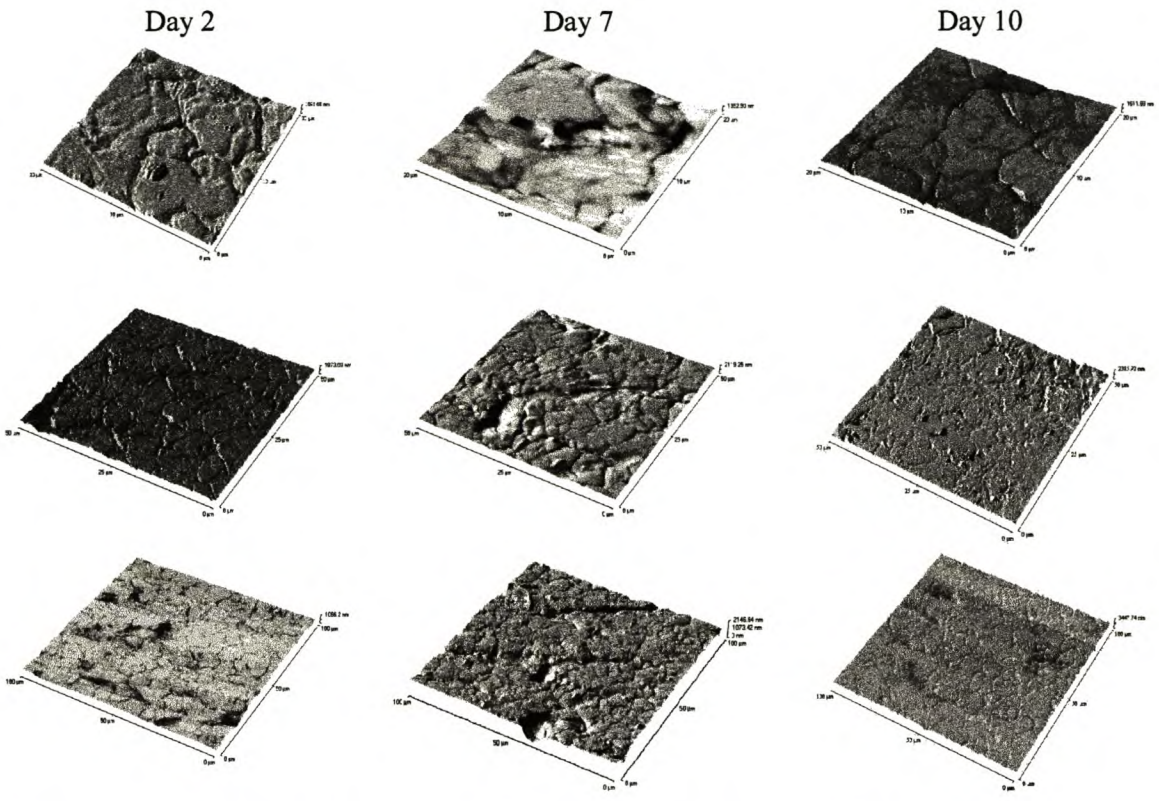

Figure 4.5 Three-dimensional AFM surface images (400 μm^2, top row; 2 500 μm^2, middle row and 10 000 μm^2, bottom row) of biofilms cultivated on polished stainless steel substrate in a modified Pederson device.

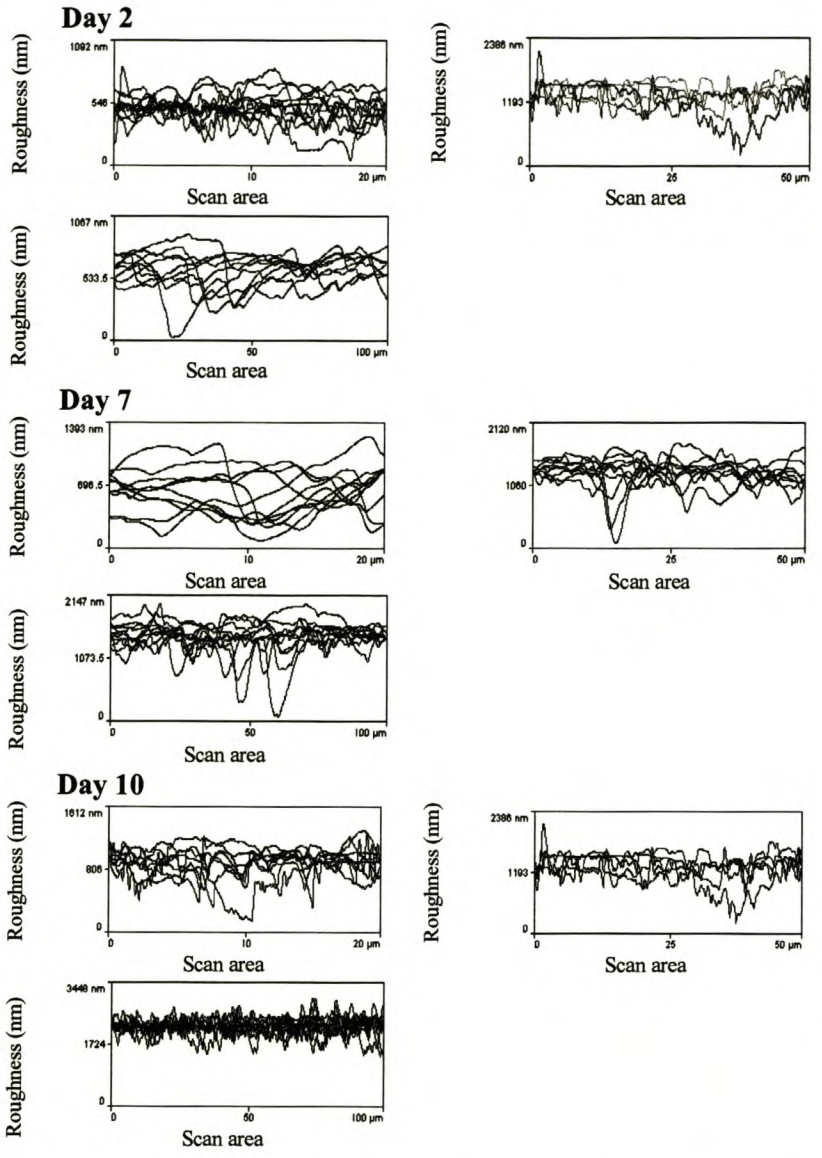

Figure 4.6 Line analysis plots (400 µm^2; 2 500 µm^2; 10 000 µm^2) of the surface roughness of biofilms cultivated on a polished stainless steel substrate in a modified Pederson device.

Table 4.1 Results of AFM images for the scan area 400 μm^2, 2 500 μm^2 and 10 000 μm^2 of biofilms cultivated on PVC, glass and polished stainless steel substrates respectively for varying periods of time. *Values in brackets represent percentage standard deviation (%).*

Substrate	Days	Average Roughness (nm)	Average Height (nm)	Fractal
400 μm^2: PVC	2	61.19 *(14)*	682.76 *(14)*	1.31 *(33)*
	7	37.71 *(22)*	722.44 *(21)*	1.38 *(37)*
	10	34.91 *(38)*	570.50 *(31)*	1.46 *(33)*
Glass	2	21.15 *(67)*	340.28 *(31)*	1.44 *(28)*
	7	38.34 *(136)*	401.99 *(41)*	1.50 *(27)*
	10	14.10 *(80)*	312.23 *(38)*	1.61 *(20)*
	13	30.57 *(114)*	255.60 *(60)*	1.75 *(27)*
Polished Stainless Steel	2	78.99 *(36)*	737.94 *(18)*	1.38 *(32)*
	7	119.49 *(46)*	1073.03 *(8)*	1.32 *(33)*
	10	161.39 *(47)*	1159.80 *(14)*	1.41 *(27)*
2 500 μm^2: PVC	2	66.84 *(19)*	731.04 *(9)*	1.16 *(23)*
	7	73.09 *(28)*	876.02 *(14)*	1.49 *(25)*
	10	165.64 *(31)*	1176.36 *(15)*	1.70 *(30)*
Glass	2	21.86 *(22)*	213.58 *(21)*	1.36 *(24)*
	7	53.19 *(75)*	883.96 *(75)*	1.39 *(18)*
	10	6.87 *(32)*	132.65 *(32)*	1.56 *(24)*
	13	6.65 *(58)*	123.75 *(34)*	1.73 *(18)*
Polished Stainless Steel	2	128.93 *(49)*	1390.47 *(19)*	1.20 *(33)*
	7	133.08 *(33)*	1834.09 *(12)*	1.37 *(27)*
	10	139.66 *(44)*	1507.62 *(4)*	1.41 *(28)*
10 000 μm^2: PVC	2	82.78 *(30)*	929.55 *(30)*	1.35 *(28)*
	7	87.53 *(22)*	1106.63 *(29)*	1.50 *(31)*
	10	487.17 *(42)*	2870.00 *(46)*	1.58 *(22)*
Glass	2	37.16 *(35)*	334.15 *(57)*	1.43 *(27)*
	7	26.29 *(17)*	491.97 *(13)*	1.50 *(28)*
	10	27.10 *(25)*	291.16 *(46)*	1.51 *(32)*
	13	27.50 *(24)*	294.87 *(42)*	1.66 *(26)*
Polished Stainless Steel	2	97.87 *(22)*	804.88 *(35)*	1.34 *(30)*
	7	148.09 *(40)*	1766.59 *(12)*	1.06 *(34)*
	10	140.78 *(35)*	2160.59 *(6)*	1.50 *(18)*

4.1.2 Effect of temperature

Biofilms were allowed to develop on a glass substrate at 8°C, 22°C and 37°C, respectively. The growth behaviour of the biofilms investigated by Witten et al. (1981) was fast and dense at higher temperatures and became slow and dispersed at lower temperatures. In the present study the same growth behaviour was shown at 8°C (Fig. 4.7) and 22°C (Fig. 4.9), the lower temperatures, respectively, and at 37°C (Fig. 4.11), the higher temperature. Similar to the results obtained for different substrates (Section 4.1.1) average roughness and average height values did not support these visual observations (Fig. 4.8; 4.10; 4.12). For example, the scan range of 2 500 μm^2 displayed decreases from 31.51 nm to 11.47 nm in average roughness values and the corresponding average height values increased from 129.76 nm to 174.53 nm (Table

4.2) during development at 8°C. At this temperature, the surface structure of the biofilms is characteristic of one or two cells after one day to a few sparsely distributed cells after four days. The surface roughness profile of typical biofilms developed at 8°C is shown as line analysis plots in Fig. 4.8. The 10 000 μm^2 area line plots consisted of slightly more clusters after four days revealing an average of two clusters at day two and eight clusters at day four. Profiles of the biofilms at 22°C (Fig. 4.10) revealed varying amounts of clusters over time, ranging from ±14, 21, 25 and 14 clusters respectively for day one to day four. The surface roughness profiles of these biofilm depositions revealed a fractal landscape covered with tiny bumps close to the second dimension (values between 1 and 2) (Table 4.2). As time progressed, the microorganisms became evenly distributed across the substrate and some formed microcolonies (Fig. 4.9). The surface roughness values at 37°C were higher than those obtained from the biofilms developed at 8°C and 22°C. After 4 days most of the surface had been colonized by rod-shaped cells with a dense distribution. In the 10 000 μm^2 plots, there were already ±19 clusters after day one with too many to distinguish after day three and day four (Fig. 4.12). Comparison of fractal dimension values suggested an increase in the three-dimensional space occupied by biofilms (Table 4.2).

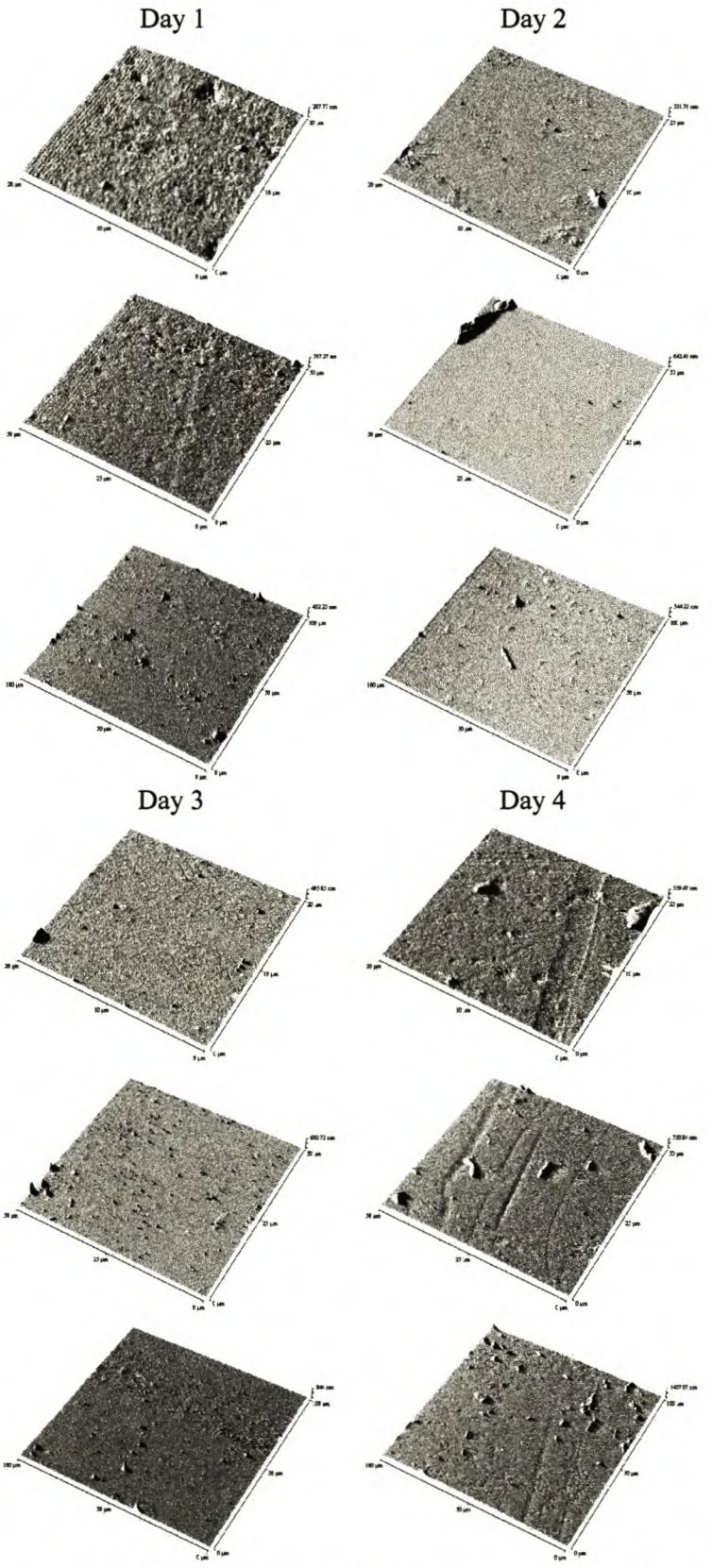

Figure 4.7 Three-dimensional AFM surface images (400 μm^2, top row; 2 500 μm^2, middle row and 10 000 μm^2, bottom row) of biofilms cultivated on a glass substrate at 8°C.

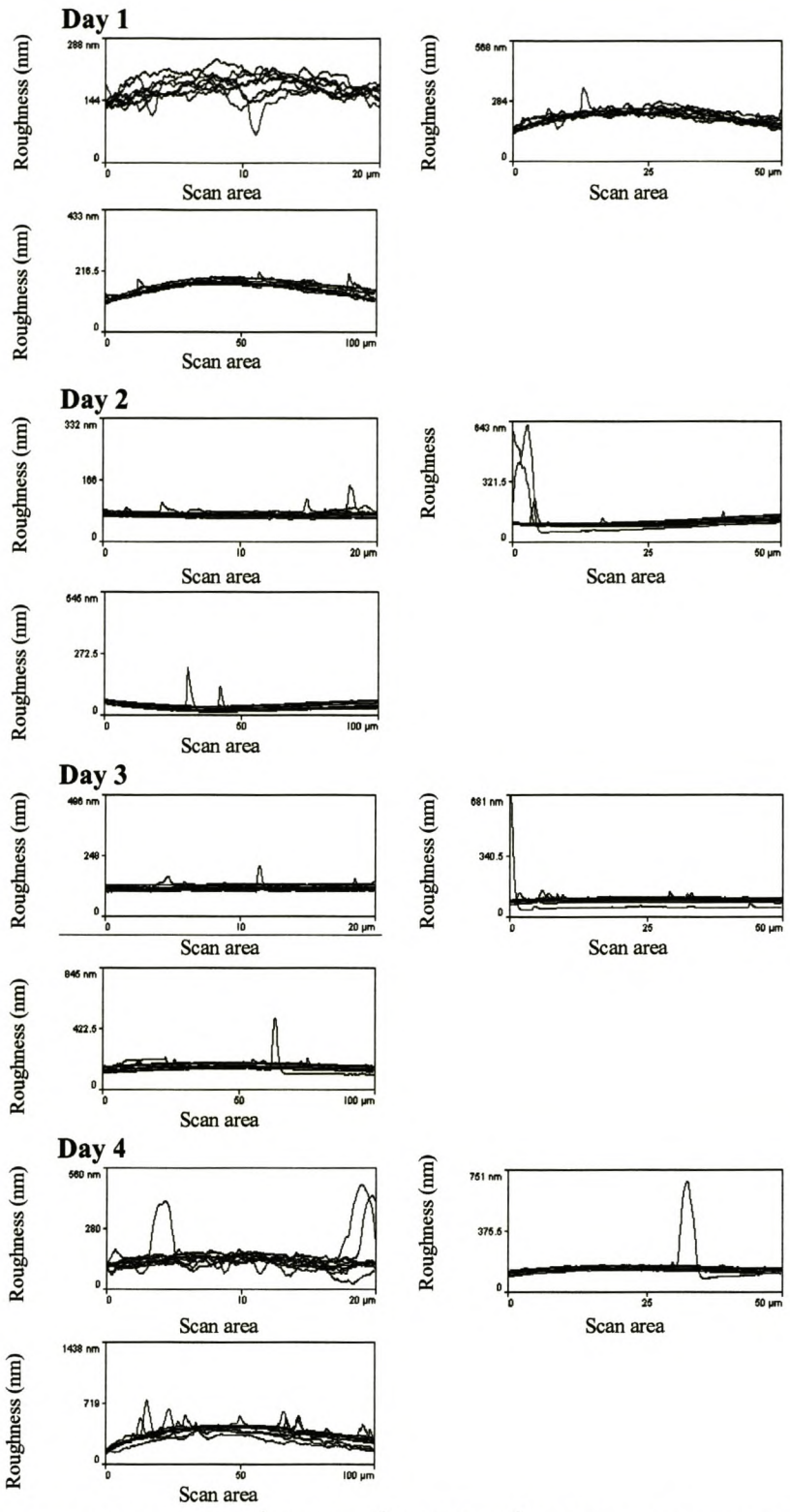

Figure 4.8 Line analysis plots (400 µm^2; 2 500 µm^2; 10 000 µm^2) of the surface roughness of biofilms cultivated on a glass substrate at 8°C.

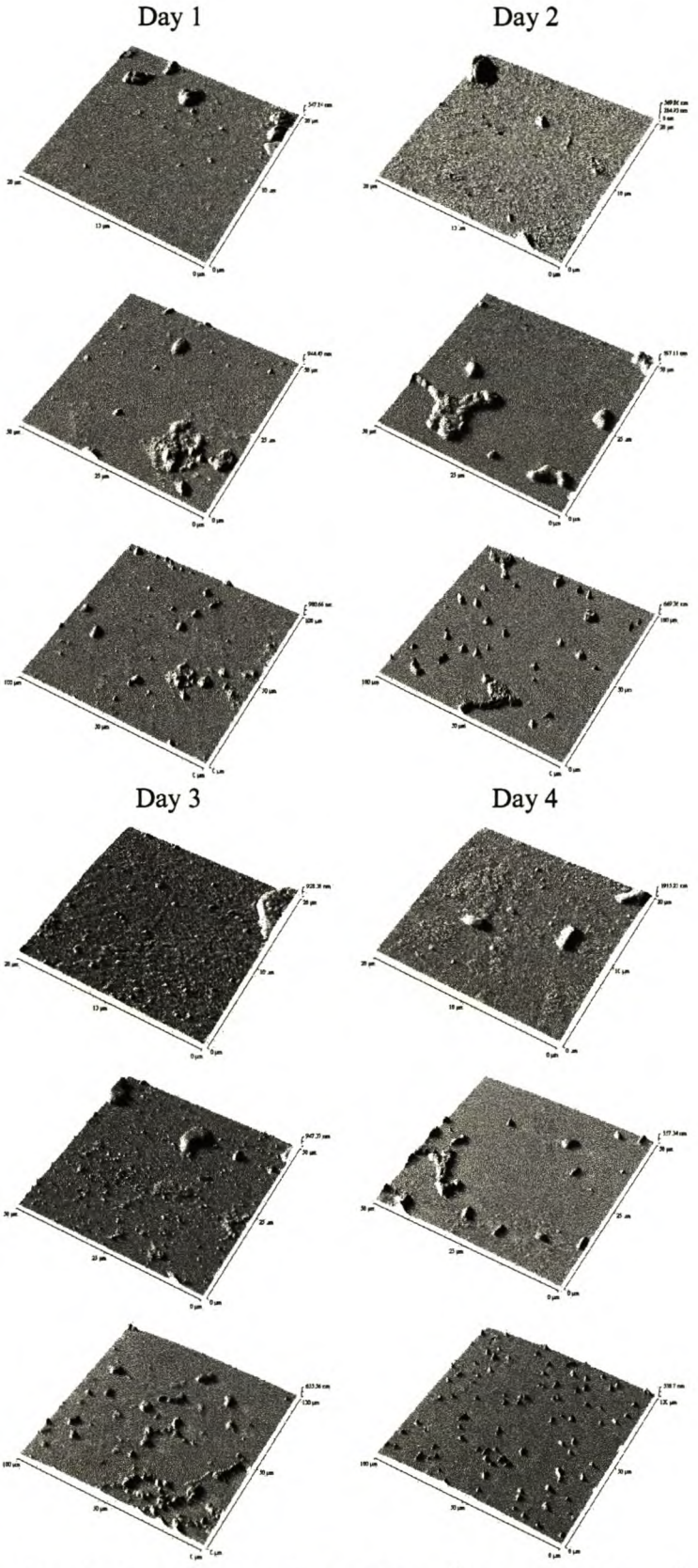

Figure 4.9 Three-dimensional AFM surface image (400 μm^2, top row; 2 500 μm^2, middle row and 10 000 μm^2, bottom row) of biofilms cultivated on glass substrate at 22°C.

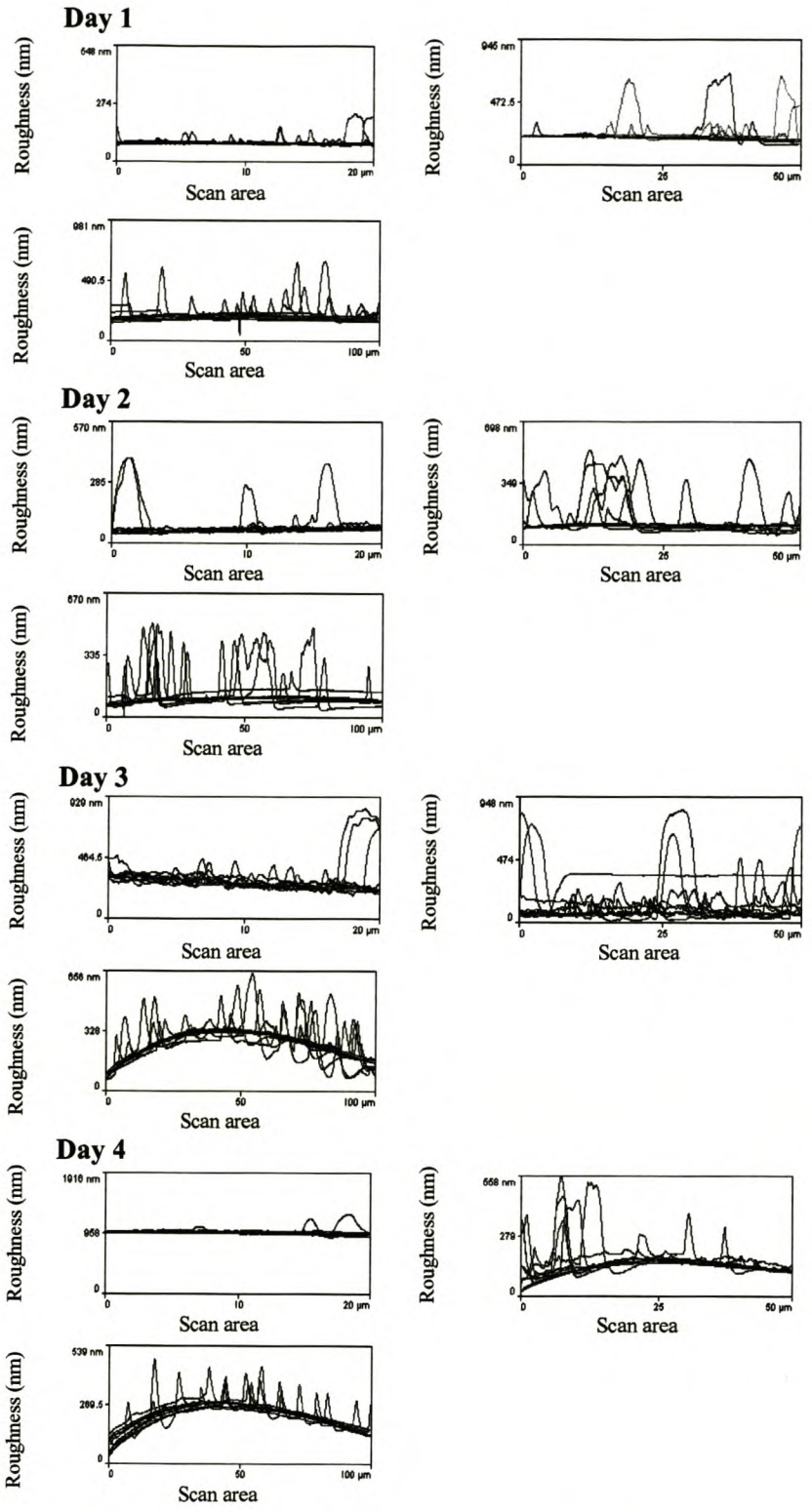

Figure 4.10 Line analysis plots (400 µm^2; 2 500 µm^2; 10 000 µm^2) of the surface roughness of biofilms cultivated on glass substrate at 22°C.

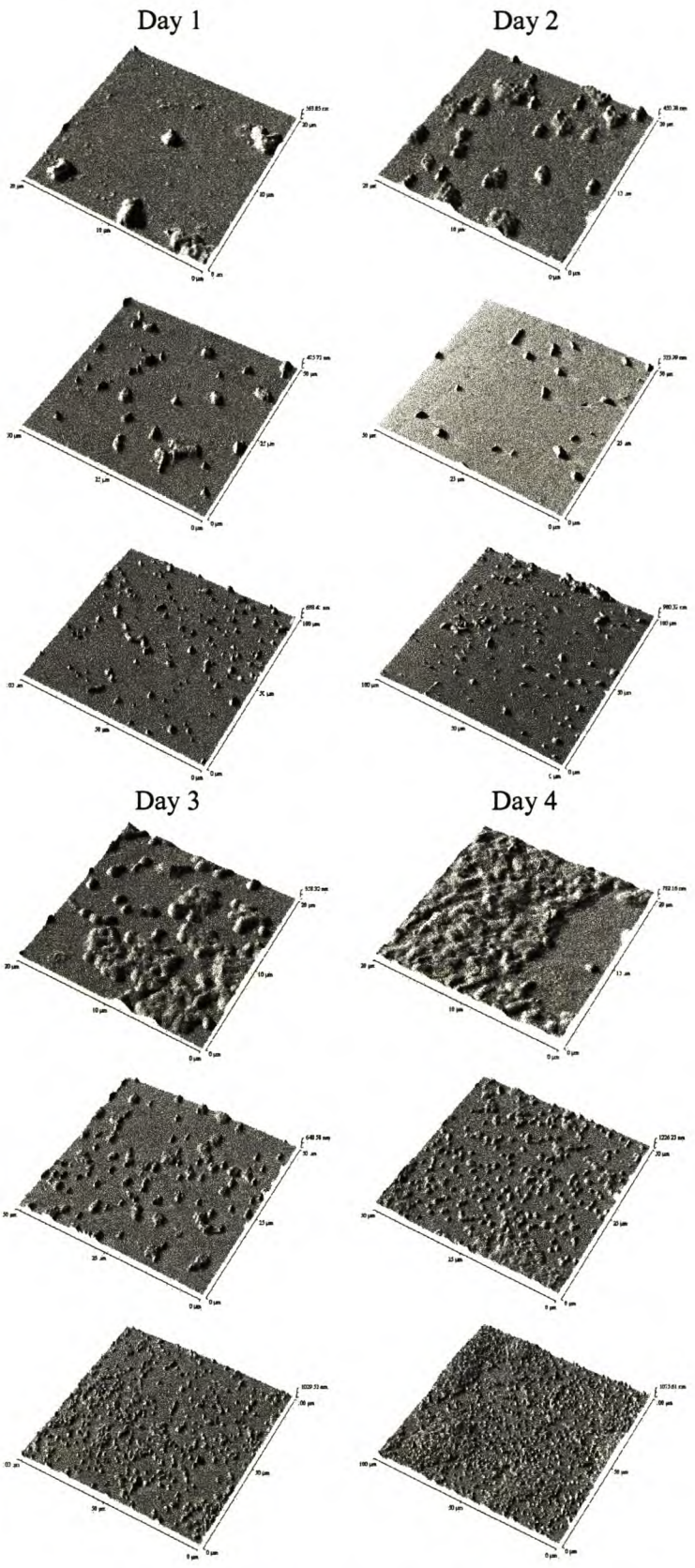

Figure 4.11 Three-dimensional AFM surface images (400 μm^2, top row; 2 500 μm^2, middle row and 10 000 μm^2, bottom row) of biofilms cultivated on a glass substrate at 37°C.

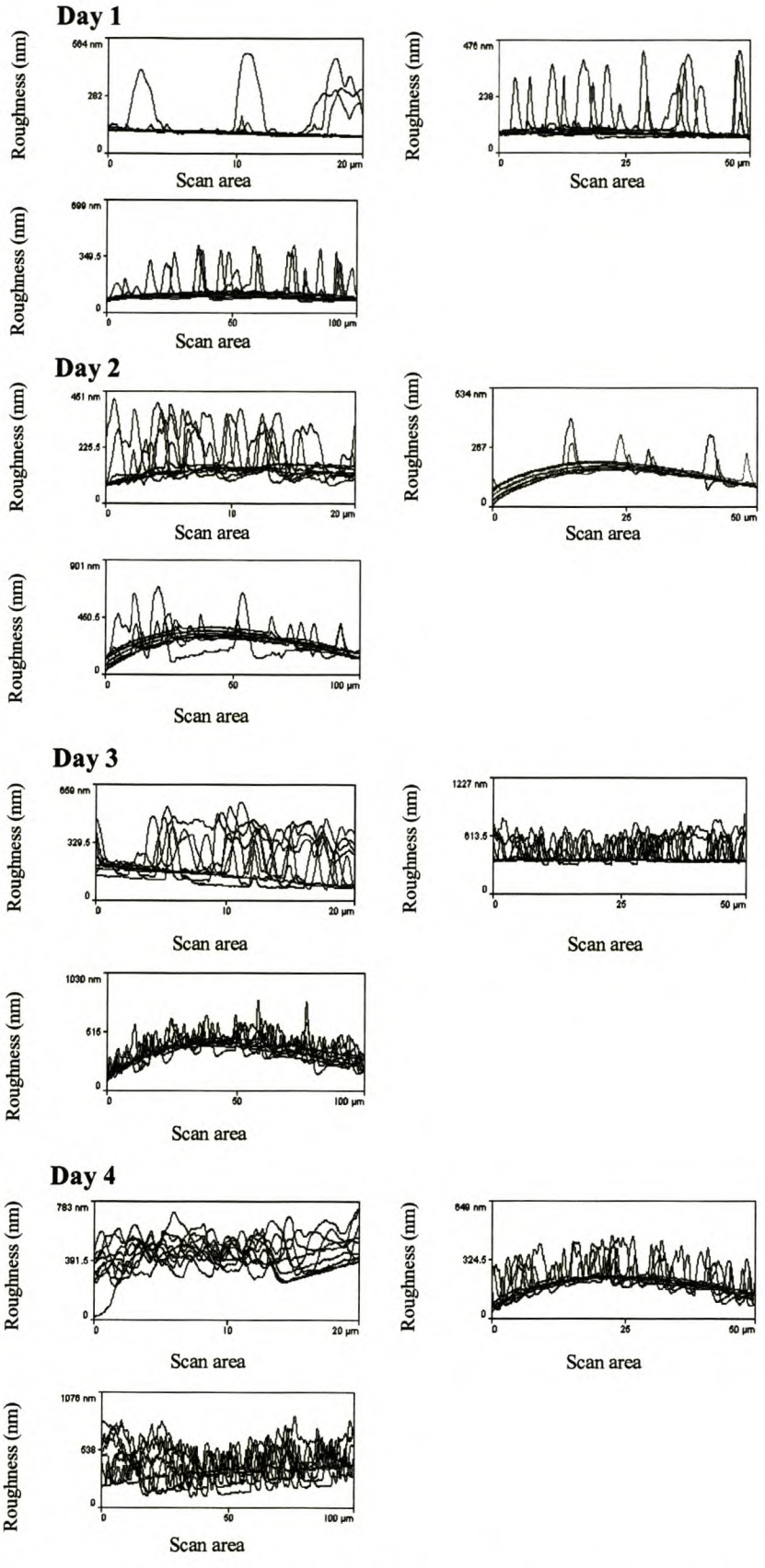

Figure 4.12 Line analysis plots (400 µm^2; 2 500 µm^2; 10 000 µm^2) of the surface roughness of biofilms cultivated on a glass substrate at 37°C.

Table 4.2 Results of AFM images for the scan area 400 μm^2, 2 500 μm^2 and 10 000 μm^2 of biofilms developed on glass at 8°C, 22°C and 37°C for varying length of time. *Values in brackets represent percentage standard deviation (%).*

Temperature	Day	Average Roughness (nm)	Average Height (nm)	Fractal
400 μm^2:	1	15.52 *(22)*	200.10 *(10)*	1.04 *(28)*
8°C	2	1.91 *(62)*	80.11 *(29)*	1.28 *(11)*
	3	2.06 *(68)*	115.00 *(31)*	1.35 *(36)*
	4	24.83 *(53)*	259.14 *(49)*	1.62 *(26)*
22°C	1	14.41 *(196)*	223.38 *(49)*	1.18 *(24)*
	2	19.27 *(92)*	203.81 *(62)*	1.30 *(26)*
	3	52.08 *(65)*	233.67 *(27)*	1.30 *(37)*
	4	14.46 *(63)*	128.84 *(23)*	1.44 *(37)*
37°C	1	26.90 *(118)*	227.40 *(54)*	1.47 *(34)*
	2	45.76 *(34)*	343.70 *(18)*	1.51 *(10)*
	3	87.20 *(24)*	475.62 *(14)*	1.68 *(9)*
	4	77.81 *(23)*	642.97 *(16)*	1.70 *(25)*
2 500 μm^2:	1	31.51 *(15)*	129.76 *(9)*	1.18 *(25)*
8°C	2	18.45 *(90)*	197.35 *(82)*	1.24 *(29)*
	3	3.91 *(103)*	130.52 *(28)*	1.68 *(32)*
	4	11.47 *(114)*	174.53 *(102)*	1.70 *(30)*
22°C	1	30.56 *(91)*	395.09 *(48)*	1.38 *(27)*
	2	42.37 *(96)*	338.83 *(57)*	1.33 *(26)*
	3	61.21 *(100)*	462.75 *(51)*	1.49 *(23)*
	4	32.40 *(28)*	342.65 *(38)*	1.66 *(22)*
37°C	1	24.83 *(73)*	293.37 *(40)*	1.43 *(17)*
	2	31.13 *(8)*	246.51 *(24)*	1.49 *(27)*
	3	81.40 *(29)*	676.87 *(7)*	1.66 *(19)*
	4	72.546 *(17)*	285.17 *(17)*	1.86 *(14)*
10 000 μm^2:	1	16.62 *(6)*	161.56 *(28)*	1.46 *(33)*
8°C	2	7.38 *(15)*	75.15 *(88)*	1.14 *(18)*
	3	9.95 *(52)*	175.82 *(57)*	1.49 *(34)*
	4	63.03 *(7)*	628.37 *(14)*	1.63 *(25)*
22°C	1	21.23 *(76)*	367.57 *(41)*	1.42 *(25)*
	2	31.73 *(73)*	418.27 *(17)*	1.40 *(20)*
	3	64.56 *(18)*	502.80 *(18)*	1.47 *(21)*
	4	43.87 *(10)*	369.80 *(13)*	1.48 *(15)*
37°C	1	25.43 *(44)*	386.44 *(33)*	1.38 *(30)*
	2	56.83 *(7)*	442.43 *(14)*	1.50 *(24)*
	3	75.00 *(13)*	557.16 *(15)*	1.57 *(26)*
	4	106.86 *(26)*	658.91 *(20)*	1.73 *(10)*

4.1.3 Effect of nutrient concentration

Biofilms were allowed to develop in different concentrations of TSB. In contrast to the lack of trends in the average roughness and average height results when the effects of substrate type and temperature (Section 4.1.1 and 4.1.2, respectively) on biofilm formation were evaluated, these measurements displayed discernable trends when the effect of nutrient concentration was studied. In the latter case, there was a positive correlation (data not shown) between biofilm development over time, and the corresponding average roughness/height measurements (Fig. 4.13 - 4.18; Table 4.3). This response was most prominent at the highest nutrient concentration (10% TSB)

studied. The biofilms were notably more dense and uniform at 10% TSB, resulting in much smaller differences in peak-valley distribution in surface profiles. In general, the fractal values showed similar increases over time as displayed by average roughness and height values.

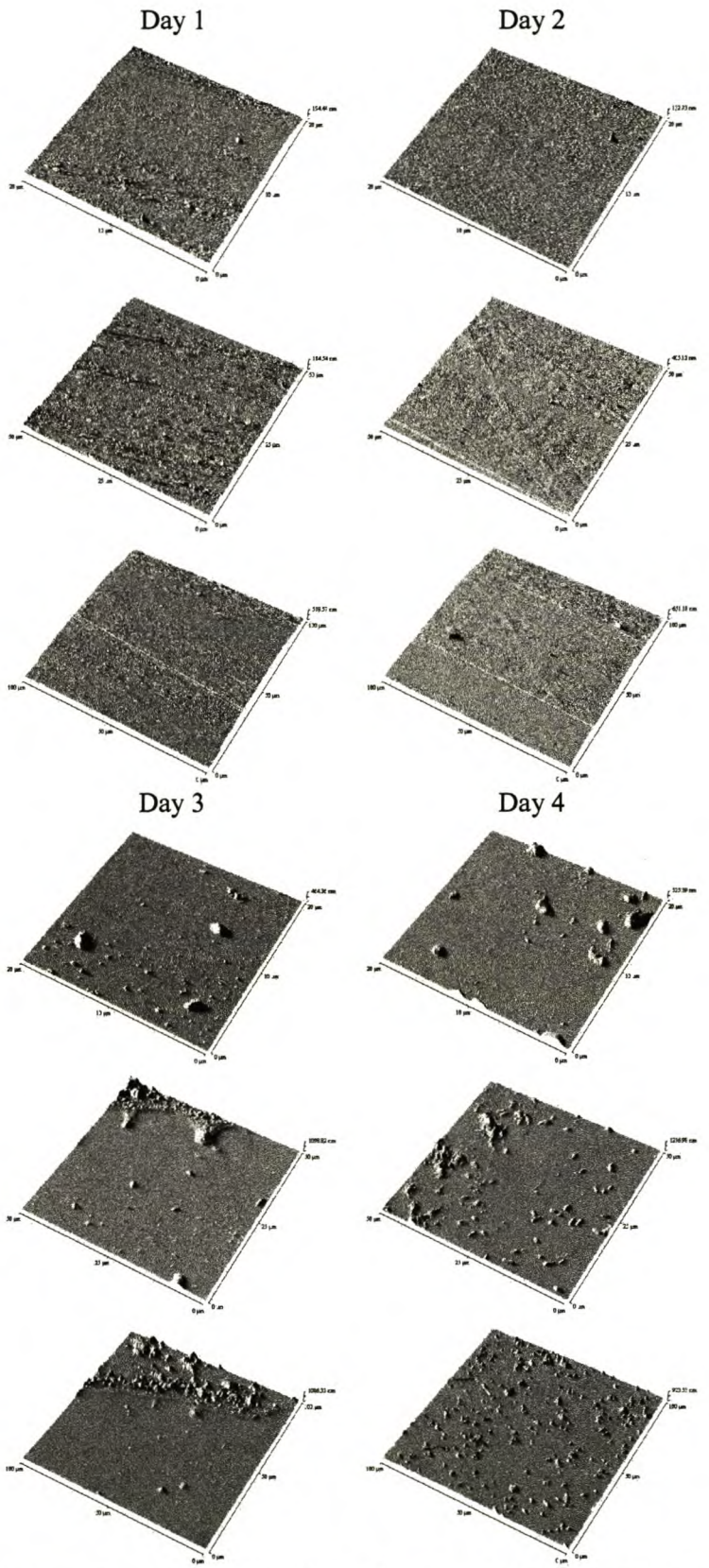

Figure 4.13. Three-dimensional AFM surface (400 µm^2, top row; 2 500 µm^2, middle row and 10 000 µm^2, bottom row) of biofilms cultivated on a glass substrate in 0.1% TSB.

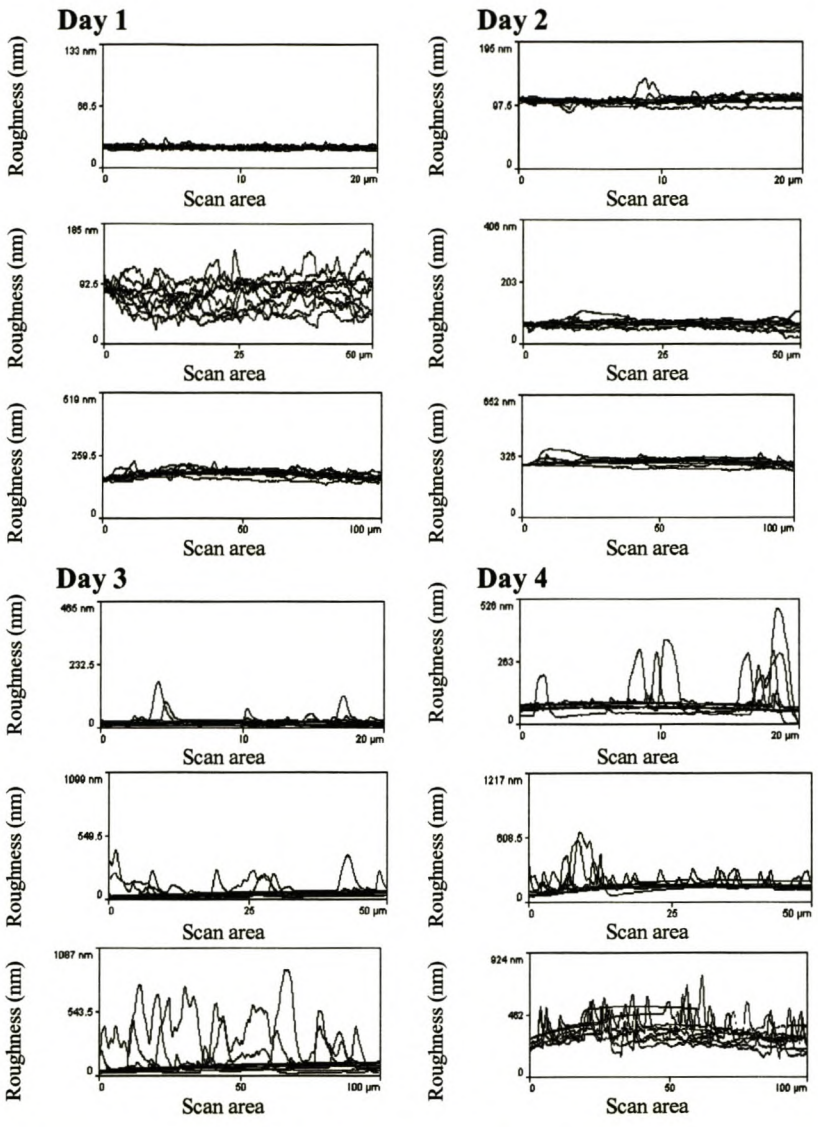

Figure 4.14 Line analysis plots (400 μm^2; 2 500 μm^2; 10 000 μm^2) of the surface roughness of biofilms cultivated on a glass substrate in 0.1% TSB.

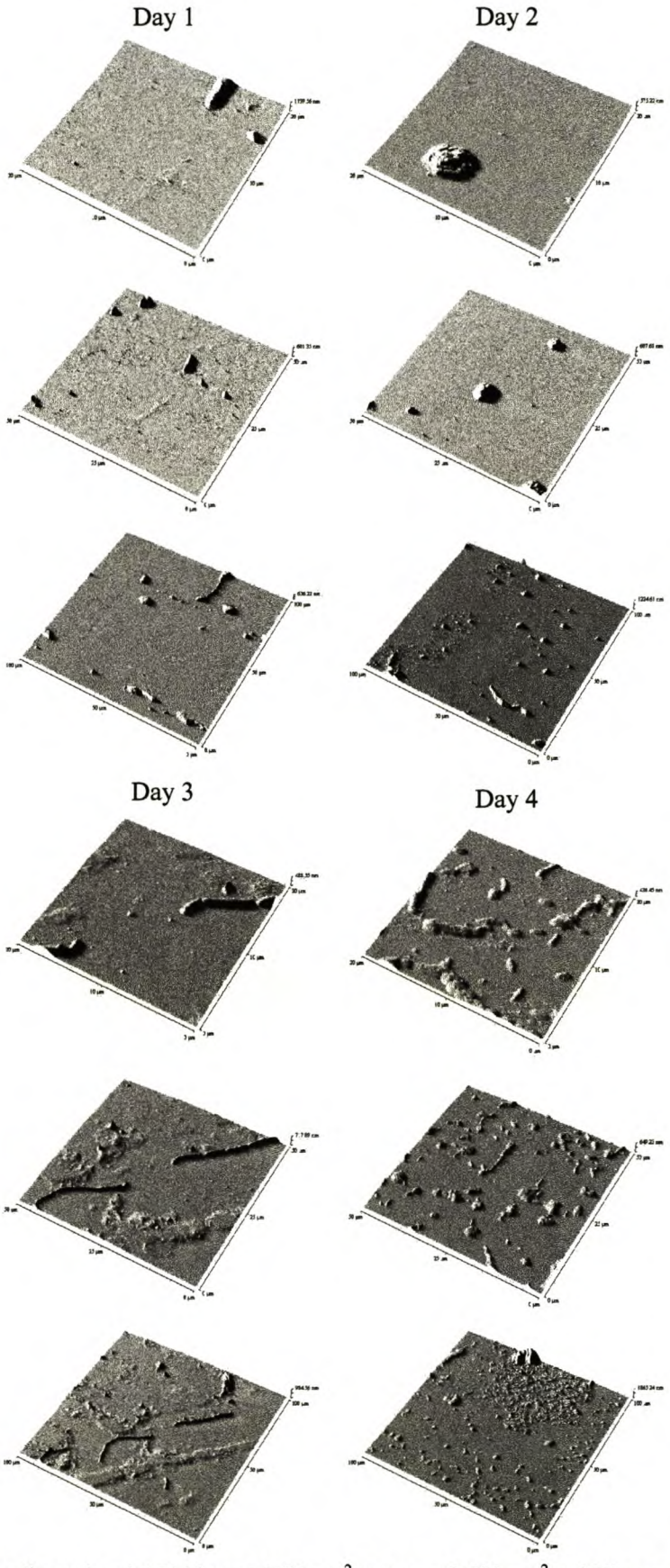

Figure 4.15 Three-dimensional AFM image (400 μm^2, top row; 2 500 μm^2, middle row and 10 000 μm^2, bottom row) of biofilms cultivated on a glass substrate in 1% TSB.

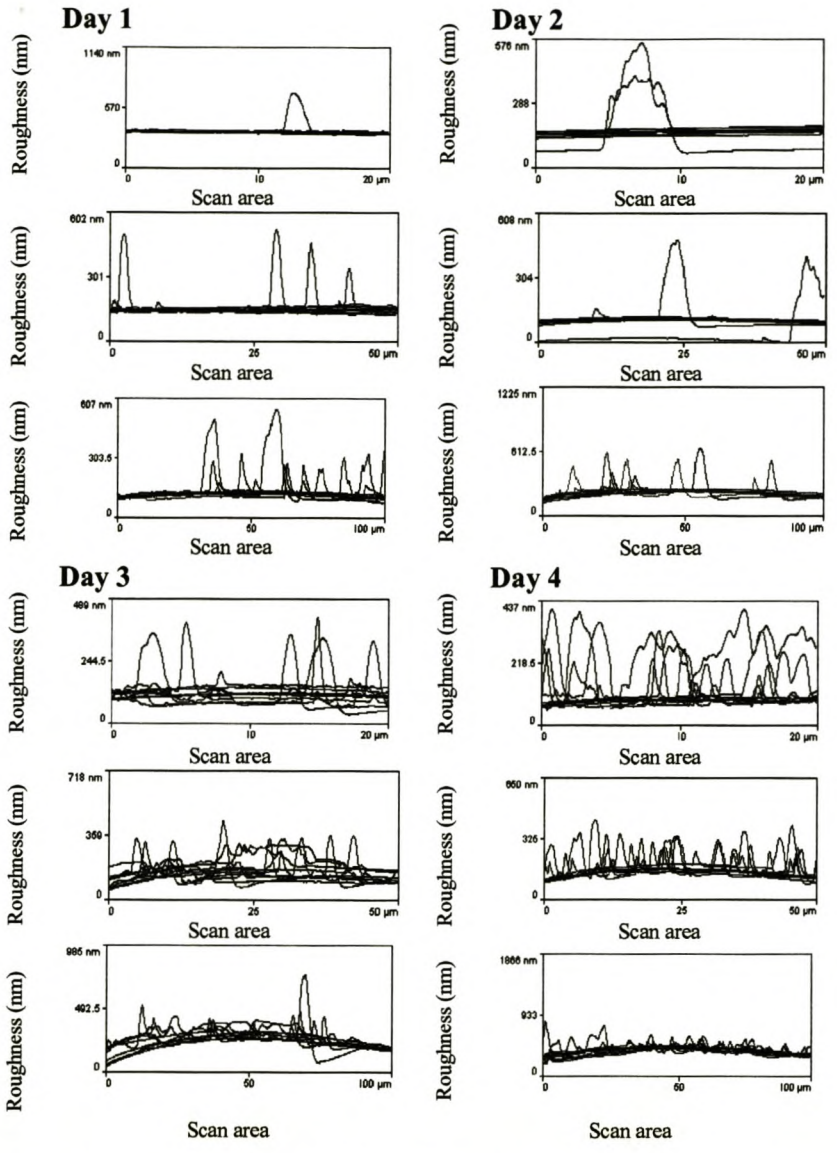

Figure 4.16 Line analysis plots (400 μm^2; 2 500 μm^2; 10 000 μm^2) of the surface roughness of biofilms cultivated on a glass substrate in 1% TSB.

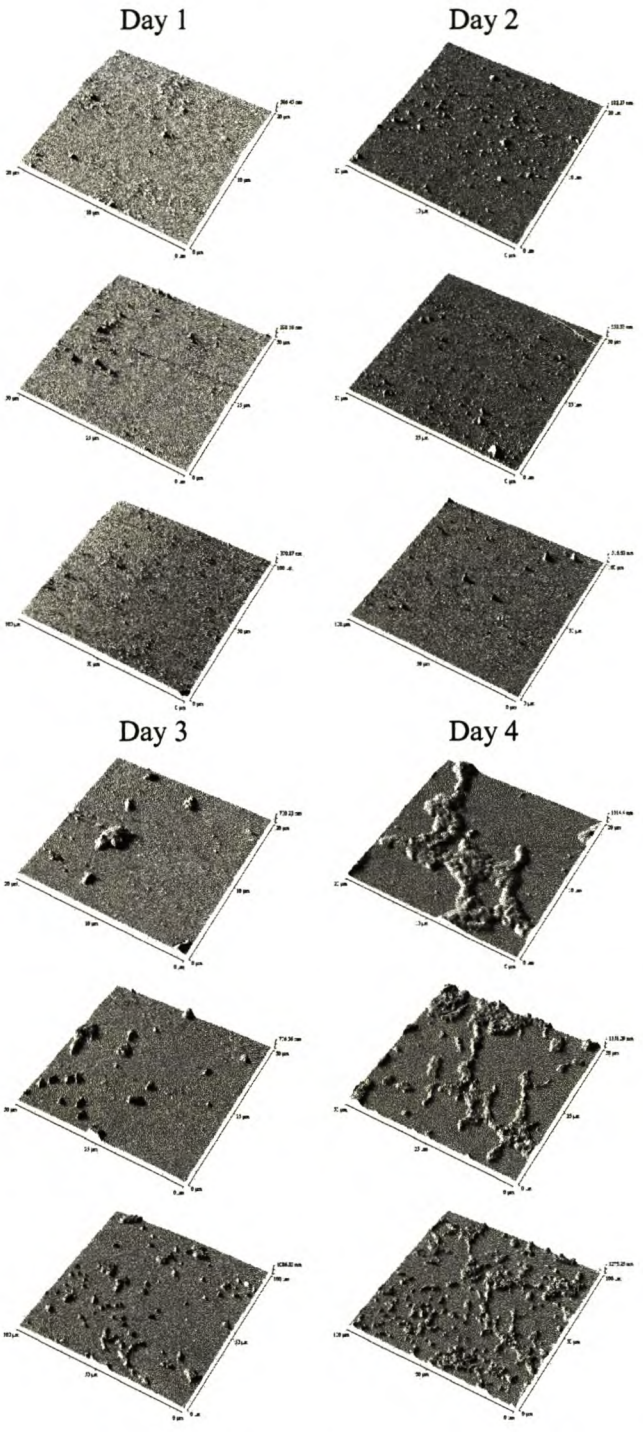

Figure 4.17 Three-dimensional AFM images (400 µm^2, top row; 2 500 µm^2, middle row and 10 000 µm^2, bottom row) of biofilms cultivated on a glass substrate in 10% TSB.

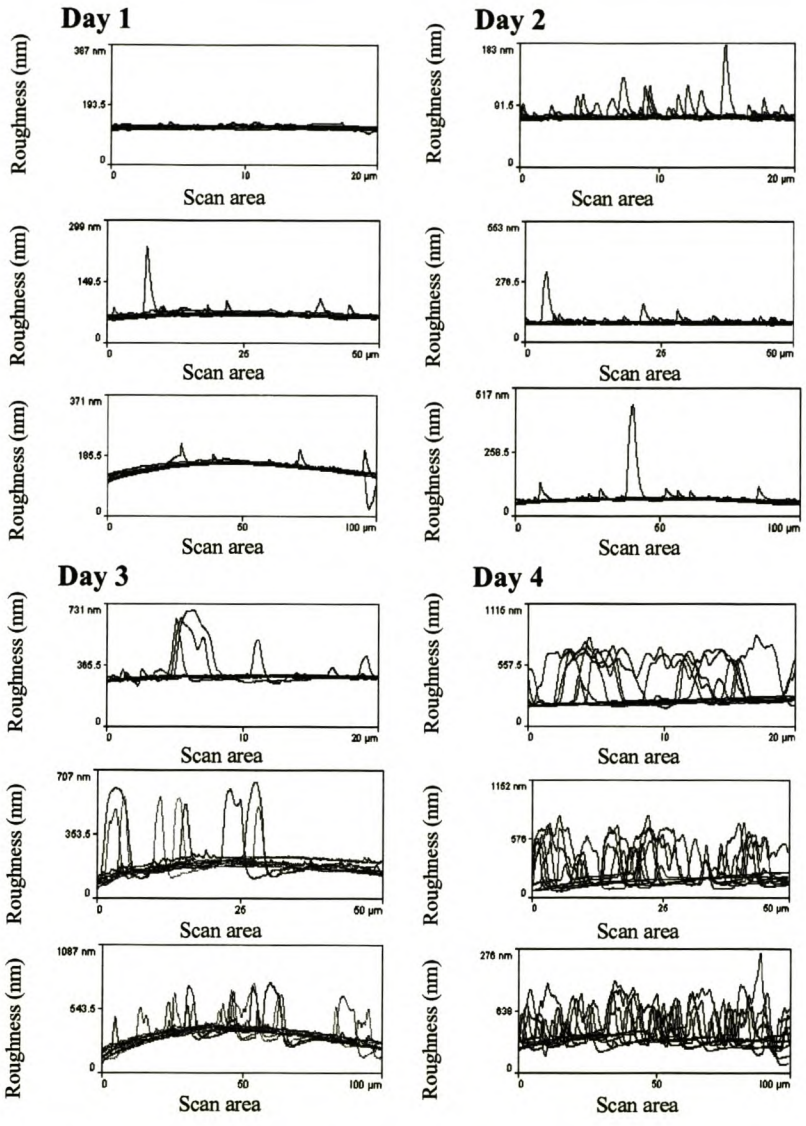

Figure 4.18 Line analysis plots (400 μm^2; 2 500 μm^2; 10 000 μm^2) of the surface roughness of biofilms cultivated on a glass substrate in 10% TSB.

Table 4.3 Results of AFM images for the scan area 400 μm^2, 2 500 μm^2 and 10 000 μm^2 of biofilms developed on glass in 0.1%, 1% and 10% TSB. *Values in brackets represent percentage standard deviation (%).*

TSB Concentration	Days	Average Roughness (nm)	Average Height (μm^2)	Fractal
400 μm^2:	1	1.14 *(22)*	34.34 *(37)*	1.40 *(37)*
0.1%	2	21.10 *(59)*	93.15 *(13)*	1.32 *(35)*
	3	3.61 *(133)*	57.15 *(75)*	1.50 *(24)*
	4	20.40 *(106)*	220.15 *(68)*	1.60 *(31)*
1%	1	21.12 *(65)*	273.64 *(43)*	1.42 *(30)*
	2	8.31 *(148)*	263.95 *(78)*	1.39 *(30)*
	3	21.34 *(166)*	135.02 *(98)*	1.46 *(30)*
	4	7.39 *(76)*	63.62 *(24)*	1.61 *(20)*
10%	1	2.39 *(45)*	214.45 *(39)*	1.17 *(37)*
	2	3.42 *(54)*	96.56 *(22)*	1.34 *(24)*
	3	21.99 *(110)*	429.65 *(36)*	1.40 *(28)*
	4	119.38 *(41)*	764.41 *(22)*	1.42 *(25)*
2 500 μm^2:	1	10.45 *(33)*	107.65 *(21)*	1.34 *(27)*
0.1%	2	5.94 *(42)*	110.89 *(26)*	1.47 *(32)*
	3	24.93 *(63)*	238.86 *(52)*	1.52 *(19)*
	4	29.43 *(64)*	297.48 *(60)*	1.60 *(23)*
1%	1	33.99 *(35)*	334.53 *(20)*	1.48 *(25)*
	2	9.95 *(93)*	248.30 *(67)*	1.36 *(28)*
	3	14.34 *(136)*	221.470 *(61)*	1.49 *(34)*
	4	26.86 *(28)*	358.38 *(18)*	1.53 *(25)*
10%	1	3.44 *(46)*	130.82 *(46)*	1.36 *(32)*
	2	4.42 *(76)*	153.46 *(46)*	1.38 *(34)*
	3	38.86 *(54)*	497.01 *(30)*	1.44 *(20)*
	4	113.85 *(46)*	820.48 *(10)*	1.66 *(15)*
10 000 μm^2:	1	9.46 *(31)*	314.89 *(35)*	1.31 *(38)*
0.1%	2	8.34 *(44)*	394.70 *(24)*	1.29 *(30)*
	3	67.27 *(99)*	416.61 *(73)*	1.54 *(18)*
	4	55.52 *(48)*	532.04 *(13)*	1.55 *(20)*
1%	1	48.27 *(23)*	471.80 *(22)*	1.36 *(25)*
	2	18.57 *(109)*	284.99 *(58)*	1.30 *(24)*
	3	30.19 *(45)*	508.00 *(31)*	1.50 *(30)*
	4	47.30 *(29)*	567.96 *(21)*	1.58 *(30)*
10%	1	11.74 *(11)*	219.86 *(19)*	1.19 *(30)*
	2	6.72 *(83)*	133.59 *(80)*	1.61 *(25)*
	3	65.43 *(17)*	664.31 *(15)*	1.62 *(19)*
	4	107.60 *(39)*	831.92 *(15)*	1.71 *(15)*

Considering the results discussed in Sections 4.1.1 - 4.1.3, it became evident that scan area has an influence on the validity of observations. Michaels (2002) showed that the measurement of small areas of a platinum catalyst on a membrane by AFM provided information on the shape, size and arrangement of platinum particles on a membrane. The measurement of larger areas (10 000 μm^2) of the platinum-containing membranes by AFM provided more accurate information on the roughness profile, fractal dimension and average height of the platinum catalyst embedded on a membrane than the 400 μm^2 and in some cases the 2 500 μm^2 scan areas. Similar conclusions extended from this study. At small measurement lengths, the average height distribution is that

of only a few features, or even a fraction of a feature, while at large lengths many features are included, including those not apparent to the eye.

The AFM results showed that biofilms comprise of cells scattered throughout the biofilm layer. The biofilms developed on the glass with a regular increase in fractal dimension (Table 4.1). This increase is possibly influenced by surface properties such as roughness and hydrophobicity (contact angle). These surface properties govern the attachment of microorganisms to surfaces especially during the early stages of biofilm formation. Comparing this phenomenon to the results of the contact angle measurements of the polished stainless steel and PVC substrates, confirmed the role that substrate properties play in the initial stages of biofilm development. Pringle and Fletcher illustrated that the increase of the hydration of the attachment surface causes a decrease in bacterial attachment (Pringle and Fletcher, 1986).

The resulting fractal dimension values (Table 4.1, 4.2 and 4.3) illustrate the advantage of using fractals to describe changes in surface profiles, which are not always clearly indicated by average height values alone as shown by Chesters *et al.* (1989) who illustrated this phenomenon in the studies of the cleanibility of different substrates. As in this study the height distribution values did not always reveal how the subject filled up the three-dimensional space.

In Sections 4.1.1, 4.1.2 and 4.1.3 the line analysis profiles did not provide sufficient evidence to describe the stages of the initial development of biofilms under all the conditions in this study. These line analysis plots may however be more useful for later development stages of biofilm development when biofilms are more dense, and their surfaces more uniform. The surface roughness, average height and fractal dimension values displayed increases over time for most of the experiments. The line analysis profiles did not always correlate with these findings and sometimes seemed to be too smooth to judge the amount of increase or decrease. The inconsistency of some of the results obtained for the average height and roughness values can be attributed to the heterogeneity in the biofilm structure.

During experiments with different temperatures and different TSB concentrations, the first two days of development did not show significant increases in average roughness and height unlike the last two. Comparison of the different growth conditions showed

different and distinct colonization pattern development. For all the experiments the surface area values (data not shown), which in general is the sum of all the areas of all the cells that cover the surface of the biofilm, seemed to be useful in describing the initial development stages of biofilms for all the scan range sizes.

4.2 Characterization of biofilms with epifluorescence microscopy

4.2.1 Effect of substrate type

The surface profile of the biofilms developed on different substrates was investigated by epifluorescence microscopy after being removed from a modified Pederson device. The results of cell distribution on PVC correlated with the observations made with AFM. The production of EPS was also observed during the investigation of AFM images. The biofilms consisted of cells of varying sizes (Fig. 4.19). After 2 days, there did not appear to be any EPS production, but after 7 and 10 days the presence of EPS is noted in the slimy matrix on the images.

Evenly distributed biofilms developed after 2 and 7 days on glass (Fig. 4.20). The biofilm on the glass comprised of small rod-shaped cells. After 10 and 13 days the biofilms were more densely packed with more cells. These observations were the same as revealed by AFM, where colony development occured more gradually than on the other substrates. The formation of biofilms on polished stainless steel resulted in cells distributed sparsely across the polished stainless steel (Fig. 4.21). The thickness of the biofilms on the surface of the polished stainless steel did not increase notably after 7 and 10 days and the distribution also remained widely spread. Epifluorescence microscopy revealed the presence of more cells on polished stainless steel than AFM. There is no conclusive explanation for this difference, although it is possible that the desiccation required for the dry scanner of the AFM, resulted in lost of cells from the polished stainless steel surface. This in turn suggests that the binding strength of cell attachment to polished stainless steel was smaller than to glass and PVC. Indeed, this is in agreement with the contact angle measurements (Table 4.4).

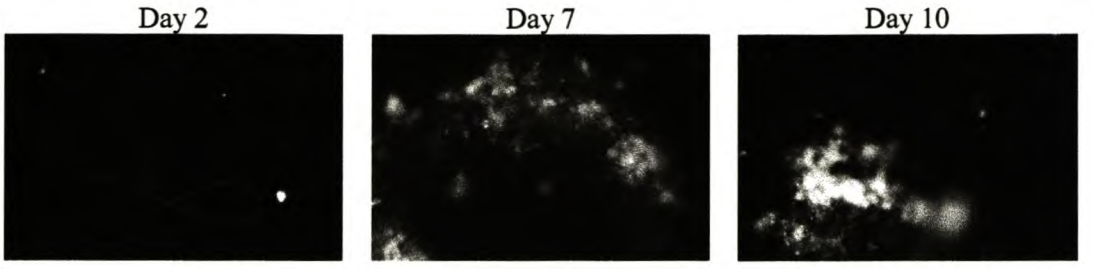

Figure 4.19 Epifluorescence images of biofilms cultivated on PVC after 2, 7 and 10 days, respectively.

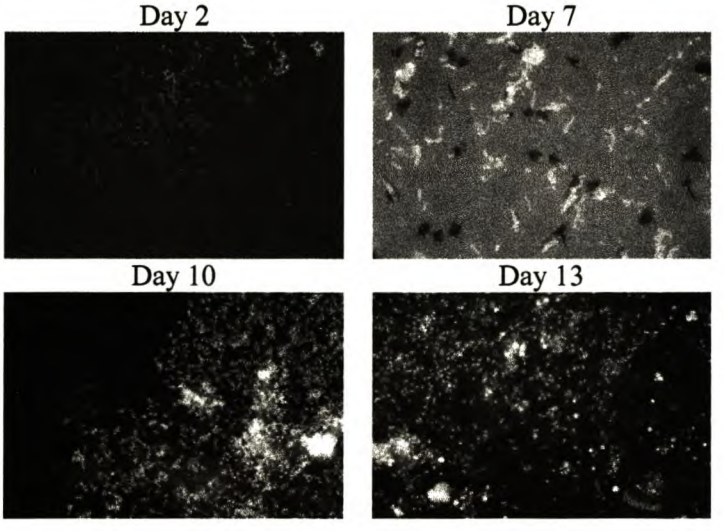

Figure 4.20 Epifluorescence images of biofilms cultivated on glass after 2, 7, 10 and 13 days, respectively.

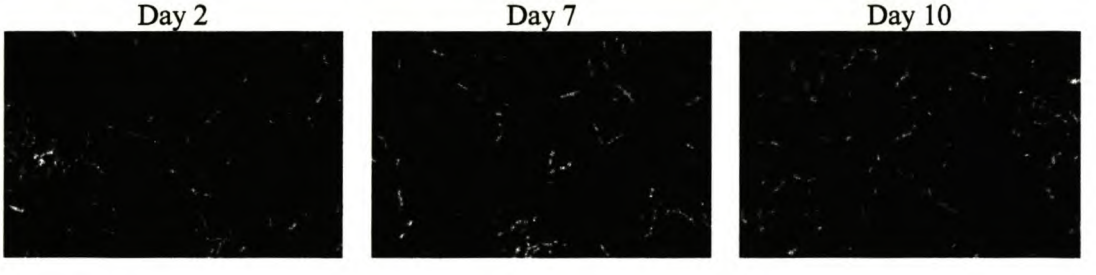

Figure 4.21 Epifluorescence images of biofilms cultivated on polished stainless steel after 2, 7 and 10 days, respectively.

4.2.2 Effect of temperature

The epifluorescence microscopy results showed that temperature had an influence on biofilm development. These patterns correlate with the images obtained with the AFM. The biofilms consisted of very little, if any cells after 1 day (Figure 4.22) at 8°C. Attached cells can be seen after 2-3 days and there was a slight increase in the number of cells. After 4 days there was a thin layer of evenly distributed cells, resulting in a

biofilm layer that was non-continuous and thin. The epiflourescence results show that the biofilms on the substrate incubated at 8°C, are less compact and dense than when biofilms were cultivated at 22°C and 37°C. The increase in temperature during the cultivation process causes the rate of the colonization to increase and this inevitably leads to greater cell distribution of the biofilm on the substrate. Biofilm development at 22°C revealed a significant distribution of cells after 1 to 3 days (Figure 4.23). After the fourth day there was a strong colony pattern and large numbers of cells were observed. The biofilms consisted of densely packed cells that formed microcolonies, and cells and EPS forming bridges that linked the microcolonies. Biofilm formation at 37°C resulted in densely packed structures (Figure 4.24) after 1 to 4 days. After 4 days, the biofilm cells were even more densely packed, and thicker distribution into the bulk of the biofilm was observed as cells divided and formed microcolonies. After four days the development of EPS is clearly visible and had increased as the microcolonies increased in size.

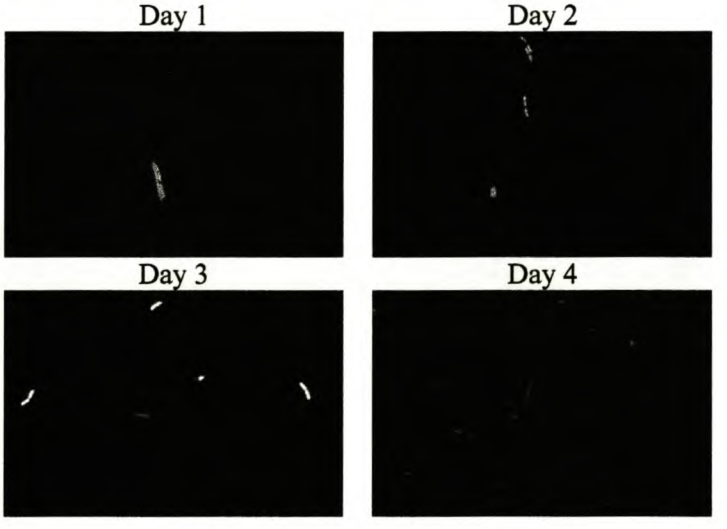

Figure 4.22 Epifluorescence images of biofilms cultivated on a glass substrate at 8°C after 1, 2, 3 and 4 days, respectively.

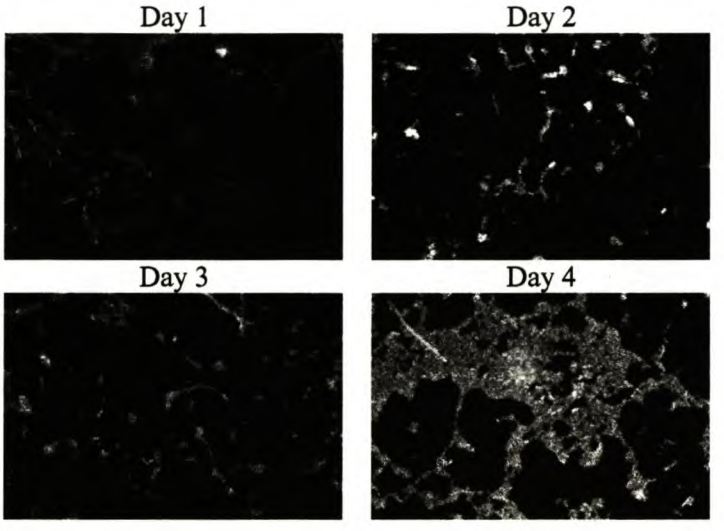

Figure 4.23 Epifluorescence images of biofilms cultivated on a glass substrate at 22°C after 1, 2, 3 and 4 days, respectively.

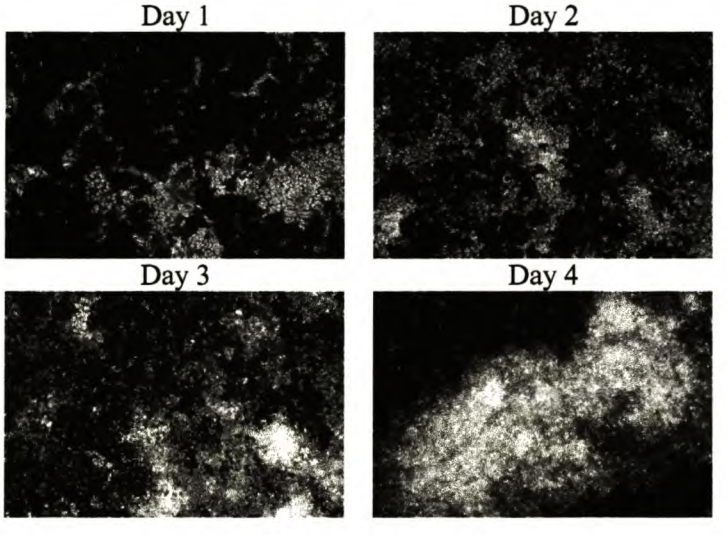

Figure 4.24 Epifluorescence images of biofilms cultivated on a glass substrate at 37°C after 1, 2, 3 and 4 days, respectively.

4.2.3 Effect of nutrient concentration

Biofilm development was investigated after 1 to 4 days in 0,1%, 1% and 10% TSB. The biofilm formation after 1 to 2 days did not reveal notable colony development and no cells could be detected (Figure 4.25). After 3 and 4 days, biofilms developed, which were similar than those observed with AFM. It was also shown that the biofilm morphology was influenced by the concentration of the TSB solution. The images below (Fig.4.25 and 4.26) show biofilm formation on a glass slide immersed for four days in a 1% TSB solution. After 1 to 2 days, cells developed (Figure 4.26) as observed by AFM. After the third and fourth days, these strings expanded and

elongated and small microcolonies became visible. After the fourth day the colonies consisted of round-shaped, rod-shaped and spiral-shaped cells with distinct colony patterns. Studies by Chang *et al.* (1991) revealed that increasing the nutrient concentration increases the biofilm thickness, which was confirmed by the results from the biofilm colony development in 10% TSB solution (Fig. 4.27).

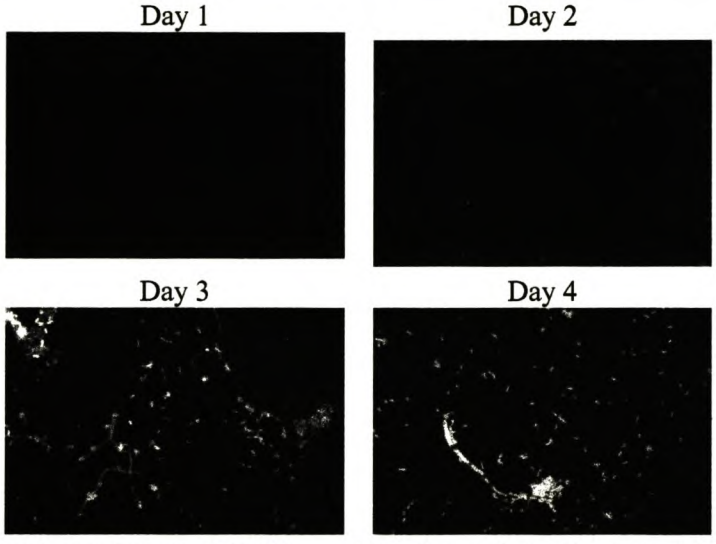

Figure 4.25 Epifluorescence images of biofilms cultivated on a glass substrate in 0.1% TSB after 1, 2, 3 and 4 days, respectively.

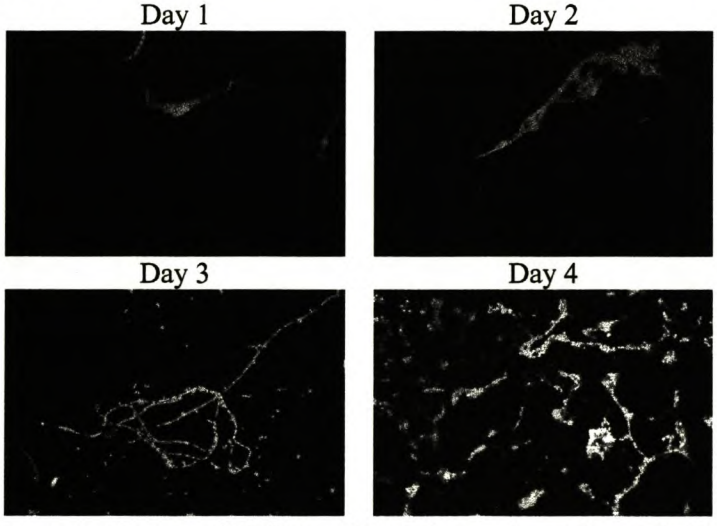

Figure 4.26 Epifluorescence images of biofilms cultivated on a glass substrate in 1% TSB after 1, 2, 3 and 4 days, respectively.

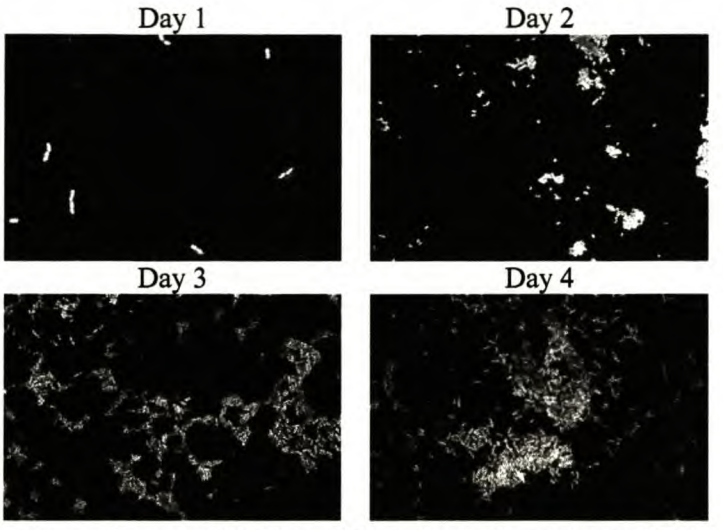

Figure 4.27 Epifluorescence images of biofilms cultivated on a glass substrate in 10% TSB after 1, 2, 3, and 4 days, respectively.

4.3 Contact angle measurements

Surface hydrophobicity is among the critical surface properties of the cell, and in biological systems, hydrophobic interactions define the unusually strong attraction between hydrophobic molecules and surfaces in water (Van Loosdrecht *et al.*, 1987). A correlation has been established between cell surface hydrophobicity, specific rate coefficient for adsorption and probability of desorption. Findings showed that *Pseudomonas fluorescens,* which has a low cell surface hydrophobocity adsorps to glass at a rate five times slower and has a 20% lower probability of desorption than *Pseudomonas aeruginosa*, which has a high surface hydrophobicity. The increase of hydration of the attachment surface has been shown to cause a decrease in bacterial attachment (Pringle and Fletcher, 1986). Hydrophobicity has been demonstrated by contact angle measurements. In Section 2.2.5, reference was made to increased surface tension corresponding to smaller contact angles. The surface tension of PVC, glass and polished stainless steel respectively is 1.30-1.40 g/cm^3, 2.47-2.57 g/cm^3 and 7.90 g/cm^3 (Ullmann's Encyclopedia). The results for the advancing minus receding cycles in this study were -0.39, -0.48 and -0.55 degrees for polished stainless steel, PVC and glass, respectively (Table 4.4). The smaller the contact angle, the better the wetting on the specific surface. The glass substrate revealed better wetting and thus a higher hydrophobicity compared to the other surfaces, which caused a reduction and delay of bacterial adherence. This supports the results from microscopic characterization and statistical analysis indicating the better cultivation of biofilms obtained on glass, and

the observation of a steady increase in biofilm development on the glass over time. These conclusions lead to the decision to choose glass as a substrate for the experiments with different concentrations of TSB and different temperatures.

Table 4.4 Results of contact angle determination of polished stainless steel, PVC and glass.

	Contact Angle (degrees)	Cos0	0.95 Confidence (degrees)	Coefficient of determination	Advancing – Receding Cycle (degrees)
Polished stainless steel: Advancing cycle	93.43	-0.06	± 0.35	0.9992	-0.39
Receding cycle	70.57	0.33	± 0.64	0.9956	
PVC: Advancing cycle	71.00	0.32	± 1.07	0.9976	-0.48
Receding cycle	37.29	0.80	± 0.56	0.9993	
Glass: Advancing cycle	72.93	0.29	± 0.24	0.9998	-0.55
Receding cycle	32.39	0.84	± 0.29	0.9999	

The results obtained with epifluorescence microscopy show that the loading of the biofilm on a glass substrate increased with time. The biofilm formation occurred in repeatable patterns on the surface of the glass substrate. The development of biofilms on the PVC and polished stainless steel substrates both were initially slow and the increase over time was not as evenly and significant as the development on the glass substrate according to the average roughness, average height and fractal values in Table 4.1. The development on the glass was more uniform with a notable amount of cells observed even from the first day. This can be explained by the fact that glass has better wetting properties.

CHAPTER 5: QUANTIFICATION OF BIOFILMS BY STATISTICAL METHODS

5.1 Quantification of AFM images of biofilm surfaces by statistical methods

Van Loosdrecht *et al.* (2002) indicated that biofilm formation depends on physical as well as biological factors. They suggested that growth yield and substrate conversion rates are basic factors governing biofilm formation. They continued to propose a mathematical model of biofilm structure. The topographic structure of surfaces can be defined in terms of surface roughness, morphological factors and geometry. Knowledge of the topographic structure of a surface can give quantitative insight into processes that produce a particular surface (Kiely and Bonnell, 1997). AFM is commonly used to obtain general statistical information about surface structures at different spatial scales. Statistical parameters of the surface height distribution function, such as the root-mean-square (rms), slope, curvature, average height, average surface area, average surface roughness, and surface fractal number (dimension) have been used to characterize surfaces. Timashev *et al.* 2000 described a new phenomenological approach to the analysis of complex membrane structures and surfaces. This included the processing of corresponding experimental data obtained, for example, from studying the roughness of structures. Application of this approach to the analysis of surface roughness of a perfluorinated cation-exchange membrane coated with a platinum layer was demonstrated by Michaels (2002). Experiments have shown that surface topography cannot be adequately described by means of statistical parameters, and that the corrugation of the surface height may have a broad bandwidth (Sayles and Thomas, 1978; Herrasti *et al.*, 1992; Yan *et al.*, 1998). Non-regularities are inherent in thin film surfaces, which are observed by SEM, AFM and STM analyses as very sharp changes in local membrane surface density and other irregularities. Sharp fluctuations in local heights of membrane and electrode surfaces were obtained, for example, by various metal deposition techniques (Timashev *et al.*, 2000).

The results of the surface roughness quantification of the biofilm surface for power spectrum, variogram and wavelet analyses are summarized in Tables 5.1-5.6. The percentage deviation of power spectrum, variogram and wavelet analyses was calculated to determine the accuracy of the different analysis for surface roughness quantification. It is important to acknowledge that the state of biofilm surfaces can determine various important characteristics of biofilms, such as cellular activity,

colony behaviour, interface formation and film growth. This also includes the non-uniformity in distribution of microorganisms on a surface, which may be determined by studies of the early stages of biofilm formation under various conditions. Although smoother surfaces delay the initial buildup of attached bacteria, smoothness does not significantly affect the total amount of biofilm on a surface after several days. It has been shown that the increase of the roughness factor does influence biofilm development in systems and might have implications on the activity of the system. Thus, the quantification of the surface profile of biofilms is important. There are different approaches to quantifying the surface roughness of biofilms. Some of these methods will be explored in this chapter.

The various analyses used for determining the Hurst exponent, such as variogram, power spectrum and wavelet, exhibited different results. This is attributed to the analyses having different degrees of error (Accuracy of different traces is provided by Benoit™ software), which can be seen in the percentage deviation results for power spectrum, variogram and wavelet analyses (Tables 5.1, 5.3 and 5.5). For all the experiments the variogram and wavelet methods proved to be the most applicable methods to describe biofilm development. The standard deviation percentages indicate that more images/line profiles is needed to accurately describe biofilm formation with Hurst exponent using the power spectrum (Tables 5.1, 5.3 and 5.5). This may reflect that the mathematical basis for power spectrum analysis is not closely related to the intrinsic process of biofilm formation or morphology. Variogram values were mainly in the range of 0.9 (Tables 5.1, 5.3 and 5.5). These values show little variation between data sets. From this it can be concluded that biofilm growth is of a consistent nature, which means that the patterns will continue to developed and distribute in the same manner. For most of the experiments the Hurst exponent was > 0.5 and thus resembles a series that covers more "distance" than a random walk. Values that are > 0.5 also indicate the probability that the surfaces of the cultivated biofilms will continue to increase in height with time. Thus, the probability that the biofilms will grow in the same fashion as they have done before, rather than developing other patterns of growth is high. If the values of Hurst were less than 0.5, the patterns of biofilm growth would have changed over time. The fractal dimension results obtained by line profiles are between 1 and 2 (Tables 5.2, 5.4 and 5.6). Since a surface with fractal dimension = 1 is featureless and a surface with fractal dimension = 2 is rough, these surfaces with

fractal dimension values between 1 and 2 can therefore be described as moderately rough (Marchese-Ragona *et al.*, 1993). The fractal dimension results obtained by the Lake-filling method for surfaces of biofilms are between 2 and 3 (Tables 5.2, 5.4 and 5.6). Again, the results show that these surfaces are so rough that they fill a three-dimensional space (Marchese-Ragona *et al.*, 1993).

5.1.2 Effect of substrate type

Table 5.1 Hurst exponents (10 line profiles) of biofilms developed on PVC, glass and polished stainless steel, analyzed after various time intervals. The Hurst exponent was determined using AFM images of scan area 400 μm^2, 2 500 μm^2 and 10 000 μm^2, respectively. *Values in brackets represent percentage standard deviation (%).*

Substrate	Days	Hurst exponent as determined by:		
		Power Spectrum*	Variogram*	Wavelets*
400 μm^2: PVC	2	0.80 *(26)*	0.73 *(10)*	0.83 *(14)*
	7	0.72 *(39)*	0.80 *(14)*	0.81 *(6)*
	10	0.72 *(39)*	0.84 *(7)*	0.78 *(7)*
Glass	2	N/A *(25)*	0.81 *(39)*	0.76 *(20)*
	7	N/A *(22)*	0.86 *(39)*	0.91 *(6)*
	10	N/A *(18)*	0.93 *(54)*	0.82 *(18)*
	13	0.75 *(41)*	0.94 *(27)*	0.91 *(9)*
Polished Stainless Steel	2	0.77 *(29)*	0.85 *(12)*	0.74 *(14)*
	7	0.91 *(50)*	0.89 *(8)*	0.84 *(9)*
	10	0.59 *(26)*	0.86 *(5)*	0.90 *(9)*
2 500 μm^2: PVC	2	0.69 *(27)*	0.84 *(7)*	0.78 *(11)*
	7	N/A *(20)*	0.80 *(23)*	0.89 *(7)*
	10	0.51 *(19)*	0.85 *(7)*	0.90 *(5)*
Glass	2	N/A *(19)*	0.75 *(26)*	0.93 *(7)*
	7	N/A *(17)*	0.78 *(45)*	0.85 *(9)*
	10	0.81 *(30)*	0.76 *(10)*	0.88 *(7)*
	13	N/A *(15)*	0.87 *(19)*	0.77 *(17)*
Polished Stainless Steel	2	0.88 *(17)*	0.87 *(20)*	0.81 *(11)*
	7	0.81 *(55)*	0.86 *(8)*	0.72 *(15)*
	10	0.64 *(25)*	0.92 *(6)*	0.64 *(14)*
10 000 μm^2: PVC	2	0.83 *(31)*	0.87 *(10)*	0.78 *(7)*
	7	0.60 *(47)*	0.91 *(14)*	0.84 *(6)*
	10	0.68 *(31)*	0.91 *(17)*	0.77 *(7)*
Glass	2	0.96 *(13)*	0.78 *(17)*	0.91 *(10)*
	7	0.80 *(14)*	0.85 *(18)*	0.90 *(9)*
	10	N/A *(26)*	0.84 *(52)*	0.61 *(53)*
	13	0.88 *(27)*	0.90 *(19)*	0.85 *(17)*
Polished Stainless Steel	2	0.93 *(36)*	0.80 *(25)*	0.85 *(9)*
	7	0.86 *(39)*	0.85 *(10)*	0.76 *(11)*
	10	0.68 *(18)*	0.80 *(13)*	0.90 *(10)*

* Benoit software was used to determine the Hurst exponent by variogram, power spectrum and wavelet analyses.

Table 5.2 Results of surface roughness characterisation of biofilms developed on PVC, glass and polished stainless steel after various time intervals. Results were determined from AFM images of scan areas of 400 μm^2, 2 500 μm^2 and 10 000 μm^2, respectively.

Substrate	Days	R_a [5]	R_{RMS} [6]	FD^{PS} #	FD^{vario} #	FD^{wave} #	FD^{line} ♦	FD^{area} √
400 μm^2: PVC	2	72.20	99.41	1.20	1.37	1.17	1.00	2.87
	7	66.68	93.12	1.18	1.50	1.19	2.00	2.45
	10	88.68	111.87	1.28	1.36	1.22	1.00	2.38
Glass	2	110.27	147.52	0.88	1.59	1.24	1.25	2.80
	7	42.47	59.62	0.93	1.54	1.09	1.45	2.54
	10	23.40	37.61	0.95	1.67	1.18	1.16	2.63
	13	37.01	65.16	1.25	1.33	1.09	1.74	2.01
Polished Stainless Steel	2	114.79	142.16	1.23	1.35	1.26	1.11	2.36
	7	106.34	141.20	1.09	1.11	1.16	1.00	2.51
	10	983.9	124.28	1.41	1.14	1.10	1.49	2.18
2 500 μm^2: PVC	2	139.60	179.48	1.31	1.36	1.22	1.30	2.56
	7	80.51	106.92	0.81	1.61	1.11	2.00	2.56
	10	97.57	125.76	1.49	1.25	1.10	1.87	2.65
Glass	2	29.02	51.32	0.70	1.65	1.07	1.13	2.45
	7	42.47	59.62	0.87	1.62	1.15	1.45	2.54
	10	19.55	26.88	1.19	0.77	1.12	1.45	1.39
	13	21.51	39.40	0.90	1.43	1.23	1.22	2.14
Polished Stainless Steel	2	150.78	198.29	1.12	1.62	1.19	1.43	2.51
	7	153.32	206.30	1.19	1.24	1.28	1.63	2.40
	10	104.99	127.25	1.36	1.28	1.36	1.00	2.19
10 000 μm^2: PVC	2	132.58	172.00	1.17	1.43	1.22	1.00	2.58
	7	111.80	143.82	1.40	1.29	1.16	2.00	2.60
	10	554.16	741.73	1.32	1.39	1.23	1.42	2.27
Glass	2	41.31	57.27	1.04	1.72	1.09	1.16	2.75
	7	29.31	45.41	1.20	1.55	1.10	2.00	2.80
	10	93.82	118.55	0.90	1.76	1.41	1.37	2.65
	13	30.80	47.14	1.12	1.50	1.15	1.40	2.65
Polishes Stainless Steel	2	185.94	265.60	0.96	1.70	1.15	143	2.51
	7	129.30	165.18	1.14	1.25	1.24	1.00	2.14
	10	152.12	206.39	1.32	1.40	1.10	1.00	2.00

[5] Average roughness of AFM image as determined by Topometrix software.
[6] Root-mean-square of AFM image as determined by Topometrix software.
Fractal dimension was determined by using the Hurst exponent in the following equation: $FD=2-H$. (*PS*=power spectrum, *wave*=wavelet and *vario*=variogram)
♦ Fractal dimension was determined by the line profile method, which uses the box-counting method (Topometrix AFM software).
√ Fractal dimension of a surface of a membrane embedded with platinum was determined by the lake-filling method (Topometrix AFM software).

5.1.3 Effect of temperature

Table 5.3 Hurst exponents (10 line profiles) of biofilms developed on glass at temperatures of 8°C, 22°C and 37°C, respectively at various time intervals. The Hurst exponent was determined using AFM images of scan area 400 μm^2, 2 500 μm^2 and 10 000 μm^2, respectively. *Values in brackets represent percentage standard deviation (%).*

Temperature	Days	Hurst exponent as determined by:		
		Power Spectrum *	Variogram*	Wavelet*
400 μm^2: 8°C	1	0.94 *(12)*	0.90 *(22)*	0.85 *(10)*
	2	0.44 *(77)*	0.87 *(37)*	0.73 *(17)*
	3	0.79 *(35)*	0.85 *(14)*	0.82 (9)
	4	0.47 *(16)*	0.84 *(22)*	0.84 *(10)*
22°C	1	0.85 *(29)*	0.85 *(32)*	0.81 *(9)*
	2	0.89 *(29)*	0.89 *(44)*	0.86 *(10)*
	3	0.76 *(36)*	0.86 *(29)*	0.77 *(8)*
	4	0.57 *(43)*	0.82 *(38)*	0.82 *(9)*
37°C	1	0.73 *(25)*	0.91 *(33)*	0.82 *(17)*
	2	0.62 *(31)*	0.87 *(9)*	0.37 *(11)*
	3	0.68 *(34)*	0.88 *(20)*	0.85 *(13)*
	4	0.70 *(28)*	0.81 *(11)*	0.90 *(8)*
2 500 μm^2: 8°C	1	0.80 *(17)*	0.88 *(19)*	0.83 *(14)*
	2	0.76 *(34)*	0.89 *(37)*	0.70 *(23)*
	3	0.93 *(30)*	0.79 *(30)*	0.76 *(16)*
	4	0.74 *(26)*	0.82 *(16)*	0.90 *(9)*
22°C	1	N/A *(34)*	0.91 *(18)*	0.70 *(20)*
	2	0.65 *(32)*	0.88 *(26)*	0.70 *(16)*
	3	N/A *(28)*	0.80 *(25)*	0.75 *(16)*
	4	0.68 *(26)*	0.86 *(27)*	0.81 *(10)*
37°C	1	0.98 *(37)*	0.91 *(17)*	0.70 *(26)*
	2	0.65 *(22)*	0.81 *(6)*	0.61 *(8)*
	3	0.70 *(37)*	0.76 *(11)*	0.86 *(11)*
	4	0.95 *(34)*	0.80 *(9)*	0.70 *(10)*
10 000 μm^2: 8°C	1	0.78 *(34)*	0.81 *(31)*	0.89 *(10)*
	2	0.66 *(61)*	0.86 *(28)*	0.83 *(7)*
	3	N/A *(14)*	0.82 *(30)*	0.89 *(9)*
	4	0.62 *(15)*	0.75 *(12)*	0.92 *(7)*
22°C	1	N/A *(31)*	0.95 *(14)*	0.68 *(18)*
	2	N/A *(35)*	0.85 *(28)*	0.78 *(20)*
	3	0.69 *(22)*	0.83 *(15)*	0.90 *(12)*
	4	0.76 *(13)*	0.88 *(19)*	0.72 *(16)*
37°C	1	N/A *(25)*	0.89 *(21)*	0.66 *(16)*
	2	0.86 *(32)*	0.88 *(16)*	0.63 *(10)*
	3	0.64 *(16)*	0.91 *(11)*	0.82 *(11)*
	4	0.70 *(44)*	0.84 *(12)*	0.75 *(16)*

* Benoit software was used to determine the Hurst exponent by variogram, power spectrum and wavelet analyses.

Table 5.4 Results of surface roughness characterisation of biofilms developed on glass at temperatures of 8°C, 22°C and 37°C, respectively at various time intervals. Results were determined from AFM images of scan areas of 400 μm^2, 2 500 μm^2 and 10 000 μm^2, respectively.

Temperature	Days	R_a [7]	R_{RMS} [8]	$FD^{PS\ \#}$	$FD^{vario\ \#}$	$FD^{wave\ \#}$	$FD^{line\ \blacklozenge}$	$FD^{area\ \surd}$
400 μm^2:								
8°C	1	19.11	24.83	1.06	1.49	1.15	1.00	2.33
	2	4.22	9.22	1.56	1.60	1.27	1.24	2.18
	3	26.55	39.30	1.21	1.66	1.18	1.19	2.10
	4	23.04	42.42	1.53	1.52	1.16	1.51	1.00
22°C	1	36.82	54.74	1.15	1.45	1.19	1.75	1.98
	2	30.73	49.95	1.11	1.51	1.14	1.25	2.15
	3	94.72	128.22	1.24	1.43	1.23	1.29	2.39
	4	287.52	352.65	1.43	1.46	1.18	2.00	2.20
37°C	1	34.61	58.17	1.27	1.40	1.18	1.46	1.90
	2	4.22	9.22	1.34	1.20	1.33	1.24	2.18
	3	98.01	115.21	1.32	1.33	1.15	1.52	2.54
	4	80.64	100.54	1.30	1.21	1.10	1.00	2.48
2 500 μm^2:								
8°C	1	24.55	31.21	1.20	1.57	1.20	1.9	2.72
	2	35.89	54.99	1.24	1.48	1.30	1.24	2.18
	3	32.08	39.30	0.97	1.70	1.24	1.19	2.00
	4	34.90	47.63	1.26	1.46	1.10	1.82	1.60
22°C	1	48.00	77.31	1.10	1.42	1.30	1.30	1.89
	2	53.03	86.85	1.35	1.23	1.30	1.75	2.37
	3	78.15	126.25	0.90	1.47	1.25	1.39	2.07
	4	34.63	56.87	1.32	1.40	1.19	1.39	2.40
37°C	1	32.88	58.10	1.02	1.42	1.30	1.49	2.33
	2	35.89	54.99	1.35	1.43	1.39	1.24	2.18
	3	83.17	105.69	1.30	1.41	1.14	1.55	2.54
	4	49.36	67.82	1.05	1.50	1.30	1.66	2.06
10 000 μm^2:								
8°C	1	30.89	38.84	1.22	1.52	1.11	1.45	2.96
	2	13.73	18.96	1.34	1.49	1.17	1.36	2.00
	3	18.96	27.23	0.91	1.63	1.11	1.25	2.50
	4	68.22	85.72	1.38	1.46	1.08	1.00	2.40
22°C	1	31.82	54.74	0.81	1.55	1.32	1.59	2.13
	2	39.12	61.50	0.97	1.58	1.22	1.50	2.50
	3	65.18	85.63	1.19	1.33	1.10	1.59	2.76
	4	45.74	58.14	1.24	1.53	1.28	1.21	2.39
37°C	1	47.20	67.70	0.99	1.50	1.34	1.55	2.31
	2	13.73	18.96	1.14	1.49	1.37	1.36	2.00
	3	72.79	92.84	1.36	1.41	1.17	1.21	2.57
	4	124.19	153.50	0.31	1.49	1.25	1.66	2.42

[7] Average roughness of AFM image as determined by Topometrix software.
[8] Root-mean-square of AFM image as determined by Topometrix software.
[#] Fractal dimension was determined by using the Hurst exponent in the following equation: $FD=2-H$. (*PS*=power spectrum, *wave*=wavelet and *vario*=variogram)
[♦] Fractal dimension was determined by the line profile method, which uses the box-counting method (Topometrix AFM software).
[√] Fractal dimension of a surface of a membrane embedded with platinum was determined by the lake-filling method (Topometrix AFM software).

5.1.4. Effect of nutrient concentration

Table 5.5 Hurst exponents (10 line profiles) of biofilms developed on glass in TSB concentrations of 0.1%, 1% and 10%, respectively at various time intervals. The Hurst exponent was determined using AFM images of scan area 400 μm^2, 2 500 μm^2 and 10 000 μm^2, respectively. *Values in brackets represent percentage standard deviation (%).*

TSB Concentration	Days	Hurst exponent as determined by:		
		Power Spectrum*	Variogram*	Wavelets*
400 μm^2: 0.1%	1	0.52 *(28)*	0.74 *(21)*	0.77 *(14)*
	2	0.87 *(34)*	0.97 *(26)*	0.78 *(17)*
	3	0.37 *(36)*	0.87 *(58)*	0.69 *(35)*
	4	N/A *(32)*	0.94 *(22)*	0.87 *(10)*
1%	1	0.71 *(38)*	0.89 *(10)*	0.81 *(8)*
	2	0.78 *(33)*	0.88 *(13)*	0.83 *(13)*
	3	0.65 *(21)*	0.85 *(32)*	0.79 *(24)*
	4	0.83 *(30)*	0.82 *(19)*	0.71 *(12)*
10%	1	0.56 *(26)*	0.95 *(10)*	0.95 *(4)*
	2	N/A *(14)*	1.00 *(8)*	0.85 *(13)*
	3	0.66 *(33)*	0.97 *(9)*	0.78 *(13)*
	4	0.79 *(24)*	0.98 *(25)*	0.79 *(15)*
2 500 μm^2: 0.1%	1	0.53 *(19)*	0.99 *(16)*	0.78 *(14)*
	2	0.82 *(31)*	0.90 *(30)*	0.72 *(13)*
	3	0.96 *(40)*	0.97 *(22)*	0.67 *(9)*
	4	N/A *(17)*	0.88 *(10)*	0.75 *(18)*
1%	1	0.89 *(22)*	0.86 *(13)*	0.74 *(19)*
	2	0.73 *(29)*	0.84 *(33)*	0.77 *(23)*
	3	0.65 *(42)*	0.89 *(52)*	0.87 *(10)*
	4	0.94 *(30)*	0.85 *(9)*	0.76 *(18)*
10%	1	0.77 *(26)*	0.88 *(17)*	0.91 *(7)*
	2	0.94 *(26)*	0.87 *(24)*	0.81 *(12)*
	3	0.81 *(32)*	0.99 *(8)*	0.57 *(17)*
	4	0.84 *(16)*	0.87 *(15)*	0.77 *(16)*
10 000 μm^2: 0.1%	1	0.58 *(25)*	0.94 *(17)*	0.82 *(13)*
	2	0.62 *(46)*	0.96 *(16)*	0.71 *(12)*
	3	0.94 *(30)*	0.88 *(12)*	0.76 *(19)*
	4	N/A *(25)*	0.81 *(14)*	0.77 *(12)*
1%	1	0.74 *(33)*	0.95 *(29)*	0.85 *(11)*
	2	0.84 *(38)*	0.96 *(20)*	0.73 *(27)*
	3	0.92 *(11)*	0.89 *(13)*	0.83 *(9)*
	4	0.95 *(25)*	0.85 *(26)*	0.78 *(16)*
10%	1	0.62 *(19)*	0.91 *(17)*	0.87 *(8)*
	2	N/A *(19)*	0.94 *(23)*	0.76 *(20)*
	3	0.92 *(28)*	0.96 *(15)*	0.64 *(25)*
	4	0.79 *(21)*	0.84 *(14)*	0.88 *(12)*

* Benoit software was used to determine the Hurst exponent by variogram, power spectrum and wavelet analyses.

Table 5.6 Results of surface roughness characterisation of biofilms developed on a glass substrate in a TSB concentration of 0.1%, 1% and 10% at various time intervals. Results were determined from AFM images of scan areas of 400 μm^2, 2 500 μm^2 10 000 μm^2, respectively.

TSB Concen.	Days	R_a [9]	R_{RMS} [10]	FD^{PS} #	FD^{vario} #	FD^{wave} #	FD^{line} ♦	FD^{area} √
400 μm^2:								
0.1%	1	10.38	11.98	1.42	1.61	1.19	1.44	1.85
	2	15.56	22.56	1.13	1.64	1.22	1.00	2.00
	3	12.03	22.11	1.63	1.65	1.31	1.34	1.60
	4	23.21	45.83	1.14	1.47	1.13	1.42	1.97
1%	1	28.28	49.18	1.30	1.35	1.19	1.39	2.45
	2	134.79	165.60	1.22	1.54	0.10	1.13	1.69
	3	59.97	84.27	1.35	1.41	1.21	1.76	2.00
	4	42.03	64.09	1.17	1.31	1.29	1.61	2.20
10%	1	62.21	76.79	1.44	1.34	1.05	1.00	2.19
	2	20.18	24.87	0.90	1.52	1.15	1.00	2.20
	3	35.99	58.58	1.34	1.24	1.22	1.55	1.73
	4	174.92	224.06	1.21	1.41	1.21	1.48	2.41
2 500 μm^2:								
0.1%	1	16.16	21.02	1.47	1.44	1.22	1.97	2.54
	2	23.30	48.50	1.18	1.62	1.28	1.55	2.30
	3	32.11	63.19	1.04	1.52	1.33	1.43	2.17
	4	29.62	60.65	0.95	1.51	1.25	1.48	2.50
1%	1	39.57	55.33	1.11	1.46	1.26	1.00	2.59
	2	25.26	39.74	1.27	1.55	1.23	1.05	2.48
	3	33.46	48.01	1.35	1.48	1.13	1.75	1.62
	4	43.23	62.71	1.06	1.46	1.24	1.90	2.29
10%	1	31.27	38.03	1.23	1.43	1.09	1.00	2.61
	2	17.61	26.04	1.06	1.62		1.10	2.00
	3	44.37	73.82	1.19	1.39	1.43	1.45	2.19
	4	125.95	164.64	1.16	1.43	1.23	1.74	2.50
10 000 μm^2:								
0.1%	1	86.16	103.21	1.42	1.52	1.18	1.00	1.73
	2	89.87	112.90	1.38	1.49	1.29	1.00	1.76
	3	70.60	110.73	1.06	1.45	1.24	1.58	2.48
	4	53.87	73.76	0.88	1.62	1.23	1.18	2.33
1%	1	58.93	77.10	1.26	1.43	1.15	2.00	2.38
	2	43.91	60.42	1.16	1.47	1.27	1.16	2.26
	3	58.48	76.84	1.08	1.50	1.17	1.07	2.14
	4	56.04	96.56	1.05	1.52	1.22	1.01	2.45
10%	1	37.30	44.11	1.38	1.49	1.13	1.00	1.52
	2	16.18	23.43	0.91	1.59	1.24	1.35	1.75
	3	121.75	159.93	1.08	1.48	1.36	1.70	2.53
	4	74.26	105.48	1.21	1.56	1.12	1.36	2.34

[9] Average roughness of AFM image as determined by Topometrix software.
[10] Root-mean-square of AFM image as determined by Topometrix software.
Fractal dimension was determined by using the Hurst exponent in the following equation: *FD=2-H*. (*PS*=power spectrum, *wave*=wavelet and *vario*=variogram)
♦ Fractal dimension was determined by the line profile method, which uses the box-counting method (Topometrix AFM software).
√ Fractal dimension of a surface of a membrane embedded with platinum was determined by the lake-filling method (Topometrix AFM software).

5.2 Quantification of epiflourescence microscopy images of biofilm surfaces by statistical methods

Box dimension was used to determine fractal dimension values (Tables 5.7-5.9). The other methods, perimeter-area dimension, information dimension, mass dimension and ruler dimension described in Sections 3.8.2-3.8.5 proved to be unsuitable (data not shown) and it was concluded that these methods cannot be applied to the studies of early stages of biofilm development. The analytical basis of these methods does not relate to biofilm growth patterns. The results using AFM images of scan area 20µm×20µm may not be as accurate as with scan areas of 100µm×100µm, since a smaller scan area provides less information on the general trend of the surface roughness profile. Over a small scan range the development of the biofilm can be explained by correlating the statistical results with the microscopy images. Tables 5.7 – 5.9 revealed that the fractal dimension values obtained by the box dimension method (a self-similar estimation method) gave useful results for all the experiments. This method proved to be suitable for description of biofilm development patterns and the values indicated a steady increase over time.

If D_p=2 when using the perimeter-area dimension method, then the surface of the biofilm is space filling and if D_p is between 1 and 2, the perimeter of the fractal figure is longer than the perimeter of a Euclidean (space that is linear and finite-dimensional) figure with the same area. This method did not fit the required criteria. Box dimension revealed values mostly ranging between 1 and 2, proving this method to be appropriate for investigations of early biofilm formation studies. These values also increased over time as biofilm development continued. As a method for determining fractals it revealed that biofilms have self-similar profiles with vertical and horizontal ranges not varying with scale.

5.2.1 Effect of substrate type

Table 5.7 Results of Epifluorescence microscopy images of the biofilms developed on PVC, Glass and Polished Stainless Steel at room temperature for varying length of time.

Substrate	Day	SELF-SIMILAR ESTIMATION METHOD: Fractal Dimension
		Box Dimension
PVC	2	1.24
	7	1.46
	10	1.63
Glass	2	1.11
	7	1.38
	10	1.53
	13	1.69
Polished Stainless Steel	2	0.70
	7	1.13
	10	1.28

5.2.2 Effect of temperature

Table 5.8 Results of Epifluorescence microscopy images of biofilms developed on glass at 8°C, 22°C and 37°C for varying length of time.

Temperature	Day	SELF-SIMILAR ESTIMATION METHODS: Fractal Dimension
		Box Dimension
8°C	1	0.99
	2	1.13
	3	1.23
	4	0.54
22°C	1	0.76
	2	1.18
	3	1.30
	4	1.52
37°C	1	1.22
	2	1.37
	3	1.56
	4	1.81

5.2.3 Effect of nutrient concentration

Table 5.9 Results of Epifuorescence microscopy images of biofilms at room temperature developed on glass in 0.1%, 1% and 10% TSB.

TSB Concentration	Day	**SELF-SIMILAR ESTIMATION METHODS: Fractal Dimension**
		Box Dimension
0.1%	1	NA
	2	NA
	3	1.21
	4	1.38
1%	1	1.10
	2	1.10
	3	NA
	4	1.26
10%	1	1.27
	2	1.30
	3	1.41
	4	1.18

CHAPTER 6: GENERAL CONCLUSIONS AND FUTURE CONSIDERATIONS

Similar to previous studies, biofilms displayed growth patterns of which the formation was influenced by environmental factors such as the type of substrate, nutrient availability and temperature. Different bacteria require different substrates for growth and the presence or absence of the appropriate nutrients can affect a bacterial cell's ability to attach, and may cause a delay in initial build-up. These observations suggested that there are consistencies in colony development and patterns of single cells forming microcolonies. Applications of the statistical methods (power spectrum; wavelet; variogram and box dimension) to analyse biofilm surfaces and their optical images are a novel area of research. It is possible to use these methods to describe, assess and predict development of biofilm communities in order to control build up of biofilms and to prevent bacteria from attaching to surfaces.

The first objective was to select a model system that would allow primary colonization of test surfaces. Polished stainless steel, PVC and glass were selected as substrates for biofilm development. Of these substrates, glass had the best wetting properties as confirmed by contact angle measurements. Earlier studies suggested that the better the wetting attributes of a surface, the slower the initial attachment behaviour of the organisms, but over time the attachment becomes stronger. The glass displayed the most consistent increase in cell numbers over time and observations of growth could be investigated over a longer period of time. The polished stainless steel and PVC substrates did not reveal this steady increase and was concluded to be less feasible substrates for the experiments that followed. The lack of cells on polished stainless steel, as observed with AFM, might be due to the inability of microorganisms to attach and grow effectively on finished surfaces, as there is less surface area to attach to. The biofilm communities tended to produce more EPS on the PVC, which may interfere with AFM imaging of cells on surfaces since the EPS will cover most of the cells. An increase in the production of highly hydrated EPS also leads to a decrease in hydrophobicity. In response the attachment of bacteria decreased.

To achieve the second and third objectives, AFM were used to observe initial stages of biofilm formation under different environmental conditions, including type of attachment surface, nutrient conditions, and temperature. The extent of biofilm development, growth patterns and behaviour observed with AFM imaging was

correlated with corresponding images from epifluorescence microscopy. Notable differences were observed between biofilms cultivated under different conditions. At 37°C the biofilm communities developed more cells after the first few days than at 22°C and 8°C. At the 0.1% and 1 % concentrations of TSB there were lower cell numbers than at 10% TSB. Biofilm thickness was limited by nutrient limitations and lower temperatures. For both the above-mentioned experimental setups, the biofilms produced a notable amount of EPS under stressed conditions, regarding nutrient concentrations and temperature settings. The increased production of EPS generally increases the hydrophibicity of the surface which leads to a decrease in the attachment of bacterial cells. In this case the production of EPS proved to be a contributing reason for unsuitable values obtained during of the calculation of maximum height and roughness values determined from the AFM images. These methods seemed to be suitable for analysis of individual cells of biofilms, but should not be used for roughness analysis of biofilm surfaces during their early-stage biofilm formation.

As the fourth and final objective, different methods were used for fractal analysis to describe primarily colonization on the different test surfaces under different environmental conditions. The AFM images were analyzed with applications of various methods for determining the Hurst exponent, such as variogram, power spectrum and wavelet. The results showed that even during early stages of biofilm formation a describable growth pattern of biofilm development could be deducted. The ability to predict patterns in which a biofilm will develop from the profiles of early stage biofilm formation will be of benefit for medical, industrial and environmental applications. Of all the methods applied, the variogram method gave the most consistent values (close to 0.9). This implies that the growth behaviour of the biofilms would continue development in a similar pattern providing the absence of feedback loops, since biofilm populations will compete for available nutrients and space as cell numbers continue to increase. Similar values which are > 0.5 also indicate the probability that the development of biofilms will continue in the same fashion as they have done before, rather than to develop other patterns of growth. The value of H=0.9 is well above 0.5 in the self-similar range proving this physical parameter to be feasible for description of initial biofilm development. Box dimension, used to determine fractal dimension values obtained form the images acquired by epi-fluorescent microscopy, revealed values mostly ranging between 1 and 2 (which were comparable to the AFM/Topometrix obtained values), proving this method to be

appropriate for investigations of early biofilm formation. Box dimension can therefore effectively be used to describe biofilm development. The statistical methods investigated in this study hold potentially promising benefits for the description of cell distributions and description of biofilm development with reliable mathematical and statistical numbers. The findings of this novel area of research contribute to the initial working hypothesis of the study, namely that the initial stages of biofilm formation inherently occur in distinct patterns that are influenced by environmental conditions.

It is evident that quantitative description of biofilm morphology is a complex issue. Especially when biofilm populations become too complex to continue obtaining realistic values using certain quantitative methods. Under less favourable conditions, not all of the methods applied followed the suspected trends. This would be an important consideration when investigating useful tools for describing the initial phases of biofilm formation. This stresses the primary importance of spreading and physical arrangement of cells and complexity of biofilm communities when using solid physical parameters to describe development of biological systems. This however, does not imply that there should necessarily be limitations to investigate various solid physical parameters as tools in the description of colony development during biofilm formation. Investigative techniques with the ability to quantify surface topographic structure in a way that can be related to biofilm structure and development will therefore always be worth exploring.

REFERENCES

Adamson, A. W. 1990. Physical Chemistry of Surfaces. 5th Ed. Wiley, New York.

Allison, C., and C. Hughes. 1992. Ability of *Proteus mirabilis* to invade human urothelial cells is coupled to motility and swarming differentiation. Infection and Immunity **60**: 4740-4746.

Arnold, J. W., and G. W. Bailey. 2000. Bacterial swarming: an example of prokaryotic differentiation and multicellular behaviour. Science Progress Edinburgh **75**: 403–422.

Barton, A.J., Sagers, R.D., and W.G. Pitt. 1996. Measurement of bacterial growth rates on polymers. J. Biomed. Mat. Res. **32:** 271-278.

Beech, I. B. 1996. The potential use of atomic force microscopy for studying corrosion of metals in the presence of bacterial biofilms- an overview. Int. Biodeterioration & iodegradation **37:** 141-149.

Beech, I. B., C. W. S. Cheung, D. B. Johnson, and J. R. Smith. 1996. Comparative studies of bacterial biofilms on steel surfaces using atomic force microscopy and environmental scanning electron microscopy. Biofouling **10:** 65-77.

Binnig, G., and H. Rohrer. 1984. Scanning tunnelling microscopy, p. 38-46. *In* J. Janta and J. Pantollick (eds.), Vol. 18, Trends in Physics.

Binnig, G., C. F. Quate, and Ch. Gerber. 1986. Atomic force microscope. Phys. Rev. Let. **56:** 930-933.

Binnig, G., Ch. Gerber, E. Stoll, T. R. Albrecht, and C. F. Quate. 1987. Atomic resolution with atomic force microscope. Europhys. Let. **3:** 1281–1286.

Blanco M. A., C. Negro, I. Gaspar, and J. Tijero. 1996. Slime problems in the paper and board industry. Appl. Microbiol. Biotechnol. **46**:203–208.

Braga, P. C., and D. Ricci. 1998. Atomic force microscopy: Application to investigation of *Escherichia coli* morphology before and after exposure to cefodizime. Antimicrob. Agents & Chemother. **42:** 18-22.

Bremer, P. J., G. G. Geesey, and B. Drake. 1992. Atomic force microscopy examination of the topography of a hydrated bacterial biofilm on a copper surface. Curr. Microbiol. **24:** 223-230.

Bryers, J. D. and, W. G. Characklis. 1982. Processes governing primary biofilm formation. Biotechnol. Bioeng. **24:** 2451-2476.

Burne, R. A., R. G. Quivey, Jr. and R. E. Marquis. 1999. Physiologic homeostasis and stress responses in oral biofilms. Meth. Enzymol. **310:** 441-460.

Busscher, H. J., R. Bos, and H. C. Van der Mei. 1995. Initial microbial adhesion is a determinant for the strength of biofilm adhesion. FEMS Microbiol. Lett. **128:** 229-34.

Campbell, R., and M. P. Greaves. 1990. Anatomy and community structure of the rhizosphere, p. 11-34. *In* J. M. Lynch (ed.), The rhizosphere. John Wiley and Sons, West Sussex, U.K.

Carlen, A., K. Nikdel, A. Wennenberg, K. Holmberg, and J. Olson. 2001. Surface characteristics and *in virto* biofilm formation on glass ionomer and composite resin. Biomaterials **22(5):** 481-487.

Chang, H.T., B.E. Rittmann, D. Amar and R. Heim. 1991. Biofilm detachment mechanisms in a liquid-fluidized bed." Biotechnol. Bioeng. 38(5): 499-506.

Characklis, W.G. 1971. Abstract 71-001: p. 171-181. Effect of hypochlorite on microbial slimes. *In* Proceedings of the 26th Industrial Waste Conference. Purdue University.

Characklis, W.G. Attached microbial growths-I. Attachment and growth, Water Res, 7:1113-1127(1973). Abstract 73-002

Characklis, W. G. and, K. E. Cooksey. 1983. Biofilms and microbial fouling. Adv. Appl. Microbiol. **29:** 93-137.

Chesters, S., H. Y. Wen, M. Lundin, and G. Kasper. 1989. Appl. Surface Sci. **40:** 155-192.

Christensen, F. R., G. H. Kirstensen, and J. la Cour Jansen. 1989. Biofilm structure; an important and neglected parameter in wastewater treatment. Water Sci. Technol. **21:** 805-814.

Costerton, J. W., and P.S. Stewart. 2001. Battling Biofilms. Scientific American **285:** 60-67.

Costerton, J. W., Z. Lewandowski, D. E. Caldwell, D. R. Korber, and H. M. Lappin-Scott. 1995. Microbial biofilms. Annu. Rev. Microbiol. **49:** 711-745.

Coutinho, C. M. L. M., F. C. M. Magalhães, and T. C. A. Jorge. 1993. Scanning electron microscope study of biofilm formation at different flow rates over metal surfaces using sulfate-reducing bacteria. Biofouling **7:** 19-27.

Dankert, J., A. H. Hogt, and J. Feijen. 1986. Biomedical polymers: Bacterial adhesion, colonization and infection. CRC Crit. Rev. Biocompat. **2:** 219-301.

Davies, J. 1994. Inactivation of antibiotics and the dissemination of resistance genes. Science, **264:** 375-382.

De Angelis, D. L. and L. J. Gross. 1992. Individual-based models and approaches in ecology. *In* Population, communities and ecosystems. Chapman and Hall, New York.

De Beer, D., P. Stoodley, and Z. Lewandowski. 1994. Effects of biofilm structures on oxygen distribution and mass transport. Biotechnol. Bioeng. **43:** 1131-1138.

De Beer, D., and P. Stoodley. 1995. Relation between the structure of an aerobic biofilm and mass transport phenomena. Water Sci. & Technol. **32:** 11-18.

De los Ríos, A., J. Wierzchos, L. G. Sancho, and C. Ascaso. 2003. Acid microenvironments in microbial biofilms of antarctic endolithic microecosystems Environ. Microbiol. **5**: 231.

Dibdin, G., and J. Wimpenny. 1999. Steady-state biofilm: practical and theoretical models. Meth. Enzymol. **310:** 296-322.

Donlan, R. M. 2002. Biofilms: Microbial life on surfaces. Emerging Infect. Diseases J. **8(9):** 881-890.

Eberl, H. J., D. F. Parker, and M. C. M. Loosdrecht. 2001. A new deterministic spatio-temporal continuum model for biofilm development. J. Theoret. Med. **3:** 161-176.

Eden, M. 1961. Vol. 4: p223. A two dimensional growth process. *In* F. Neyman (ed.), Proceedings of the Fourth Berkeley Symposium on Mathematical Statistics and Probability. University of California Press, Berkeley.

Feder, J. 1989. Fractals (Plenum Press, New York and London), pp213-228.

Flemming, H. C., and G. G. Geesey (Eds.) 1991. Biofouling and Biocorrosion in Industrial Water Systems, Springer-Verlag, New York.

Flemming, H. C. 1996. Economical and technical overview, p.5-14. *In* E. Heitz, H.-C. Flemming, and W. Sands (eds), Microbially influenced corrosion of metals. Springer-Verlag, Berlin, Heidelberg.

Fletcher, M., and J. H. Pringle. 1986. Influence of substratum hydration and absorbed macromolecules on bacterial attachment to surfaces. Appl. Environ. Microbiol. **51:** 1321-1325.

Flint, S. H., P. J. Bremer, and J. D. Brooks. 1997. Biofilms in dairy manufacturing plant description. Biofouling **11:** 81-97.

Gardiner, R. H., B. T. Milne, M. G. Turner, and R. V. O'Neill. 1987. Natural models for the analysis of broad-scale landscape patterns. Landscape Ecol. **1:** 5-18.

Geesey, G. G., M. W. Mittelman, T. Iwaoka, and P. R. Griffiths. 1986. Role of bacterial exopolymers in the deterioration of metallic copper surfaces. Mat. Performance **25:** 37-40.

Genevaux, P., S. Muller, and P. Bauda. 1996. A rapid screening procedure to identify mini-Tn*10* insertion mutants of *Escherichia coli* K-12 with altered adhesion properties. FEMS Microbiol. Lett. **142:** 27-30.

Gerson, D. F., and J. E. Zajic. 1979. The biophysics of cellular adhesion, p.2957. *In* Venkatsubramanian K, (ed), Immobilized microbial cells. ACS symposium series, vol.106. American Chemical Society, Washington, D.C.

Gilbert, P., J. Das, and I. Foley. 1997. Biofilms susceptibility to antimicrobials. Adv. Dent. Res. **11:** 160-167.

Gorlin, A. I., M. M. Gabriel, L. A. Wilson, and D. G. Ahearn. 1996. Effect of adhered bacteria on the binding of *Acanthamoeba* to hydro gel lenses. Arch. Ophthalmol. **114:** 576-580.

Gorman S. P., D. S. Jones, W. M. Mawhinney, J. G. McGoven, and C. G. Adair. 1997. Conditioning fluid influences on the surface properties of silicon and polyurethane peritineal catheters: implications for infection. J. Mat. Sc.: Mat. Med. **8:** 631-635.

Gouyet, J. -F. 1996. Physics and fractal structures. New York: Springer.

Goulian, M., and S. M. Simon. 2000. Tracking single proteins within cells. Biophys. J. **79(4):** 2188-2198.

Grimm, V. 1999. Ten years of individual-based modelling in ecology: what have we learned and what could we learn in the future? Ecol. Model **115:** 129-148.

Gristina, A. G. 1987. Biomaterial-centered infection: microbial adhesion versus tissue integration. Science **237:** 1588-1595.

Gunning, P. A., A. R. Kirby, M. L. Parker, A. P. Gunning, and V. J. Morris. 1996. Comparative imaging of *Pseudomonas putida* bacterial biofilms by scanning electron microscopy and both dc contact and ac contact non-contact atomic force microscopy. J. Appl. Bacteriol. **81:** 276-282.

Hermanowicz, S. W., U. Schindler, and P. Wilderer. 1995. Fractal structure of biofilms: New tools for investigation of morphology. Water Sci. & Technol. **32(8):** 99-105.

Herrasti, P., P. Ocon, L. Vazquez, R. C. Salvarezza, J. M. Vara, and A. J. Arvia. 1992. Scanning tunnelling microscopy study on the growth mode of vapour-deposited gold films. Phys. Rev. A **45:** 7440-7447.

Hattori, T., and R. Hattori. 1976. The physical environment in soil microbiology: an attempt to extend principles of microbiology to soil micro-organisms. Crit. Rev. Microbiol., **4:** 423-461.

Huston, M. A., D. L. DeAngelis, and W. Post. 1988. New computer models unify ecological theory. Bioscience, **38:** 682-691.

Israelachvili, J. N. 1985. Intermolecular and surface forces. Academic Press: London. Ch 11.

Jarlier W., and H. Nikaido. 1994. Mycobacterial cell wall: structure and role in natural resistance to antibiotics. FEMS Microbiol Lett. **123**:11-18.

Jaschke, M., H. -J. Butt, and E. K. Wolff. 1994. Imaging flagella of Halobacteria by atomic force microscopy. Analyst **119:** 1943-1946.

Jolley, J. G., G. G. Geesey, M. R. Hankins, R. B. Wright, and P. L. Wichlacz. 1988. Auger electron spectroscopy and X-ray photoelectron spectroscopy of the biocorrosion of copper by gun Arabic, BCS and *Pseudomonas atlantica* exopolymer. J. Surface & Interface Anal. **11:** 371-376.

Kaandorp, J. 1994. Fractal modelling growth and form in biology. Springer: Berlin.

Kasas, S., B. Fellay, and R. Cargnello. 1994. Observation of the action of penicillin on Bacillus-subtilis using atomic force microscopy-techniques for the preparation of bacteria. Surface & Interface Anal. **21:** 400-401.

Kiely, J. D., and D. A. Bonnell. 1997. Quantifying surface topography and scanning probe image reconstruction. J. Vaccine Sci. & Technol. B **15(4).**

Kinniment, S. L., J. W. T. Wimpenny, D. Adams, and P. D. Marsh. 1996. Development of a steady-state oral microbial biofilm community using the constant-depth film fermenter. Microbiol. **142:** 631-638.

Kolenbrander, P. E., and J. London. 1993. Adhere today, here tomorrow: oral bacterial adherence. J. Bacteriol. **175:** 3247-3252.

Kolenbrander, P. E., R. N. Andersen, K. Kazmerzak, R. Wu, and R. J. Palmer, Jr. 1999. Spatial organization of oral bacteria in biofilms. Methods in Enzymol. **310:** 322-332.

Kreft, J. -U., C. Picioreanu, J. W. T. Wimpenny, and M. C. C. van Loosdrecht. 2001. Individual-based modelling of biofilms. Microbiol. **147:** 2897-2912.

Landa, A. S., H. C. Van der Mei, and H. J. Busscher. 1996. A comparison of the detachment of an adhering oral streptococcal strain stimulated by mouth rinses and a pre-brushing rinse. Biofouling, **9:** 327-339.

Lawrence, J. R., and D. E. Caldwell. 1987. Behaviour of bacterial stream populations within the hydrodynamic boundary layers of surface microenvironments. Microb. Eco. **14:** 15-27.

Lawrence, J. R., D. R. Korber, B. D. Hoyle, J. W. Costerton, and D. E. Caldwell. 1991. Optical sectioning of microbial biofilms. J. Bacteriol. **173:** 6558-6567.

Marchese-Ragona, S. P., and B. Christie. 1993. Surface characterization using fractal analysis. Topometrix Technical Notes. No.2-0493-009.

Marsh, P. D. 1999. Microbiologic aspects of dental plaque and dental caries. Dental Clinic North America **43:** 599-614.

Massol-Deya, A. A., J. Whallon, R. F. Hickey, and J. M. Tiedje. 1995. Channel structure in aerobic biofilms of fixed film reactors treating contaminated groundwater. Appl. Environ. Microbiol. **61:** 769-777.

Matsuura, S., and S. Miyazima. 1992. Self-affine fractal growth front of *Aspergillus oryzae*. Physica A191: 30-34.

Maurice, P., J. Forsythe, L. Hersman, and G. Sposito. 1996. Application of atomic force microscopy to studies of microbial interactions with hydrous Fe(III)-oxides. Chem. Geol. **132:** 33-43.

McCoy W. F., J. D. Bryers, J. Robbins, and J. W. Costerton. 1981. Observations of fouling biofilm formation. Can. J. Microbiol. **27:** 910-917.

McLaughlin-Borlace, L., F. Stapleton, M. Matheson, and J. K. G. Dart. 1998. Bacterial biofilm on contact lenses and lens storage cases in wearers with microbial keratitis. J. Appl. Microbiol. **84:** 827-838.

Meadows, P. S. 1971. The attachment of bacteria to solid surfaces. Arch. Microbiol. **85:** 374-381.

Michaels, W. C. 2002. Microheterogeneous solid polymer electrolyte (SPE) membranes for electrocatalysis. Doctoral Thesis, University of Stellenbosch.

Morra M., and C. Cassinelli. 1996. *Staphylococcus epidermidis* adhesion to films deposited from hydroxyethylmethacrylate plasma. J. Biomed. Mat. Res. **31:** 149-155.

Morris, V. J., A. R. Kirby, and A. P. Gunning. eds. 1999. Atomic force microscopy for biologists. Imperial College Press.

Müller, D.J., Schabert, F.A., Buldt, G., and A. Engel. 1995. Imaging purple membranes in aqueous solutions at subnanometer resolution by atomic force microscopy. Biophys. J. **68:** 1681-1686.

Nagao, E., and Dvorak, J. A. 1998. An integrated approach to the study of living cells by Atomic Force Microscopy. J. Microscopy **191:** 8-19.

Nicolella, C., S. Chiarle, R. Di Felice and M. Rovatti. 1997. Mechanisms of biofilm detachment in fluidized bed reactors. Water Sci. & Technol. **36(1):** 229–235.

Noble D. 1995. Magnetic resonance force microscopy. Anal. Chem. November: 671A-673A.

Noguera, D. R., G. Pizarro, D. A. Stahl, and B. E. Rittmann. 1999b. Simulation of multispecies biofilm development in three dimensions. Water Sci. & Technol. **39(7):** 123-130.

Notermans, S., J. A. Dormans, and G. C. Mead. 1991. Contribution of surface attachment to the establishment of micro-organisms in food processing plants: a review. Biofouling, **5:** 21-36.

Nyvad, B., and M. Kilian. 1990. Comparison of the initial streptococcal microflora on dental enamel in caries-active and in caries-inactive individuals. Caries Res. **24:** 267-272.

Nguyen, L. K., and N. L. Schiller. 9189. Identification of a slime exopolysaccharide depolymerise in mucoid strains of Pseudomonas aeroginosa. Curr. Microbiol. **18:**323-329.

Ohnesorge, F., W. M. Heckl, W. Harberle, D. Pum, M. Sara, H. Schindler, K. Schilcher, A. Kiener, D. P. E. Smith, U. B. Sleytr, and G. Binnig. 1992. Scanning force microscopy studies of the S-layers from *Bacillus coagulans* E38-66, *Bascillus sphaericus* CCM2177 and of an antibody binding process. Ultramicroscopy, **42-44:** 1236-1242.

O'Toole, G. A., and R. Kolter. 1998. Flagellar and twitching motility are necessary for *Pseudomonas aeruginosa* biofilm development. Mol. Microbiol. **30:** 295-304.

O'Toole, G. A., K. A. Gibbs, P. W. Hager, P. V. Phibbs, Jr., and R. Kolter. 2000. The global carbon metabolism regulator *CRC* is a component of a signal transduction pathway required for biofilm development by *Pseudomonas aeruginosa.* J. Bacteriol. **182:** 425-431.

Parker, M.L., T. F. Brocklehurst, P. A. Gunning, H. P. Coleman, and M. M. Robins. 1995. Growth of food-borne pathogenic bacteria in oil-water emulsions: I Methods for investigating the form of growth. J. Appl. Bacteriol. **78:** 601-608.

Pasmore, M., P. W. Todd, B. Pfiefer, M. Rhodes, and C. N. Bowman. 2002. Effect of polymer surface properties on the reversibility of attachment of *Pseudomonas aeruginosa* in the early stages of biofilm development. Biofouling, **18(1):** 65-71 Abstract 02-018.

Pederson, K. 1982. Method for studying microbial biofilms in flowing water systems. Appl. Environ. Microbiol. **43:** 6-13.

Picioreanu, C., van Loosdrecht, M. C. M. & Heijnen, J. J. (1998). A new combined differential-discrete cellular automaton approach for biofilm modeling: application for growth in gel beads. *Biotechnol Bioeng* **57:** 718–731

Poulsen, L. K., G. Ballard, and D. A. Stahl. 1993. Use of rRNA fluorescence in situ hybridization for measuring the activity of single cells in young and established biofilms. Appl. Environ. Microbiol. **59:** 1354-1360.

Power, K., and, K. C. Marshall. 1988. Cellular growth and reproduction of marine bacteria on surface-bound substrate. Biofouling **1:**163-174.

Pratt, L. A., and R. Kolter. 1998. Genetic analysis of *Escherichia coli* biofilm formation: defining the roles of flagella, motility, chemotaxis and type I pili. Mol. Microbiol. **30:** 285-294.

Pringle, J. H., and M. Fletcher. 1986. Influence of substratum hydration and adsorbed macromolecules on bacterial attachment to substrates. Appl. Environ. Microbiol. **51(6):** 1321-1325.

Rajyaguru, J. M., M. Kado, M. C. Richardson, and M. J. Musznki. 1997. X-ray micrography and imaging of *Escherichia coli* cell shape using laser plasma pulsed point X-ray sources. Biophys. J. **72:** 1521-1526.

Razatos, A., Y.-L. Ong, M. M. Sharma, and G. Georgiou. 1998. Molecular determinants of bacterial adhesion monitored by atomic force microscopy. Proc. Natl. Acad. Sci. USA **95:**11059–11064.

Rupp, F., D. Axmann, C. Ziegler, and J. Geis-Gerstorfer. 2002. Adsorption/desorption phenomena on pure and Teflon((R)) AF-coated titania surfaces studied by dynamic contact angle analysis. J. Biomed. Mat. Res. **62(4):** 567-578.

Ruppersberg, J. P., J. K. H. Horber, Ch. Gerber, and G. Binnig. 1989. Imaging of cell membraneous and cytoskeletal structures with a scanning tunnellisng microscope. FEBS Let. **257:** 460-464.

Russ, J. 1994. Fractal Surfaces. Plenum Press: New York.

Russell P., and D. Batchelor. 2001. SEM and AFM: Complementary techniques for surface investigations, Microscopy and Analysis, Asia/Pacific edition, Iss 22 (July), 13-16.

Sauer, K, A.K. Camper, G.D. Ehrlich, J.W. Costerton, and D.G. Davies. 2002. *Pseudomonas aeruginosa* Displays Multiple Phenotypes during Development as a Biofilm. J. Bacteriol, **184(4):**1140-1154.

Sayles, R. S., and T. R. Thomas. 1978. Surface topography as a non-stationary random process. Nature, **271:** 731-434.

Schabert, F. A., A. Hefti, K. Goldie, A. Stemmer, A. Engel, E. Meyer, R. Overney, and H. J. Guntherdodt. 1992. Ambient pressure Scanning Probe Microscopy of 2D regular protein arrays. Utramicroscopy, **42-44:** 1118-1124.

Schabert, F. A., and A. Engel. 1994. Reproducible acquisition of *Escherichia coli* porin surface topographs by atomic force microscopy. Biophys. J. **67:** 2394-2403.

Schabert, F. A., C. Henn, and A. Engel. 1995. Native *Escherichia coli* ompF porin surface topographs by atomic force microscopy. Science, **268:** 92-94.

Shapiro, J. 1987. Organization of developing *Escherichia coli* colonies viewed by scanning electron microscopy. J. Bacteriol. **52:** 142-156.

Singleton, S., R. Treloar, P. Warren, G. K. Watson, R. Hodgson, and C. Allison. 1997. Methods for microscopic characterization of oral biofilms: analysis of colonzation, microstructure, and molecular transposrt phenomena. Advances Dent. Res. **11:** 133-149.

Sissons, C. H. 1997. Artificial dental plaque biofilm model systems. Advances Dent. Res. **11:** 110-126.

Southam, F., M. Firtel, B. L. Blackford, M. H. Jericho, W. Xu, P. J. Mulhern, and T. J. Beveridge. 1993. Transmission electron microscopy, scanning tunnelling microscopy, and atomic force microscopy of the cell-envelope layers of the archaeobacterium: *Methanospirillium hungatei* GP1. J. Bacteriol. **175:** 1946-1955.

Steele, A., D. T. Goddard, and I. B. Beech. 1994. An atomic force microscopy study of the biodeterioration of polished stainless steel in the presence of bacterial biofilms. Int. Biodet. & Biodeg., **341:** 34-46.

Stickler, D. J., J. B. King, C. Winters, and S. L. Morris. 1993. Blockage of urethral catheters by bacterial biofilms. J. Inf., **27:** 133-135.

Stoodley, P., Z. Lewandowski, J. D. Boyle, and H. M. Lappin-Scott. 1999. Structural deformation of bacterial biofilms caused by short-term fluctuations in fluid shear: An in situ investigation of biofilm rheology. Biotechnol. Bioeng. **65:** 83- 92.

Surman, S. B., J. T. Walker, D. T. Goddard, L. H. G. Morton, C. W. Keevil, W. Weaver, A. Skinner, K. Hanson, D. Caldwell, and J. Kurtz. 1996. Comparison of microscope techniques for the examination of biofilms. J. Microbiol. Meth., **25:** 57-70.

Tessele, F., G. Englert, and L. O. Monteggia. 2002. Biofilm development in down flow anaerobic fluidised bed reactors under transient conditions Water Sci. & Technol. **46(1-2):** 253–256.

Timashev, S. F., D. G. Bessarabov, R. D. Sanderson, S. Marais, and S. G. Lakeev. 2000. Description of non-regular membrane structures: A novel phenomenological approach. J. Mem. Sci., **170:** 191-203.

Toerien, D. F., A. Gerber, L. H. Lotter, and T. E. Cloete. 1990. Advances in Microbiology Ecology Ed. Marshall K.C. Plenum Press, New York. **11**: 173-230.

Tommaso G., M. B. Varesche, M. Zaiat, R. F. Vazoller, and E. Foresti. 2002. Morphological observation and microbial population dynamics in anaerobic polyurethane foam biofilm-degrading gelatin. Braz. J. Chem. Eng. **19(3):** 287-292.

Ullmann's Encyclopedia of Industrial Chemistry, Fifth, Completely Revised Edition, **A10**: 465.

Qian, P. -Y., D. Rittschof, and B. Screedhar. 2000. Macrofouling in unidirectional flow: miniature pipes as experimental models for studying the interaction of flow and surface characteristics on the attachment of barnacle, bryozoan and polychaete larvae. Mar. Ecol. Prog. Ser. **207**: 109-121.

Van Loosdrecht, M. C., J. Lyklema, W. Norde, G. Schraa, and A. J. B. Zehnder. 1987. The role of bacterial cell wall hydrophobicity in adhesion. Appl. Environ. Microbiol. **53:** 1893-1897.

Van Loosdrecht, M. C. M., J. J. Heijnen, H. Eberl, J. Kreft, and C. Picioreanu. 2002. Mathematical modelling of biofilm structures. Antonie van Leeuwenhoek Int. J. Gen. & Mol. Microbiol. **81(1-4):** 245-256.

Van Oss, C. J. 1994. Polar or Lewis acid-base interactions. *In:* Interfacial forces in aqeous media. Edited by Van Oss, C.J. (Marcel Dekker, New York):18-46.

Vesenka, J., C. Mosher, S. Schaus, L. Ambrosio, E. Henderson. 1995. Combining optical and atomic force microscopy for life sciences research. Biotechniques, **19:** 240-253.

Vicsek, T., M. Cserzo, and V. K. Horvath. 1990. Self-affine growth of bacterial colonies. Physica A167: 315-321.

Vidal, O., R. Longin, C. Prigent-Combaret, C. Dorel, M. Hooreman, and P. Lejune. 1998. Isolation of an *Escherichia coli* K-12 mutant strain able to form biofilms on inert surfaces: involvement of a new *ompR* allele that increases *curli* expression. J. Bacteriol. **180:** 2442-2449.

Wang, J., S. Lory, R. Ramphal, and S. Jin. 1996. Isolation and characterization of *Pseudomonas aeruginosa* genes inducible by respiratory mucus derived from cystic fibrosis patients. Mol. Microbiol. **22:** 1005-1012.

Whittaker, C. J., C. M. Klier, and P. E. Kolenbrander. 1996. Mechanisms of adhesion by oral bacteria. Ann. Rev. Microbiol. **50:** 513-552.

Williams, V., and M. Fletcher. 1996. *Pseudomonas fluorescence* adhesion and transport through porous media are affected by lipopolysaccharide composition. Appl. Environ. Microbiol. **62:** 100-104.

Wimpenny, J. W. T., and R. Colasanti. 1997. A unifying hypothesis for the structure of microbial biofilms based on cellular automaton models. FEMS Microbiol. Ecol. **22:** 1-16.

Witten, T. A., and L. M. Sander. 1981. Diffusion--limited aggregation, a kinetic critical phenomenon Phys. Rev. Let. **47**: 1400-1403.

Xu, W., P. J. Mulhern, B. L. Blackford, M. H. Jericho, M. Firtel, and T. J. Beveridge. 1996. Modelling and measuring the elastic properties of an arhaeal surface, the sheath of *Methanospirillum hungatei*, and the implication for methane production, J. Bacteriol. **178:** 3106-3112.

Yan, W., and K. Komvopoulos. 1998. Contact analysis of elastic-plastic fractal surfaces. J. Appl. Phys. **84**: 3617-3624.

Zottola, E. A. 1997. Special techniques for studying microbial biofilms in food systems. *In* Food Microbiological Analysis—New Technologies, M.L. Tortorello and S.M. Gendel. Marcel Dekker (eds.). New York.